2014

Defect Mediated Electrochemical Hydrogenation of Epitaxial Graphene: Towards Graphene Based Microbial Fuel Cells

Kevin Michael Daniels
University of South Carolina - Columbia

DEFECT MEDIATED ELECTROCHEMICAL HYDROGENATION OF EPITAXIAL GRAPHENE: TOWARDS GRAPHENE BASED MICROBIAL FUEL CELLS

by

Kevin Michael Daniels

Bachelor of Science
University of South Carolina, 2009

Master of Engineering
University of South Carolina, 2012

Submitted in Partial Fulfillment of the Requirements

For the Degree of Doctor of Philosophy in

Electrical Engineering

College of Engineering and Computing

University of South Carolina

2014

Accepted by:

MVS Chandrashekhar, Major Professor

Tangali S. Sudarshan, Committee Member

Goutam Koley, Committee Member

Alan W. Decho, Committee Member

Lacy Ford, Vice Provost and Dean of Graduate Studies

DEDICATION

To my family

ACKNOWLEDGEMENTS

I am very thankful for so many people whom this work would not have been possible. I would like to first thank my adviser Dr. MVS Chandrashekhar for his guidance over the last four years. His enthusiasm for research and his vast knowledge of the field led to many discussions which I have found to be invaluable not only for this work but for my future career. I would also like to thank Dr. Sudarshan, whom I have had the pleasure of working with the past eight years. It is because of him that I decided to pursue my doctorate and through his continued support that I submit this thesis. I would also like to thank Dr. Goutam Koley and Dr. Alan Decho for being a part of my committee, providing valuable feedback throughout my study and ensuring the quality of this work.

I would like to thank Dr. Alan Decho and Kristen Miller from environmental health sciences for all their help with the graphene biosensor experiments. Their experience with biological systems and the many hours Kristen spent on the growth of the bacteria was invaluable. I would also like to thank Dr. Navid Saleh and Nuripam Aich from environmental engineering for their collaboration with this experiment. I would like to thank Dr. Chris Williams and Dr. John Weidner from chemical engineering for their invaluable knowledge of electrochemical systems. I also thank Dr. Chris Williams for the use of his Raman system. I am thankful for the help of Dr. John Staser, for without his expertise I would still be stuck trying to obtain cyclic voltammetry data from the wrong range. I thank Nistha Srivastava and Randall Feenstra from the department of physics at

Carnegie Mellon University for STS measurements and data interpretation. I would also like to thank Dr. Ulrich Starke and Camilla Coletti for ARPES measurements.

I thank Dr. Kurt Gaskill and Dr. Chip Eddy Jr. for the wonderful research experience at the Naval Research Laboratory after obtaining my Bachlors'. It was here I learned about the fabrication of graphene, making the transition to the material system in graduate school seamless.

I would like to thank SREB, SEAGEP and AAPP for their financial support throughout my graduate study. I sincerely thank Dr. John McFadden, AAPP Director and Ms. Rhittie Gettone, AAPP/SEAGEP Coordinator for providing what I and many in the program would call a loving support system, providing an invaluable service to minority graduate students that I would be remise not to give my praise to one of the best programs at the university.

I am deeply grateful to my lab mates, mentors and mentees throughout the last eight years, Dr. Biplob Daas, Dr. Tawhid Rana, Dr. Haizheng Song, Shamaita Shetu, Sabih Omar, Gabriel Brown, Dr. Iftekhar Chowdhury, Robert Kennedy, Zegilor Laney, Akeem Obe, Dr. Alexander Grekov, Dr. Peter Muzykov, Dr. Alex Bolotnikov, Dr. Eugene Toupitsyn, Dr. Amitesh Shrivastava, Chris Morgan for their endless support and discussions and for providing amazing work and life experiences. Many of my most memorable times at the university are thanks to these amazing individuals and I would hope to remain friends and collaborators with them in the future.

Lastly but not least I would like to thank my family for their endless emotional and spiritual support. My father (Marvin Daniels) and mother (Mary Ellen Daniels) for their constant support, the daily phone calls seeing how my day was going, the home

cooked meals and the sacrifices they have made throughout my life to give me this opportunity. My sister (Allison P. Gadsden) and brother (Marvin Edward Walter Daniels Jr.) for the games played on Xbox Live to help me unwind after barrage of work and the all-nighters spent to reach this point in my life. I would also like to thank my fiancée, Jenny Lee Afkinich for supporting me throughout my studies.

Kevin Michael Daniels

December 2013, Columbia, SC USA

ABSTRACT

Microbial fuel cells (MFCs) are seen as a promising complementary technology to alleviate the exponentially increasing worldwide energy demand. MFCs use bacteria to extract energy from biomass, where choice of electrode materials has a strong impact on energy extraction and efficiency. Graphene, a single monolayer of carbon with exceptional electrical conductivity and high surface area, is seen as a promising material with the potential of improving charge transfer and bacterial adhesion. To probe this reactivity, a novel means of hydrogenation of graphene by electrochemistry is demonstrated.

In this thesis, electrochemical hydrogenation of epitaxial graphene (EG), graphene grown on silicon carbide (SiC), shows new pathways of carbon chemistries for electrodes and hydrogen storage. The difficulty with reacting hydrogen with graphene is the need for atomic hydrogen, as hydrogen gas, H2, does not react directly with carbon. H+ ions in acidic electrolyte readily react with negatively biased graphene, revealing the reactivity of graphene and forming localized insulator-like states. Incorporating hydrogen into graphene, forming graphane, has also been shown as a means to create an engineered bandgap in semi-metal graphene, from ~0-3.5eV, allowing for traditional device architectures. This hydrogenation was shown to be thermally and electrochemically reversible, ideal for batteries and fuel cells, and history dependent, impacting H loading.

An electrochemical impedance model was developed for the electrochemical cell, with reactivity of graphene shown to be strongly dependent on defect density, edges, grain boundaries and point defects in the material, impacting the degree of hydrogenation. Addition of metal catalysts was shown as a means to overcome electrochemical hydrogenation defect dependence by lowering activation potential and offering additional pathways for hydrogen to adsorb.

Lastly, the biocompatibility of bacteria on graphene was confirmed by fluorescence confocal microscopy. Bacterial sensing by graphene demonstrated, with the ability to monitor bacterial activity through changes in EG electrical conductivity, allowing for its use as sensitive, real-time sensor for detecting biological activity. With biocompatibility established, graphene, as well as other carbon materials can be investigated by electrochemistry for optimization of MFCs.

TABLE OF CONTENTS

LIST OF TABLES

LIST OF FIGURES

LIST OF SYMBOLS

e	Electron charge (1.6×10^{-19} C)
Å	Angstrom (10^{-10})
n	Number of graphene monolayers (ML)
ML	Monolayers
E_F	Fermi energy
n_s	Sheet carrier density
μ	Mobility (cm^2/Vs)
m	Fluorescent slope
s	Normalized fluorescent slope
$E(t)$	Potential (E) as a function of time (t)
E_o	Signal amplitude
f	Frequency
t	Time
$I(t)$	Current (I) as a function of time (t)
I_o	Current amplitude
φ	Phase
Z	Impedance
R_s	Solution resistance
C_{dl_CPE}	Double layer capacitance
R_{ct}	Charge transfer resistance

R_{ad}	Adsorption resistance
C_{ad}	Adsorption capacitance
R_r	Resistance non-idealities
R_{cat}	Resistance non-idealities
C_r	Capacitance non-idealities
C_{cat}	Capacitance non-idealities.
F	Farad
Ω	Resistance
k	Wave vector
K	Boltzmann Constant
n_d	Defect density

LIST OF ABBREVIATIONS

AFM ..... Atomic Force Microscopy

Au ..... Gold

CMP ..... Chemical Mechanical Polish

CNT ..... Carbon Nanotube

CPE ..... Constant Phase Element

CV ..... Cyclic Voltammetry

CVD ..... Chemical Vapor Deposition

DAPI ..... 4',6-diamidino-2-phenylindole

DI ..... De-ionized

E-beam ..... Electron Beam

E-k ..... Energy-momentum

EG ..... Epitaxial Graphene

EIS ..... Electrochemical Impedance Spectroscopy

ELISA ..... Enzyme-Linked Immunosorbent Assay

EPS ..... Extracellular Polymers

FTIC ..... Fluorescein isothiocyanate

FTIR ..... Fourier Transform Infrared Spectroscopy

FWHM ..... Full Width Half Maximum

H^+ ..... Hydrogen Ions

H_2SO_4 ..... Sulfuric Acid

$HClO_4$ ..... Perchloric Acid

HSQ ..... Hydrogen silsesquioxane

IR ..... Infrared

MFC ..... Microbial Fuel Cell

SiC ..... Silicon Carbide

PEM ..... Proton Exchange Membrane

PCR ..... Polymerase Chain Reaction

Pt ..... Platinum

STM ..... Scanning Tunneling Microscopy

STS ..... Scanning Tunneling Spectroscopy

TCE ..... Trichloroethylene

UHV ..... Ultra High Vacuum

UV ..... Ultraviolet

XPS ..... X-ray Photoelectron Spectroscopy

CHAPTER 1

INTRODUCTION

In this chapter, the motivations, background and objectives of this research, titled, "***Influence of Defects in Epitaxial Graphene: Towards Graphene Based Microbial Fuel Cells***" are presented. This work looks at the reactivity and biocompatibility of graphene, towards the application of microbial fuel cells. Microbial fuel cells are seen as a promising complementary technology to alleviate the exponentially increasing global energy demand. MFCs use bacteria to extract energy from biomass, where choice of electrode materials has a strong impact on energy extraction and efficiency. Graphene has the potential of improving charge transfer with high surface area for improved bacterial adhesion. To probe this reactivity, a novel means of hydrogenation of graphene by electrochemistry is demonstrated. Incorporation of hydrogen into graphene transforms the material into graphane, forming a bandgap in the material and transforming semi-metal graphene into an insulator with further implications of hydrogen storage and atomic device engineering. Finally, the biocompatibility of epitaxial graphene is demonstrated, with the realization of a real-time bacteria sensor based on electrical resistance response. Presented in this chapter are major contributions of this work, the organization of this thesis and presentations and publications by the author.

1.1. BACKGROUND

Fossil fuels such as coal, oil and natural gas are unsustainable energy sources, further pushing the need for renewable resources such as wind, solar, geothermal and obtaining energy from biomass [1 2]. Biomass can be used to produce biofuels through direct combustion, though this is not ideal as the efficiency is low at 30% and its combustion results in higher carbon dioxide (CO_2) emissions than fossil fuels [3]. The burning of fossil fuels results in the emission of CO_2, which causes environmental problems such as global warming.

Microbial Fuel Cells (MFCs) use microorganisms to break down and use the energy stored in biomass to generate electricity, which serves a dual purpose: power generation and waste remediation [4-6]. The efficiency of MFCs to use the energy stored in biomass has been shown to be greater than 90% [4,7] due to no thermal losses. MFCs are also able to generate electricity with zero net carbon emission, and are an ideal alternative energy source since biomass is a renewable resource. Currently, however, MFCs are limited by their low power density and high cost compared to traditional energy sources, limiting practical uses for this device [4].

MFCs consist of two electrodes, an anode and a cathode housed in separate chambers separated by a proton exchange membrane (PEM) as shown in Figure 1.1 [4,8]. On the anode side, the anode, bacteria and biomass are held in an anaerobic or oxygenless chamber. The bacteria oxidize the biomass, generating electrons and protons. With the chamber being free of oxygen, the electrons are collected by the anode and sent to the cathode by a resistance load outside the cell. The protons enter into the cathode's

aerobic or oxygenful chamber by way of PEM where they combine with oxygen to form harmless water. Electricity is generated by taking away much easier respiration pathways for bacteria to unload electrons and protons gained from the biodegradation of biomass, such as oxygen and other acceptors. This forces bacteria to share electrons and protons to the anode and cathode respectively.

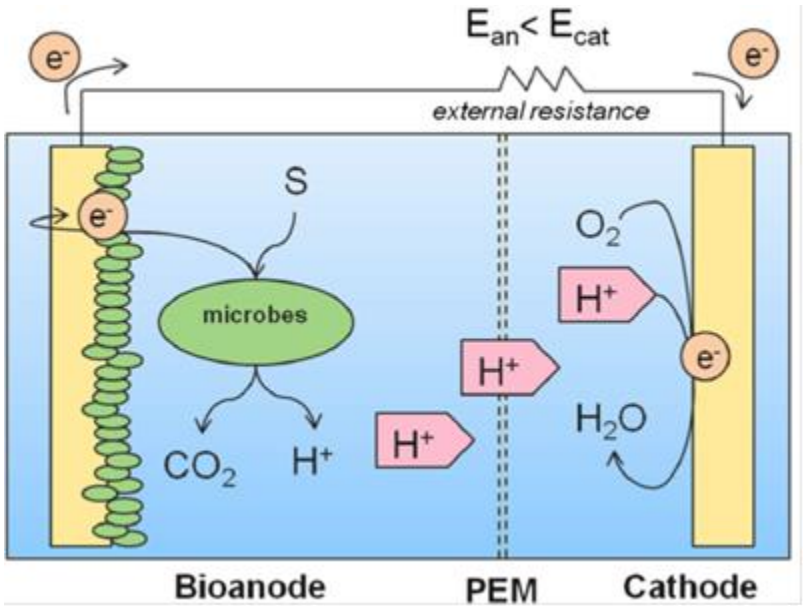

Figure 1.1. Schematic of typical microbial fuel cell

Before current can flow, activation overpotential or electron transfer overpotential must be overcome. This overpotential depends greatly on the material of the electrodes as well as the rate at which bacteria transfers electrons [8,9]. Increase in operating temperature [10] as well as the presence of mediating [11] and catalytic compounds can be used to overcome this overpotential. Other substantial losses occur in MFCs as shown in Figure 1.2, such as the addition of internal resistances of the MFC [9].

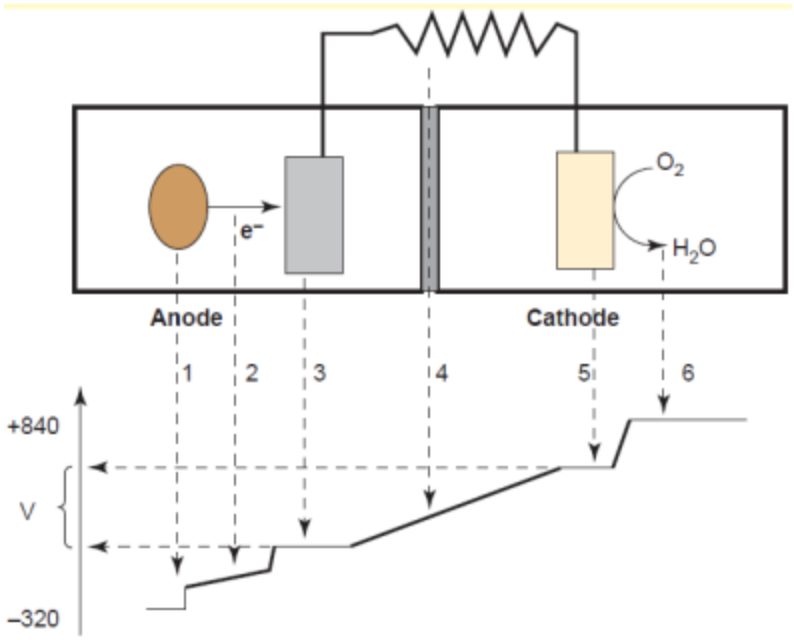

Figure 1.2. Potential losses in MFC. 1. Losses in bacteria electron transfer. 2. Losses in solution resistance. 3. Losses at anode. 4. Losses at PEM. 5. Losses at cathode. Losses at electron reduction.

Power density and cost are the two limiting factors of MFCs, both of which are governed by the materials used for electrodes [12]. For both anode and cathode electrodes, carbon materials appear to be the ideal choice, comparing performance and costs, as long as surface area is substantially large Currently, MFC's performance is governed by the low surface area of the electrodes, resulting in poor bacterial adhesion and low power density. .For achieving high power density, a planer structure with high surface area like graphene is an ideal material to minimize electrode distance and internal resistance while maximizing bacterial adhesion and charge transfer.

1.2. MOTIVATION

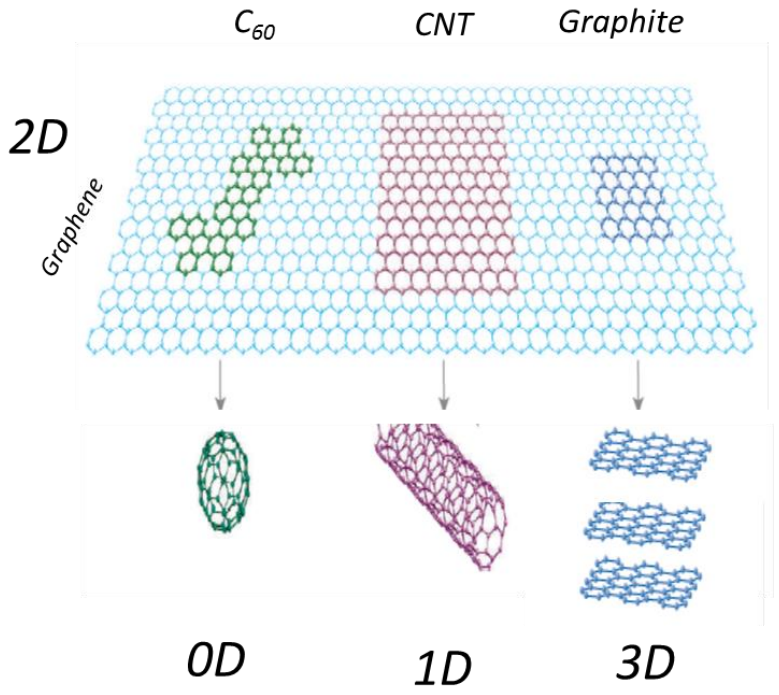

Figure 1.3: Diagram showing 2D graphene and other dimensional carbons

Graphene is a single atomic layer of carbon atoms arranged in a hexagonal lattice. Another way to look at this 2D carbon is as the planer version of 1D carbon nanotubes (CNT), 0D C_{60} buckyballs and a single layer of bulk 3D graphite [13] as shown in Figure 1.3. Because of this 2-dimensionality, graphene also has an exceptionally high surface area of 2630 m^2 g^{-1}, due to every atom in the layer being exposed to the environment. This is compared to bulk graphite which is much lower at <10 m^2 g^{-1} and CNT at half the surface area of graphene at 1315 m^2 g^{-1}[13]. Graphene also has high electrical and thermal conductivity, high room temperature mobility (>15,000 cm^2/V s)[14], high tensile strength due to the C-C bond, quasi-ballistic transport of carriers due to a linear

dispersion relation, where carriers move without mass in the material and low noise[14-17], these phenomenal characteristics of graphene have made it an appealing material for electrodes[18-23] ultra-sensitive sensors[24,25] and ultrafast logic switching [26].

To determine the reactivity of graphene as an electrode material in microbial fuel cells, we make the transition from biochemical to electrochemical processes. Complex biological systems are removed, so the purely electrochemical behaviors of the electrode are observed. A dilute acidic solution is used to maintain the proton chemistries observed in microbial fuel cells, where atomic hydrogen is attracted to a negatively biased electrode. In this thesis we demonstrate that incorporation of hydrogen into the graphene lattice is not only possible by electrochemistry but also electrochemically reversible, giving possibilities of not only inducing a substantial bandgap in the material, as supported by theory, but implications of graphene as a stable hydrogen storage medium.

1.3 Major Contribution of this thesis

The major contribution of this thesis are summarized as follows

I) Comprehensive literature review of the chemical and biological reactivity of graphene. We explore work in molecular absorption/adsorption and sensing on epitaxial graphene. Previous work in hydrogenation of graphene for hydrogen storage applications and bandgap engineering is then explored in detail. As most of these methods are in situ and require thermal annealing to desorb adsorbed hydrogen, an ex situ electrochemical means was developed as a less expensive and possibly reversible means of hydrogen incorporation into graphene.

II) A home-built electrochemical cell was designed and built to test hypothesis of hydrogen adsorption via electrochemistry. Positive hydrogen ions in dilute acidic solution are attracted to negatively biased EG where they are adsorbed and form C-H bonds with graphene.

III) Hydrogen adsorption by electrochemistry was proven by a detailed study using Raman spectroscopy, Atomic Force Microscopy (AFM) and Scanning Tunneling Spectroscopy (STS). Increases in sp^3 content, adsorption of hydrogen on the π-bonds of sp^2 bonded graphene, was observed by increases in D peak intensity in the Raman spectra and a fluorescence background was observed in hydrogenated material, which is only observed in hydrocarbons. Stress and strain caused by changes in C-C bond length, from 1.42 Å to 1.54 Å, was observed not only by peak shifts in the Raman spectra but strain in the graphene layer observed by AFM. Evidence of localized states was also observed by STS, revealing that hydrogenation is not continuous throughout the layer but in clusters. Possible substrate/sample dependence was also observed.

IV) To overcome this substrate/sample dependence, catalytic metals, Gold (Au) and Platinum (Pt) were deposited on the surface to serve the following purposes:

i) Decrease the activation energy required to form C-H bonds

ii) Offer a different, easier pathway for hydrogen to react, where hydrogen can dissociate and adsorb on graphene

Concentration of hydrogen adsorbed on graphene increased beyond that of hydrogenated EG without catalyst. Samples with gold nanoparticles were shown

to have higher hydrogen adsorption than those with platinum nanoparticles despite having lower catalytic activity than Pt by two orders of magnitude. This could simply be due to nanoparticles adhesion or size during hydrogenation.

V) Hydrogen desorption from electrochemically hydrogenated samples was demonstrated, proving hydrogenation of graphene over damage. Electrochemical reversibility was shown, revealing history dependence and lattice strain after each cycle as observed by Raman.

VI) Mechanism of hydrogen adsorption of epitaxial graphene was observed to be dependent on defects in EG as observed by cyclic voltammetry, electrochemical impedance spectroscopy and Raman.

VII) Impedance model of electrochemical cell was derived from EIS measurements.

VIII) Biocompatibility of epitaxial graphene demonstrated by fluorescence confocal microscopy. EG bacteria sensor was fabricated with sensor responding electrically in real-time with bacteria and biofilm growth via changes in material resistance.

1.4 Organization of Thesis

The reactivity and biocompatibility of epitaxial graphene will be discussed over the next six chapters, towards its application in microbial fuel cells. Theory and comprehensive literature review of the chemical reactivity of graphene and the kinetics behind molecule adsorption and sensing are presented in Chapter 2. Chapter 3 demonstrates a novel means of incorporating hydrogen into graphene electrochemically

where hydrogen ions, from an dilute acidic solution, are attracted to negatively biased epitaxial graphene on semi-insulating SiC, forming a hydrocarbon . Chapter 4 expands on this by enhancing hydrogen adsorption by adding catalytic metals to graphene to lower the activation energy necessary to form C-H bonds as well as add additional sites for hydrogen to adsorb and spillover onto graphene. Chapter 5 investigates reversibility of electrochemical hydrogen adsorption by thermal anneal and demonstrates electrochemical cycling of hydrogen by potential reversal. In Chapter 6, the mechanism of electrochemical hydrogenation of graphene is investigated by cyclic voltammetry and electrochemical impedance spectroscopy, demonstrating a clear dependence on defect density of graphene with hydrogen adsorption and reactivity. In Chapter 7, the biocompatibility of graphene is demonstrated in the form of a real-time bacteria bio-sensor measuring the change in conductivity of graphene in response to bacterial activity. Finally, chapter 8 summarizes the results observed in the dissertation and future prospects for additional development graphene as an all-purpose platform for material tuning and sensing.

1.5 PUBLICATIONS AND PRESENTATIONS

The following are publications and presentations resulting from research conducted at the University of South Carolina in the area of graphene technology. Items pertaining to research presented in this work are marked with (*) preceding

Publications (12 Journal [4 First Author], 4 conference papers [2 First Author])

1. ***Kevin M. Daniels**, A. Obe, B. K. Daas, J. Weidner, C. Williams, T. S. Sudarshan, MVS Chandrashekhar,"Metal Catalyzed Electrochemical Formation of Graphane" **[Full Manuscript in Preparation]**

2. ***Kevin M. Daniels**, S. Shetu, J. Staser, J. W. Weidner, C. Williams, T. S. Sudarshan, MVS Chandrashekhar., "Mechanisms of Electrochemical Hydrogenation of Epitaxial Graphene: Roles of Defects" [**Full Manuscript in Preparation**]

3. ***Kevin M. Daniels**, N. Aich, K. P. Miller, B. K. Daas, N. Saleh, A. W. Decho, T. S. Sudarshan, MVS Chandrashekhar "Real-Time Sensing of *E.coli* biofilm Growth Using Epitaxial Graphene ", *Sensors, 2013 IEEE*, pp. XX-XX (2013)

4. ***Kevin M. Daniels**, S. Shetu, J. Staser, J. W. Weidner, C. Williams, T. S. Sudarshan, MVS Chandrashekhar., "Electrochemical Hydrogenation of Dimensional Carbon" ECS Transactions. Vol. 58 (4). 439-445 (2013)

5. ***Kevin M. Daniels**, B. K. Daas, N. Srivastava, C. Williams, R. M. Feenstra, T. S. Sudarshan, MVS Chandrashekhar "Evidences of electrochemical graphene functionalization and substrate dependence by Raman and scanning tunneling spectroscopies" Journal of Appl. Phys. Vol 111, 114306 (2012)

6. ***Kevin M. Daniels**, B. K. Daas, N. Srivastava, C. Williams, R. M. Feenstra, T. S. Sudarshan, MVS Chandrashekhar "Evidence of Electrochemical Graphene Functionalization by Raman Spectroscopy" Mater. Sci. Vol. 717-720 661-664 (2012)

7. C. Coletti, S. Forti, A. Principi, K.V. Emtsev, A.A. Zakharov, **K.M. Daniels**, B.K. Daas, M.V.S. Chandrashekhar, T. Ouisse, D. Chaussende, A. H. MacDonald, M. Polini, U. Starke, "Revealing the electronic band structure of trilayer graphene on SiC" Phys. Rev. B 88, 155439 (2013)

8. S. S. Shetu, S. Omar, **K. Daniels**, B. Daas, J. Andrews, S. Ma, T. S. Sudarshan., "Si-adatom kinetics in defect mediated growth of multilayer epitaxial graphene films on 6H-SiC" accepted Journal of Applied Physics (2013)

9. B. K. Daas, **K. M. Daniels**, S. Shetu, T.S. Sudarshan, M.V.S. Chandrashekhar "Epitaxial Graphene Growth on non polar SiC faces" Mater. Sci. Vol. 717-720 633-636 (2012)

10. B. K. Daas, W. K. Nomani, **K. M. Daniels**, T. S. Sudarshan, G. Koley and MVS Chandrashekhar "Molecular Gas Adsorption Induced Carrier Transport Studies of Epitaxial Graphene using Polariton Enhanced IR Reflection Spectroscopy", Mater. Sci. Vol. 717-720 665-668 (2012)

11. B. K. Daas, O. Sabih, S. Shetu, **K. M. Daniels**, S. Ma, T. S. Sudarshan, MVS Chandrashekhar "Comparison of epitaxial graphene growth on polar and non-polar 6H-SiC faces: On the growth of multilayer films" Journal of Crystal Growth and Design. 12 Vol 7, 3379-3387 (2012)

12. B. K. Daas, **K. M. Daniels**, T. S. Sudarshan and M.V.S. Chandrashekhar "Polariton Enhanced IR Reflection Spectra of Epitaxial Graphene on SiC" Vir. J. Nan. Sci. & Tech. Volume 25 Issue 1 (2012)

13. B. K. Daas, **K. M. Daniels**, T.S. Sudarshan and M.V.S. Chandrashekhar "Polariton Enhanced IR Reflection Spectra of Epitaxial Graphene on SiC" Journal of Appl. Phys. Vol. 110, Issue 11 ,113114 (2011)

14. J. L. Tedesco, G. G. Jernigan, J. C. Culbertson, J. K. Hite, Y. Yang, **K. M. Daniels**, R. L. Myers-Ward, C. R. Eddy, Jr., J. A. Robinson, K. A. Trumbull, M. T. Wetherington, P. M. Campbell, and D. K. Gaskill "Morphology characterization of argon-mediated epitaxial graphene on C-face SiC" Appl. Phy. Lett. 96, 222103 (2010)

15. D. J. Meyer, R. Bass, D. S. Katzer, D. A. Deen, S. C. Binary, **K. M. Daniels**, C. R. Eddy Jr "Self-aligned ALD AlO_x T-gate insulator for gate leakage current suppression in SiN_x passivated AlGaN/GaN HEMTs" Solid-State Electronics 54, 1098-1104 (2010)

Presentations (6 oral presentations, 2 poster presentations)

1. ***Kevin M. Daniels**, N. Aich, K. P. Miller, B. K. Daas, N. Saleh, A. W. Decho, T. S. Sudarshan, MVS Chandrashekhar "Real-Time Sensing of *E.coli* biofilm Growth Using Epitaxial Graphene ", IEEE Sensors, Baltimore, MD (2013)

2. ***Kevin M. Daniels**, S. Shetu, J. Staser, J. W. Weidner, C. Williams, T. S. Sudarshan, MVS Chandrashekhar, "Electrochemical Hydrogenation of Dimensional Carbon", 244th ECS Meeting, San Francisco , CA (2013)

3. ***Kevin M. Daniels**, S. Shetu, J. Staser, J. W. Weidner, C. Williams, T. S. Sudarshan, MVS Chandrashekhar, "History Dependence of Reversible Electrochemical Hydrogenation of Epitaxial Graphene/SiC", 244th ECS Meeting, San Francisco , CA (2013)

4. ***Kevin M. Daniels**, N. Aich, K. P. Miller, B. K. Daas, N. Saleh, A. W. Decho, T. S. Sudarshan, MVS Chandrashekhar "Biological Sensing Applications of Epitaxial Graphene". Electronic Material Conference (2012)

5. ***Kevin M. Daniels**, B. K. Daas, N. Srivastava, C. Williams, R. M. Feenstra, T.S. Sudarshan, MVS Chandrashekhar "Evidence of Electrochemical Graphene Functionalization by Raman and Scanning Tunneling Spectroscopy ", ICSCRM Conference, Cleveland, OH (2011)

6. ***Kevin M. Daniels**, B. K. Daas, R. Zhang, J. Weidner, C. Williams, T.S. Sudarshan, MVS Chandrashekhar "Electrochemical Graphane Conversion using

E-beam Evaporated Metals for Catalytic Enhancement ” Electronic Material conference, Santa Barbara, CA (2011)

7. ***Kevin M. Daniels**, B. K. Daas, R. Zhang, J. Weidner, C. Williams, T.S. Sudarshan, MVS Chandrashekhar” Graphene to Graphane: Novel Electrochemical Conversion and Possible Applications” Electronic Material conference, Notre Dame (2010)

8. **Kevin. M. Daniels**, Z. Laney, F. Zhao, T. S. Sudarshan. “A Novel Etching Technique for Crystallographic Study of SiC Materials” ISDRS, University of Maryland (2009)

REFERENCES

[1] M.Zhou et al., Journal of Chemical Technology & Biotechnology 88.4, 508-518 (2013)

[2] R. S. Dhillon and G. von Wuehlisch., Biomass and Bioenergy 48, 75-89 (2013)

[3] P. McKendry., Bioresource Technology 83.1, 37-46 (2002)

[4] Z. Du, H. Li and T. Gu., Biotechnology Advances 25.5, 464-482 (2007)

[5] D. Jiang and B. Li., Biochemical Engineering Journal 47.1–3, 31-37 (2009)

[6] Feng et. al., Journal of Power Sources 195.7, 1841-1844 (2010)

[7] D. R. Lovley and K. P. Nevin., "Electricity Production with Electricigens." (2008): 295–306.

[8] A. ElMekawy et al. Bioresource Technology 142, 672-682 (2013)

[9] K. Rabaey and W. Verstraete., Trends in Biotechnology 23.6, 291-298 (2005)

[10] V.B. Oliveira et al., Biochemical Engineering Journal 73, 53-64 (2013)

[11] D.R. Lovely., Nature Reviews Microbiology 4.7 497-508 (2006)

[12] B.E. Logan., Nature Reviews Microbiology 7.5, 375-381 (2009)

[13] A. C. Brownson and C. E. Banks., Analyst 135, 2768-2778 (2010)

[14] A.K. Geim, K.S. Novoselov, Materials Science 6, 183-191 (2007)

[15] W.A de Heer, C. Berger, X. Wu, P. N. First, E. H. Conrad, X. Li, T. Li, M. Sprinkle, J. Hass, M. L. Sadowski, M. Potemski, G. Martinez, Solid State Communications 143 (2007) 92-100

[16] A.H. Castro Neto, F. Guiena, N.M.R. Peres, K.S. Novoselov, A.K. Geim., Rev. Mod. Phys. 81, 109-162 (2009)

[17] J. L. Tedesco, B. L. VanMil, R. L. Myers-Ward, J. M. McCrate, S. A. Kitt, P. M. Campbell, G. G. Jernigan, J. C. Culbertson, C. R. Eddy, D. K. Gaskill., Applied Physics Letters 12, 122102-122102-3(2009)

[18] Y. Zhang et al., Journal of Power Sources 239, 169-174 (2011),

[19] H. Choi et. al., Nano Energy 1.4, 534-551 (2012)

[20] Z. He et al., Nano Letters 12.9, 4738-4741 (2012)

[21] J. Liu et al, Bioresource Technology 144, 275-280 (2012)

[22] J. Hou, Z. Liu and P. Zhang., Journal of Power Sources 224, 139-144(2013)

[23] L. Xiao et al., Journal of Power Sources208, 187-192 (2012)

[24] F. Schedin et. al., Nature Mat. 6, 652-655 (2007)

[25] B. K. Daas, W. K. Nomani, K. M. Daniels, T. S. Sudarshan, G. Koley and MVS Chandrashekhar., Mater. Sci. Vol. 717-720 665-668 (2012)

[26] L. Liao et. al. Nature, vol. 467, 305-308, 2010

CHAPTER 2

REACTIVITY OF GRAPHENE

Graphene has a linear dispersion relation where the conduction and valance band meet, as shown in the E-k diagram in Figure 2.1(i). Consequently, intrinsic graphene is a semi-metal with zero/near zero bandgap [1]. Unlike semiconductors like silicon, which require energy for carriers to jump from the valence to the conduction allowing logic switches like transistors to turn off and stop conducting. Graphene always conducts due to band to band tunneling resulting in very small on/off ratio, despite being capable of reaching speeds up to 300GHz [2]. A low on/off ratio makes it increasingly difficult to determine state changes [1]. Having a device always conducting is not only energy inefficient but generates unnecessary heat for systems. With this a major issue with graphene devices, researchers have investigated a few ways of creating a bandgap in graphene.

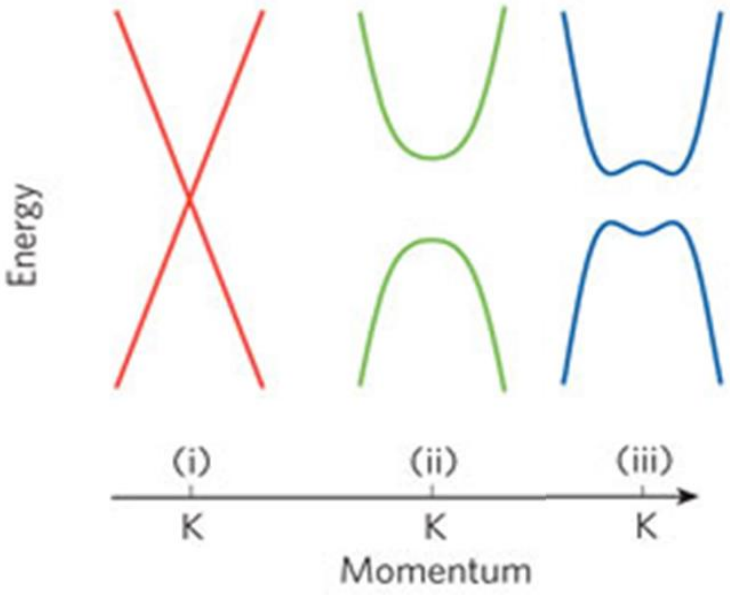

Figure 2.1: E-k diagram of monolayer graphene, graphene nanoribbon and bilayer graphene

One method of creating a bandgap in graphene is the formation of graphene nanoribbons. The bandgap is dependent on the width and crystallographic orientation of the nanoribbion is formed due to carrier confinement, similar to carbon nanotubes. As shown in Figure 2.1 (ii) the E-k diagram becomes parabolic with a bandgap of around 0.25eV [3]. Bilayer and trilayer graphene also create a bandgap as shown in Figure 2.1 (iii), which is formed by stain between the two layers (AB Bernel Stacking) [4]. With strain being the key to opening a bandgap in the material, reacting graphene with atoms and molecules to apply strain to the layer is investigated.

2.1: REACTIVITY OF GRAPHENE

In graphene and graphite, carbon atoms are sp^2 hybridized, which means that three electrons form σ-bonds with neighboring carbon atoms and the fourth bond, a π-bond, where electrons can freely travel. This accounts for graphene's high electrical

conductivity [1]. Graphene and graphite consist of two planes, basal plane which is perpendicular to the π-bond network and edge plane consisting of dangling σ-bonds as shown in Figure 2.2. Unlike graphite, graphene has an exceptionally high surface area, with the entire monolayer of carbon atoms exposed to chemical reactants. In the absence of π- π interaction from other graphitic layers, graphene has the affinity for chemically induced changes, of which are not stable in the presence of bulk due to necessary deformation of the layer [5].

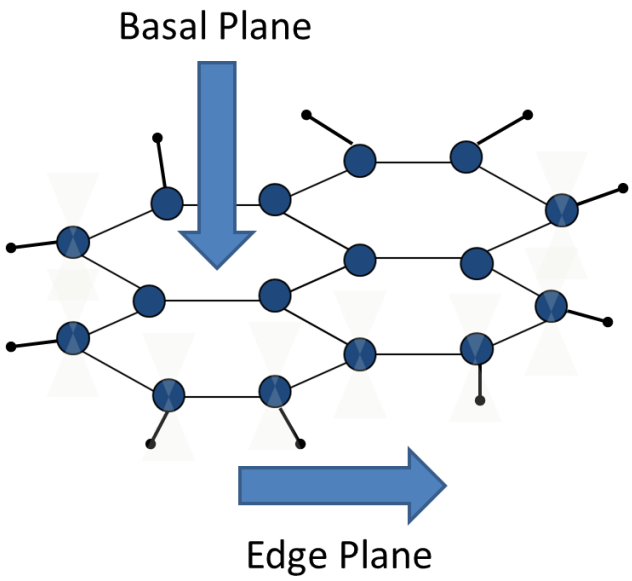

Figure 2.2: Diagram showing inert basal and reactive edge plane of graphene/graphite

Other potential factors influencing the reactivity: a) The presence of ripples and curvature of the graphene surface in graphene [5,6], which are not present in graphite and b) electron-hole puddles from surface impurities leading to local enhancement of chemical reactivity in the basal plane. Defects could also be a major contributor for

enhanced reactivity, as more dangling bonds, like those found on the edge plane of graphene, present in these areas provide more sites for reactions to occur [7]. Finally, varying the stacking of graphene from Bernal AB stacking (as in Si-Face growth) to turbostratic (as in C-face growth) [8] could also influence reactivity.

Bulk graphite has been observed to be chemically inert compared to graphene. Sharma et. al. demonstrated graphene's enhanced chemical reactivity by functionalizing it with 4-nitrobenzene diazonium tetrafluoroborate on a single monolayer, bi-layer and bulk graphite as shown in Figure 2.3. This showed that a single monolayer of graphene is not only more reactive than bulk graphite, but up to ten times more reactive than even a bi-layer of graphene. The extent of the reactivity of graphene was quantified by an increase in graphene's Raman D peak (~1350 cm^{-1}) resulting in a higher I(D)/I(G) ratio after functionalization [7], where the G peak is graphene's intrinsic G peak (1580 cm^{-1}) and I(D) and I(G) refers to the amplitude of the D peak and G peak respectively. The D peak corresponds to disorder while the G peak corresponds to lattice vibrations. Raman spectroscopy of graphene and functionalized graphene will be covered in more detail in Chapter 3.

The enhanced reactivity was attributed to substrate induced electron transfer between the substrate and graphene, leading to a shift in the energetics of the graphene layer compared to bulk graphite, and consequently affecting the reactivity. Since the electrostatic screening length in graphene is ~1 monolayer (ML), only the first layer exhibits this enhanced reactivity [7, 9]. This first monolayer experiences potential fluctuations from external impurity charges while subsequent graphene layers are electrically neutral, exhibiting the reactivity of bulk graphite. With the reactivity of

graphene established, it is necessary to look at the two methods of interaction atoms and molecules have with graphene, physisorption and chemisorption.

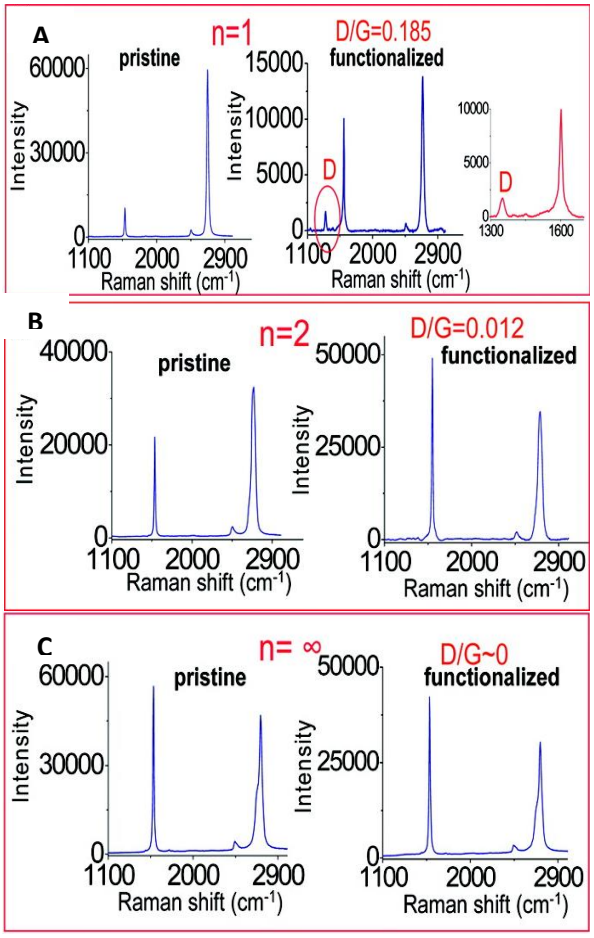

Figure 2.3: Graphene functionalization and Raman spectroscopy by Sharma et. al showing layer dependent reactivity of graphene [7]

2.2: PHYSISORPTION ON GRAPHENE

Physisorption involves basic attraction of atoms or molecules caused by van der Waals forces where the binding energy is relatively weak compared to covalent bonds. In this manner, molecules arrange themselves randomly and apply negligible strain on the material. Graphene, being all surface, is an ideal candidate for the sensing of molecules.

Schedin et. al was able to show single molecule detection based on conductivity changes in the presence of gas molecules [10]. This was due to graphene's high conductivity, low noise, and few crystal defects allowing detection of molecules in concentrations as small as 1ppb. These molecules act as donors/acceptors on graphene, showing significant changes in carrier concentration as shown in Figure 2.4.

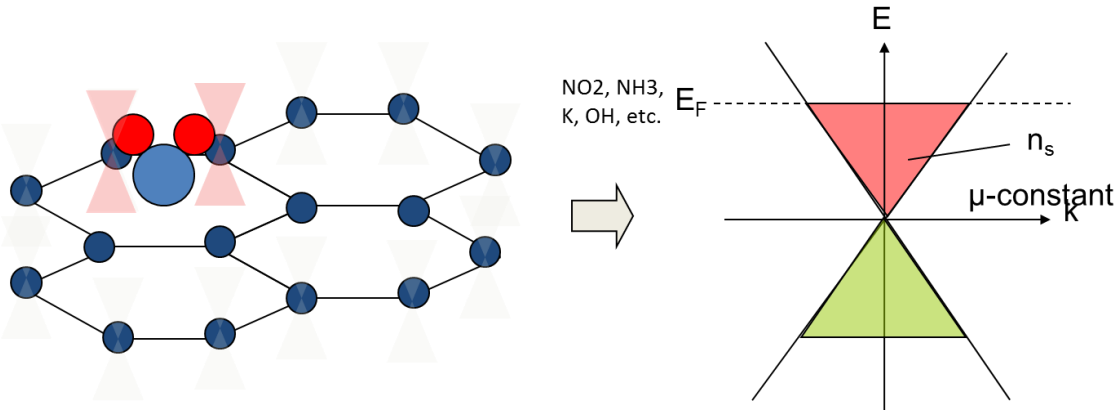

Figure 2.4. Physisorbed species on graphene resulting in conductivity change

This was also shown by Daas et. al where FTIR reflection measurements on epitaxial graphene were conducted in gas environments. NO_2 and NH_3 were chosen as electron accepting and electron donating respectively with N_2 chosen as a control due to it being inert. He was able to observe conductivity changes as changes in reflectivity and confirm doping of the EG layer as shown in Figure 2.5 [11].

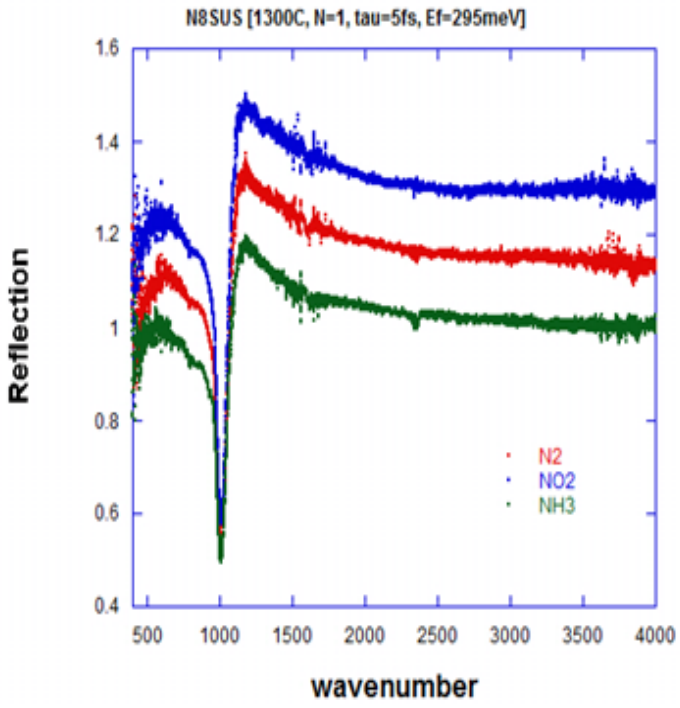

Figure 2.5: Gas adsorption experiment by Daas et. al showing change in conductivity in presence of donor/acceptor gases [11]

Biomolecules are partly governed by van der Waals forces for adhesion to surfaces within short distances to surfaces and are essentially charged macromolecules [12]. Exposing graphene to these molecules, one would expect to see conductivity changes within the material in the presence of even minute concentrations. Bacteria sensing using this principle will be discussed later in Chapter 7.

2.3: CHEMISORPTION ON GRAPHENE

Unlike physisorption, chemisorption involves chemical reactions, changing the electrical, chemical and optical properties of a material when ions/cations form covalent bonds with atoms in a crystal. This happens in a periodic, rather than a random nature as shown in physisorption and requires a certain input of energy in order to break bonds to

generate energetic ions to attach to the crystal as well as energy to break created bond. These ions bond to the conductive π-bonds in graphene, forming σ-bonds and converting material from sp^2 to sp^3; semi-metal to insulator as shown in Figure 2.6 [1].

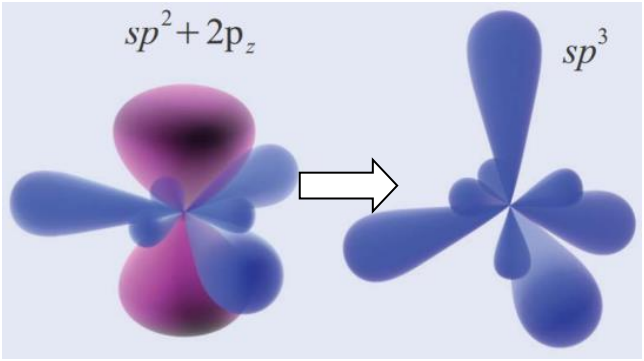

Figure 2.6. sp^2 to sp^3 bond transition

There are a few atoms/molecules that have been used to chemically modify graphene, both induces a wide bandgap into the material: one is fluorinated graphene F^- which is formed by obtaining atomic F by decomposition of xenon diffluoride [13], and the other, hydrogenated graphene, better known as graphane [5, 6, 14], where this work is focused.

2.4: GRAPHANE

Graphane was theoretically predicted in 2007 by Sofo by density functional theory (DFT) calculations [15], demonstrating the most energetically favorable configurations, the chair (3.5eV) and boat (3.7eV) , with the chair, shown in Figure 2.7, being the most stable configuration[15]. Transforming from sp^2 to a sp^3 configuration the C-C bond length of graphene was calculated to be 1.52Å, which is larger than that of pristine graphene at 1.42Å and much closer to insulating diamond 1.53Å. Since, graphane has been synthesized by a number of means [5, 6, 14]. The difficulty with

functionalizing graphene with hydrogen is the need for atomic hydrogen, since hydrogen gas H_2 does not directly react with carbon.

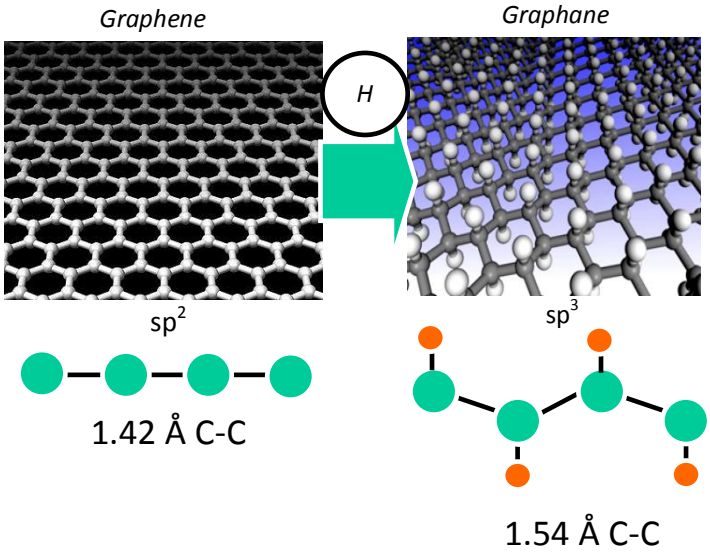

Figure 2.7: Diagram of lattice changes from graphene functionalization with atomic hydrogen

2.4.1: GRAPHANE SYNTHESIS

As H_2 does not react with carbon in its molecular state, techniques for generating atomic hydrogen have been used for hydrogenating graphene. The first to demonstrate this, Elias et al, hydrogenated exfoliated graphene on SiO_2 and free standing graphene by generating atomic hydrogen by DC plasma. Low pressure hydrogen/argon mixture (10% hydrogen) was ignited between two aluminum electrodes 30 cm away from discharge zone for two hours. At this distance the chance of impact with energetic Ar^+ ions are minimized and it is reasonable to assume only H^+ ions reach the sample. After hydrogenation the samples were annealed at 450°C in Ar to remove bond hydrogen from graphene [15].

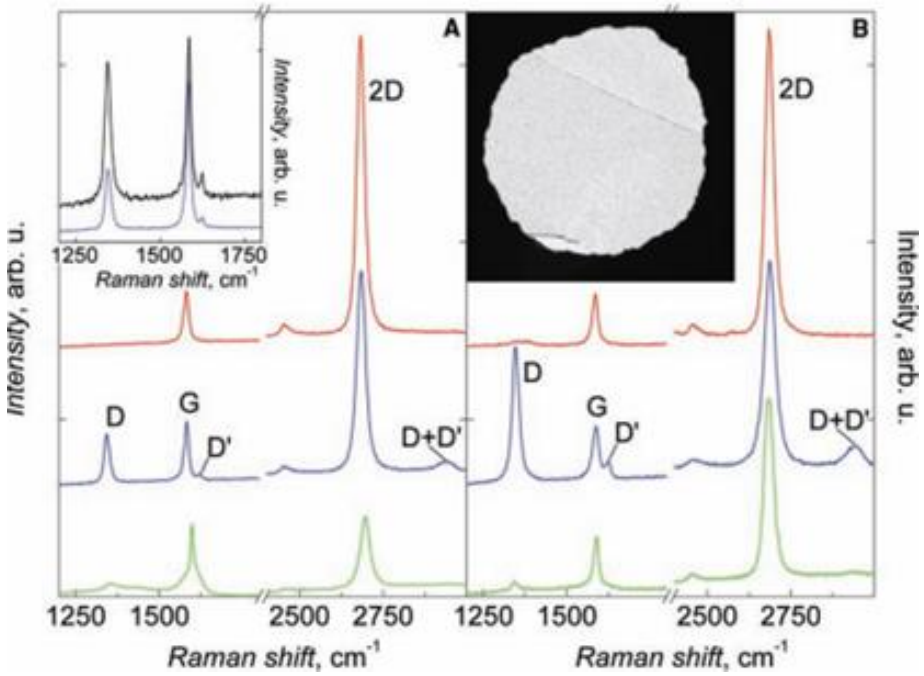

Figure 2.8. Raman spectra of pristine (Green), hydrogenated (Blue) and annealed (Red) graphene, **A** on SiO_2 and **B** free standing [15]

After hydrogenation, a sharp D peak appeared, much narrower than that seen in disordered carbon materials as shown in Figure 2.8. This further supports the formation of sp^3 bonds. This peak was also shown to be much higher for free standing graphene than graphene on SiO_2 as both sides were exposed to atomic hydrogen for free standing as opposed to a single side on SiO_2. Hall bars were fabricated on graphene showing a mobility of 14000cm^2/Vs before hydrogenation and 10cm^2/Vs after hydrogenation supporting the transition from semi-metal to insulator. After thermal, samples reverted back to graphene with desorption of hydrogen and mobility recovered to 3500 cm^{-2} [15]. Wojtaszek et al. observed similar changes in Raman spectroscopy hydrogenating graphene by reactive ion etching (RIE) plasma from Ar/H_2 gas as shown in Figure 2.9 [16].

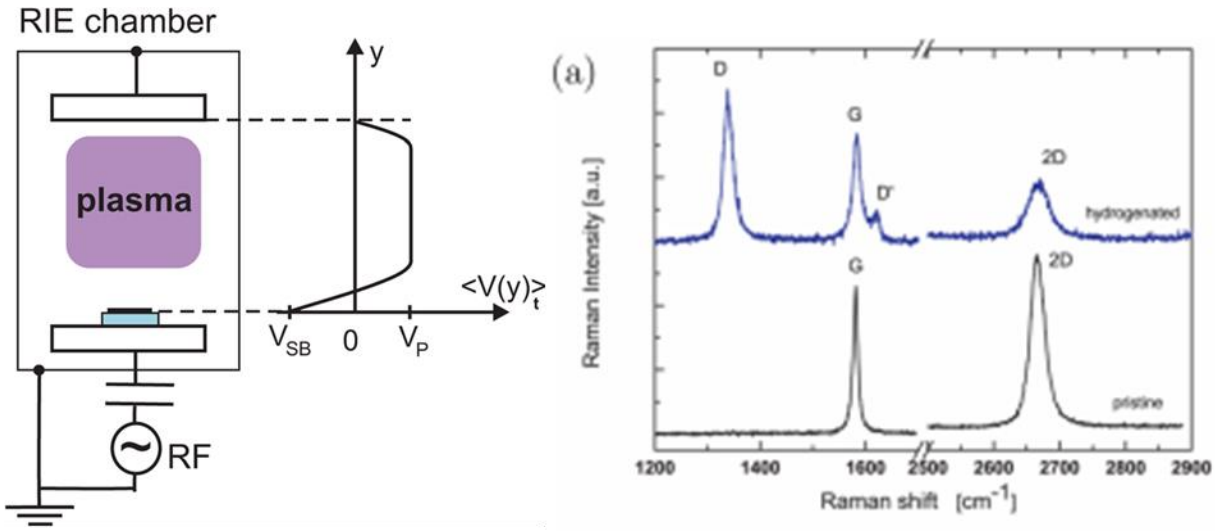

Figure 2.9. Graphane synthesis via reactive ion etching (RIE) plasma with Raman spectra showing pristine graphene and hydrogenated graphene [16]

Balog et al. employed a different approach by hydrogenating epitaxial graphene grown on the Si-face of SiC by a 1600 K D-atom beam (hot hydrogen beam) for 5 seconds at a flux of 10^{12}-10^{13} atoms/cm^2 [17]. In low dosages, hydrogenation was shown to be preferentially adsorbed along the 6 x 6 modulation on the SiC surface as shown in Figure 2.10. At high dosage, 90 second exposure, no preferential sites were observed. Hydrogen desorption was observed by an 800°C thermal anneal.

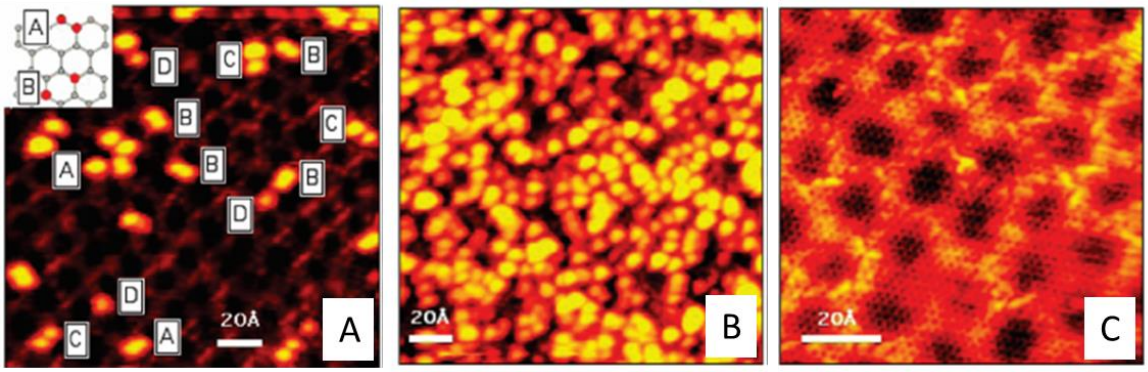

Figure 2.10. Scanning tunneling microscopy images of **A** preferential hydrogenation at low hydrogen dosage, **B** at high dosage showing no preferential sites and **C** thermal anneal at 800°C removing hydrogen from the graphene lattice [17]

Techniques implemented by other groups involve *in situ* development of atomic hydrogen by plasma-assistance which can cause damage due to energetic ions [6] or hot filaments [14], as the H-H bond in hydrogen gas requires high energy/temperature to break [6]. Others have hydrogenated graphene by electron-induced dissociation of hydrogen silsesquioxane (HSQ) [5].

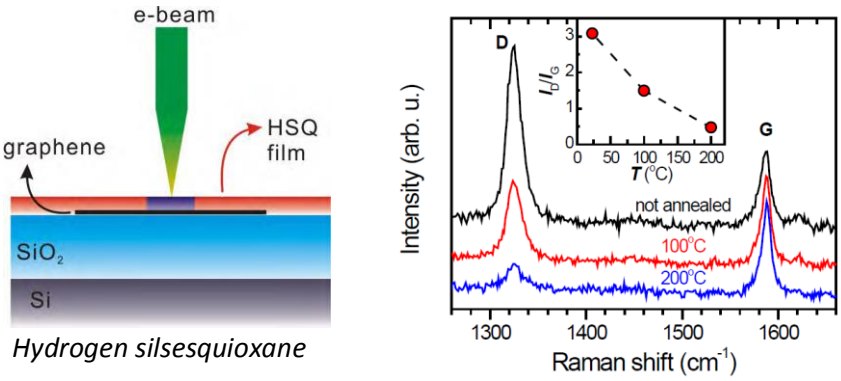

Figure 2.11: Experimental setup by Ryu et. al. of graphene formed by electron-induced dissociation of HSQ with resulting Raman spectra and thermal anneal [5]

Atomic hydrogen is formed in situ by breaking the H-Si bond of HSQ by e-beam, which diffuses to form covalent bonds with graphene. Large increase in D peak as observed in previous hydrogenation techniques signifies the formation of sp^3 and the formation of graphane, which was reversed by 200 °C thermal anneal as shown in Figure 2.11 with decrease in D peak [5]. Jones et. al hydrogenated exfoliated graphene from highly ordered pyrolitic graphite (HOPG) using a similar e-beam irradiation technique, but makes the claim that the few monolayers of H_2O on the surface was sufficient in producing graphene [18]. They observe, as shown in Figure 2.12, a narrow D peak with full-width half max (FWHM) of $20cm^{-1}$, which is an order of magnitude lower than that observed with disordered or nanocrystalline carbon with comparable I(D)/I(G) ratio. Hydrogen desorption was possible by a 590°C thermal anneal.

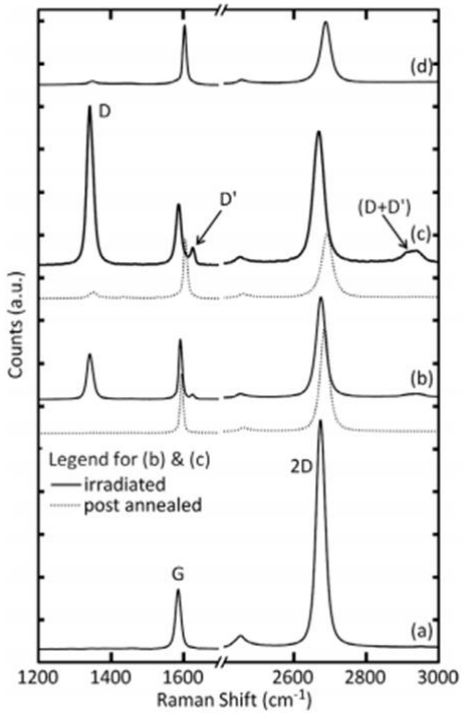

Figure 2.12. Raman spectra of graphene hydrogenated by electron irradiation of H_2O adsorbates on the surface and hydrogen desorption by 590°C thermal anneal [18]

From the literature review of graphane synthesis, confirmation of graphene hydrogenation centers around Raman spectroscopy and hydrogen desorption by high temperature thermal anneal. Formation of sp^3bonds were evident by large increases in D-peak position and deformation of the ideal graphene lattice, increases in C-C bond length with formation of C-H bond, manifested in the Raman spectra as a D' shoulder peak and introduction of a D + D' peak, or C-H peak. This process, in all cases, was shown to be thermally reversible by a wide range of temperatures (200°C, 450°C, 590°C and 800°C). Hydrogen desorption returns the material back to sp^2 bound carbon, with little residual damage observed by the process. With the limitations of current techniques to form graphane presented, notably the need for *in situ* synthesis under vacuum, an alternative, *ex situ* electrochemical [19] means is demonstrated.

REFERENCES

[1] Novoselov, K. S. Rev. Mod. Phys. 2011, 83 (3), 837−849

[2] L. Liao et. al. Nature, vol. 467, 305-308, 2010

[3] M. Y. Han, B. Ozyilmaz, Y. Zhang, P. Kim., PRL 98, 206805 (2007)

[4] B. Verberck, B. Partoens, F. M. Peeters and B. Trauzettel., Phys. Rev. B 85, 125403

[5] S. Ryu, M. Y. Han, J. Maultzsch. T. F. Heinz, P. Kim, M. L. Steigerwald and L. E. Brus., Nano Lett., Vol. 8, No. 12, 2008

[6] D. C. Elias, R. R. Nair, T. M. G. Mohiuddin, S. V. Morozov, P. Blake, M. P. Halsall, A. C. Ferrari, D. W. Boukhvalov, M. I. Katsnelson, A. K. Geim, K. S. Novoselov., Science 30, Vol. 323, No. 5914, 610-613 (2009)

[7] R. Sharma, J. H. Baik, C. J. Perera, M. S. Strano., Nano Letters 10, 398-405 (2010)

[8] R. Sprinkle, J. Hicks, A. Tejeda, A. Taleb-Ibrahimi, P. Le Fèvre, F. Bertran, H. Tinkey, M. C. Clark, P. Soukiassian, D. Martinotti, J. Hass and E. H. Conrad., J. Phys D : Appl. Phys. 43, 374006 (2010)

[9] Y. Lin and P. Avouris., Nano Lett. Vol. 8, No. 8 (2008)

[10] F. Schedin et. al., Nature Mat. 6, 652-655 (2007)

[11] B. K. Daas, W. K. Nomani, K. M. Daniels, T. S. Sudarshan, G. Koley and MVS Chandrashekhar., Mater. Sci. Vol. 717-720 665-668 (2012)

[12] S.K. Lower et. al Geochimica et Cosmochimica Acta, Vol. 64, No. 18, pp. 3133–3139, 2000

[13] Nair et. al., small 6, No.24, 2877-2884 b

[14] C. Riedl, C. Coletti, T. Iwasaki, A. A. Zakharov and U. Starke., PRL 103, 246804 (2009)

[15] Jorge O. Sofo, Ajay S. Chaudhari, Greg D. Barber., Physical Review B 75, 153401 (2007)

[16] M. Wojtaszek, N. Tombros, A. Caretta, P. H. M. van Loosdrecht, B. J. van Wess J. Appl. Phys. 110, 063715 (2011)

[17] R. Balog, B. Jørgensen, J. Wells, E. Lægsaard, P. Hofmann, F. Besenbacher, L. Hornekær., J. Am. Chem. Soc. 131, 8744-8755 (2009)

[18] J. D. Jones, K. K. Mahajan, W. H. Williams, P. A. Ecton, Y. Mo, J. M. Perez., Carbon 48, Issue 8, 2335-2340 (2010)

[19] K. M. Daniels, B. K. Daas, N. Srivastava, C. Willams, R. M. Feenstra, T. S. Sudarshan, MVS Chandrashekhar., J. Appl. Phys. 111, 114306 (2012)

CHAPTER 3

ELECTROCHEMICAL HYDROGENATION OF EPITAXIAL GRAPHENE

Electrochemistry offers the most controlled route to systematic hydrogenation, as the extent of the hydrogenation of graphene can be precisely controlled by changing the current level (or voltage) and time with the possibility of hydrogenation electrochemically reversible for further fine tuning. Such tunability is not easily achievable using the other techniques described in Chapter 3. Furthermore, through electrochemistry, reactions can be conducted at ambient conditions, opposed to *in situ* as in other techniques. The convenience and controllability of electrochemical hydrogenation of graphene therefore provides a more realistic approach for a tunable bandgap in graphene and an ideal means for hydrogen storage. First, synthesis of epitaxial graphene will be discussed.

3.1 GROWTH OF GRAPHENE

Graphene was thought to be impossible to isolate as a free standing layer until its experimental discovery by mechanical exfoliation, "scotch tape method", from bulk graphite by Giem and Novoselov in 2004 [1-4]. While exfoliated graphene yields high quality graphene layers, low production yield and small sample sizes [5] have led to groups to develop other ways of creating graphene, such as chemical exfoliation using graphite oxide [6], chemical vapor deposition (CVD) grown on single crystal copper, Cu

(111) and nickel (Ni) by dissociation of organic precursors and epitaxial graphene grown on silicon carbide (SiC) by sublimation of silicon and the subsequent graphitization of the carbon atoms [7]. Epitaxial graphene, method used to grow graphene in the Clean Energy Laboratory here at the University of South Carolina, will be discussed in greater detail.

3.1.1 USC GROWTH OF EPITAXIAL GRAPHENE AT USC

Figure 3.1 Hot Wall RF reactor outside (left) and inside (right) of growth reactor showing induction coils and graphite crucible.

Epitaxial growth of graphene at USC is performed using a hot wall RF reactor, shown in Figure 3.1, under ultra-high vacuum (UHV) and high temperature [8]. Thermal gradients in the reactor are minimized by housing the sample in a graphite crucible which is surrounded by graphite foam for further insulation as shown in Figure 3.2 [8]. The Si-C bond breaks and Si sublimates from SiC under these conditions, leaving carbon atoms behind to rearrange in a hexagonal lattice forming graphene as shown in Figure 3.3 [8].

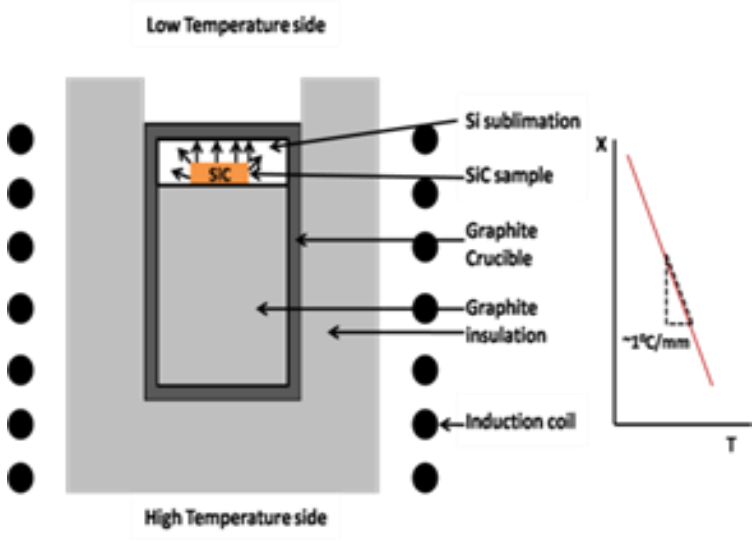

Figure 3.2 Schematic of RF reactor interior.

Epitaxial graphene is grown by thermal decomposition of 4H and 6H SiC substrates under the conditions described above. This produces from a couple layers up to >50 monolayers (ML) of graphene depending on growth condition, substrate and growth face. Before growth, $10mm^2$ samples were cleaned using trichloroethylene (TCE), acetone and methanol. They were then rinsed with DI water to remove the solvents and HF was used to remove the native oxide on the SiC.

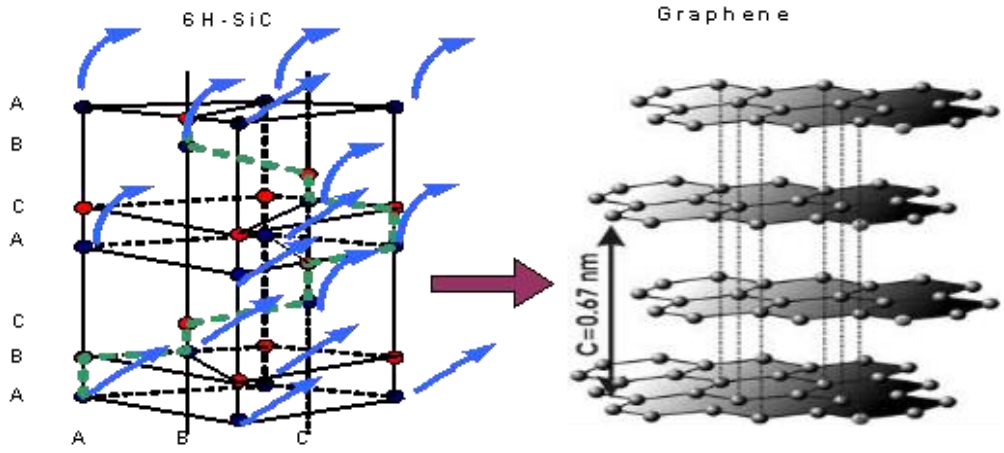

Figure 3.3 Sublimation of Si from SiC and subsequent graphitization forming graphene.

The SiC is then placed in the graphite crucible and that is placed in the RF reactor where it follows the growth parameters described in Figure 3.4. The system is pumped down to a vacuum of $<10^{-6}$ Torr and baked out between 14-17 hours at 1000°C to remove any oxygen present in the reactor, which adversely affects the growth of graphene. No graphitization occurs during this step. The samples are only held at the growth temperature 1300-1600°C for an hour, with slow ramp up and ramp down temperatures to prevent thermal stress on the grown graphene layer(s). All of the starting graphene samples in this work were grown in this manner.

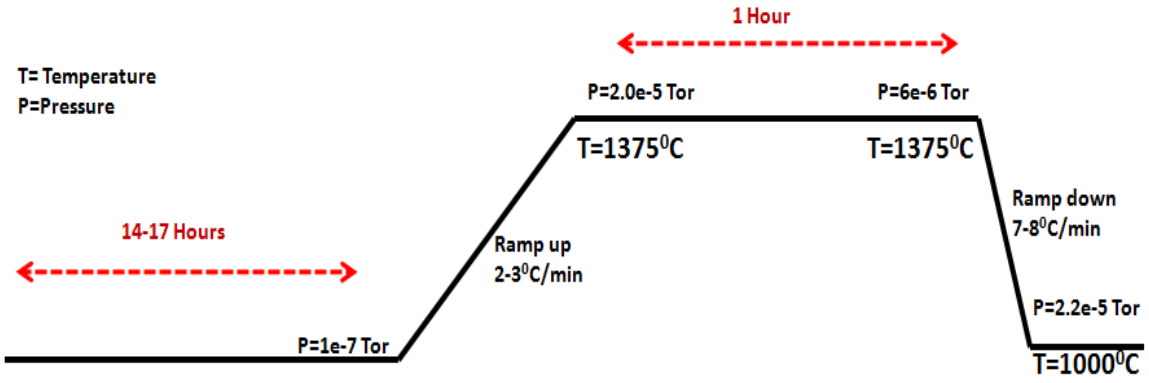

Figure 3.4 Pressure and temperature profile of typical EG growth.

3.2: ELECTROCHEMICAL CELL DESIGN AND OPERATION

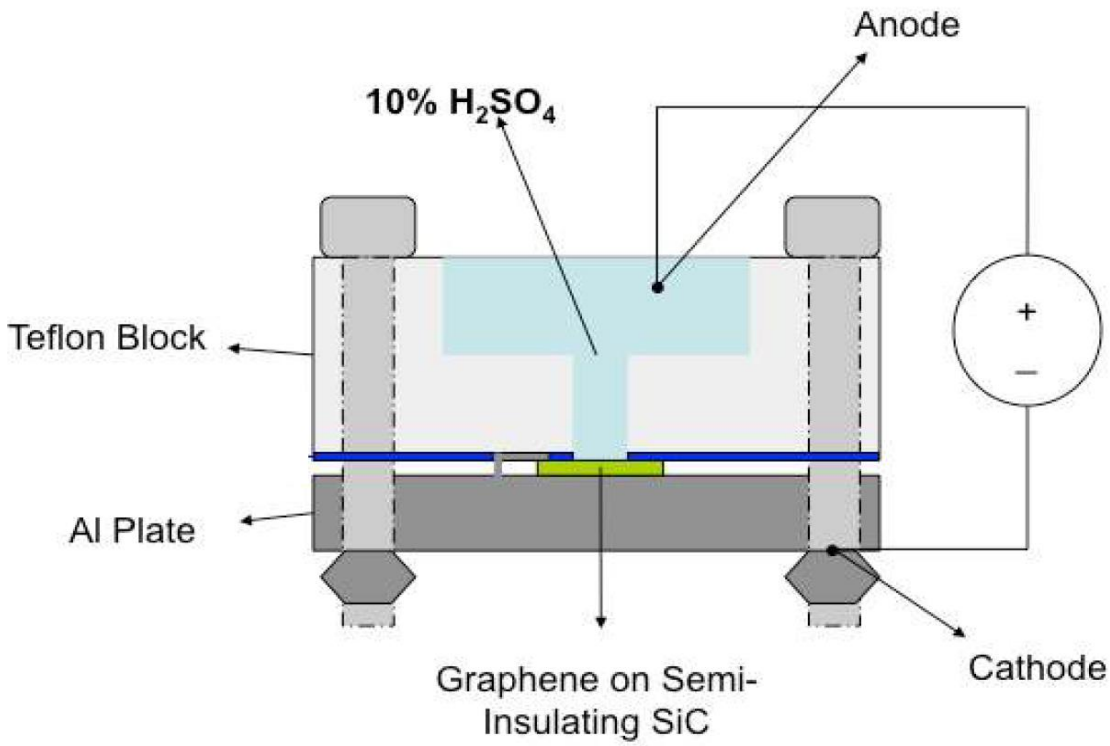

Figure 3.5 Diagram of lattice changes from graphene hydrogenation with atomic hydrogen

Atomic hydrogen was generated using a home-built electrochemical setup (Figure 3.5), with current applied though a 10% H_2SO_4 acid solution. A 99.6% Pt wire and exposed EG (approximately a 4mm diameter circular area) were used as the anode and cathode, respectively. With this setup, H+ ions in the H_2SO_4 electrolyte are attracted to the exposed graphene. Under applied voltage, H+ cations are attracted to the negatively charged graphene cathode electrostatically where they are reduced. If reduction does not occur then no current would be observed. Oxidation occurs at the Pt anode during this

process, and has been investigated and discussed in greater detail elsewhere [9, 10]. Thus, in this investigation, we limit ourselves to the reduction of the graphene cathode.

3.3. EXPERIMENTAL SETUP

Three 6H SiC semi-insulating, nominally on-axis wafers axis ,~0.02°, 0.5° and 1.0° in the 11-20 direction and EG was grown as described in Chapter 1. Growth of epitaxial graphene (EG) was done only on the Si-face with quality of EG growth verified by Raman spectroscopy, atomic force microscopy (AFM) [11, 12]. EG layer thicknesses were estimated by x-ray photoelectron spectroscopy, Raman spectroscopy [13] and infrared transmission measurements [14]. All of the samples used in this study displayed thicknesses of ~2-3ML, which was verified using XPS. Nanocrystalline graphene layers grown on non-polar faces of SiC [7,8] were used as control samples for the hydrogenated graphene on Si-face to distinguish hydrogenation from damage.

It is known that metal reduction occurs ~0.2V below the evolution of H_2 similar to that seen with other metal hydrides [9, 10]. A voltage < 1.2V was used to prevent the splitting of H_2O which causes the formation of H_2 bubbles. By using a potential below 1.2V, chances of H+ reduction by H_2 evolution was eliminated. Thus, an EG reduction anode/cathode voltage of ~1V was chosen, following similar reduction potentials shown in metals below the H_2 evolution potential [15]. Using these conditions, hydrogenation were performed until the current through the resulting material decreased <10nA from a starting value of ~0.1μA independent of substrate with typical current (I) vs. time (t) curve shown in Figure 3.6. In order to keep variables to a minimum, a set time of one hour was used for all experiments.

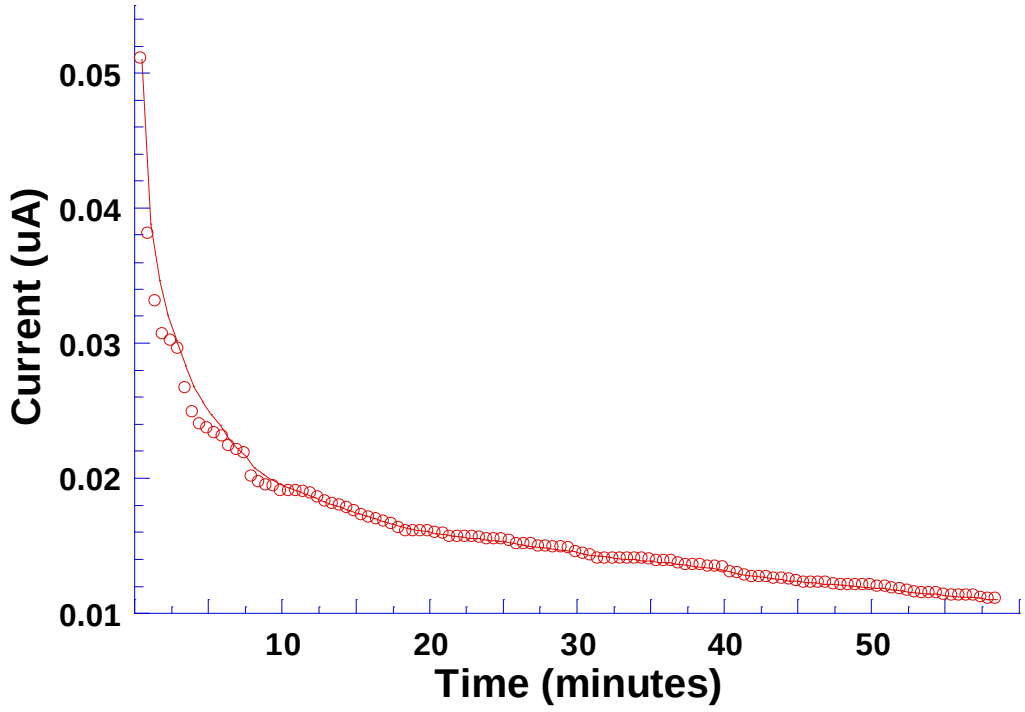

Figure 3.6 I vs. t curve for electrochemical hydrogenation of graphane. About 1 monolayer of hydrogen was calculated from the total integrated charge for 2 monolayers of graphene

3.4. CHARACTERIZATION OF GRAPHENE AND GRAPHANE

3.4.1. RAMAN SPECTROSCOPY OF GRAPHENE AND GRAPHANE

Raman spectroscopy was performed using a micro-Raman setup with laser excitation wavelength at 632nm and a spot size of ~2 µm. The Raman system was calibrated using the known Si peak at 520.7 cm^{-1}. Reference blank SiC substrate spectra were scaled appropriately and subtracted from the EG/SiC spectra to show only the graphene and hydrogenated graphene peaks [12,16]. All the spectra shown in this paper are difference Raman spectra obtained in this manner. There are three peaks associated with graphene: The D peak (~1345 cm^{-1}) corresponds to the disorder and diamond like sp^3 content in the material, The G peak (~ 1595 cm^{-1}) corresponds to the in plane

vibration of the graphene lattice and the 2D peak(~2650 cm^{-1}) due to double resonance [16].

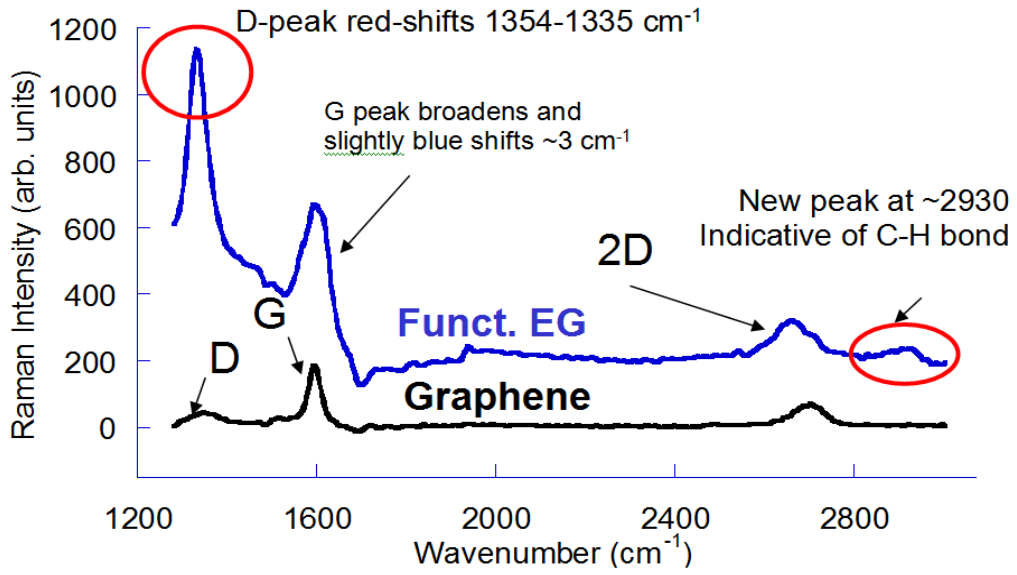

Figure 3.7 Raman spectra of graphene before and after hydrogenation

Raman was used as an indication of hydrogenation by the behavior of the D, G and 2D peaks, as well as a C-H bond peak or D+D' peak introduced at ~2930 cm^{-1} (Fig.10) [16]. A fluorescence background was also observed in the working area, which is only observed in hydrocarbons. Such a fluorescence background was not observed in the starting EG, and was used as a means for distinguishing hydrogenated graphene from damage.

3.4.1.1. FLUORESENCE OBSERVED IN RAMAN AFTER HYDROGENATION

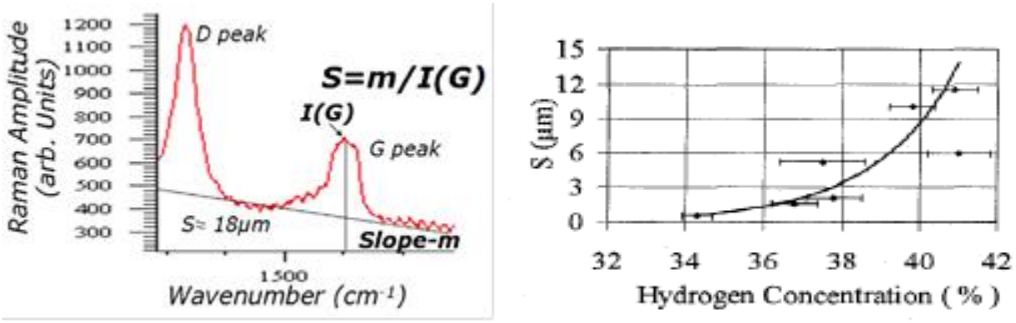

Figure 3.8 Fluorescence slope resulting from formation of hydrocarbon with chart of hydrogen content

Hydrogenated graphene is a direct gap material [12], resulting in a fluorescence background being seen in the Raman spectra. The presence of fluorescence could be due to defect induced midgap states or band-to-band recombination, as certainty of which mechanism is responsible is unclear. However, either mechanism indicates the presence of a bandgap [17].This fluorescence background can be quantified by the fluorescence slope, m, defined as the photoluminescence background present in samples as a result of hydrogenation. Extraction of slope m from the Raman signature is performed by applying a linear fit on the background of the spectra. This slope m is normalized against the intensity of the G peak, I(G) by m/I(G), which was used to measure H-content bonded to carbon [12] in studies of hydrocarbons. This can also be used to measure what fraction of sp^3 content is present in the material and therefore estimate of the extent of EG [12]. Based on these indications of hydrogenation, differences between substrates were examined.

3.4.1.2. GRADIENT AS OBSERVED BY RAMAN

As shown in Fig. 3.9, there was also a gradient associated with the conversion, where, according to Raman, the center showed significant hydrogenation when compared to other parts within the functionalized area. This gradient showed significant red shifting of the D peak, 1349 to 1328 cm^{-1}, from just outside the conversion area to the center, as well as a considerable red shift in the 2D peak from 2700 to 2626 cm^{-1}. The intensity of the D peak also increases, and as a result, the D/G ratio also changes within the gradient, with the ratio changing from 0.06 outside the conversion area to 1.35 at the center. This gradient in functionalization could be caused by the graphene becoming electrically decoupled from the substrate during the hydrogenation process [18], though it is most likely caused by the meniscus formed in the electrochemical cell causing a gradient in the available hydrogen ions on the surface.

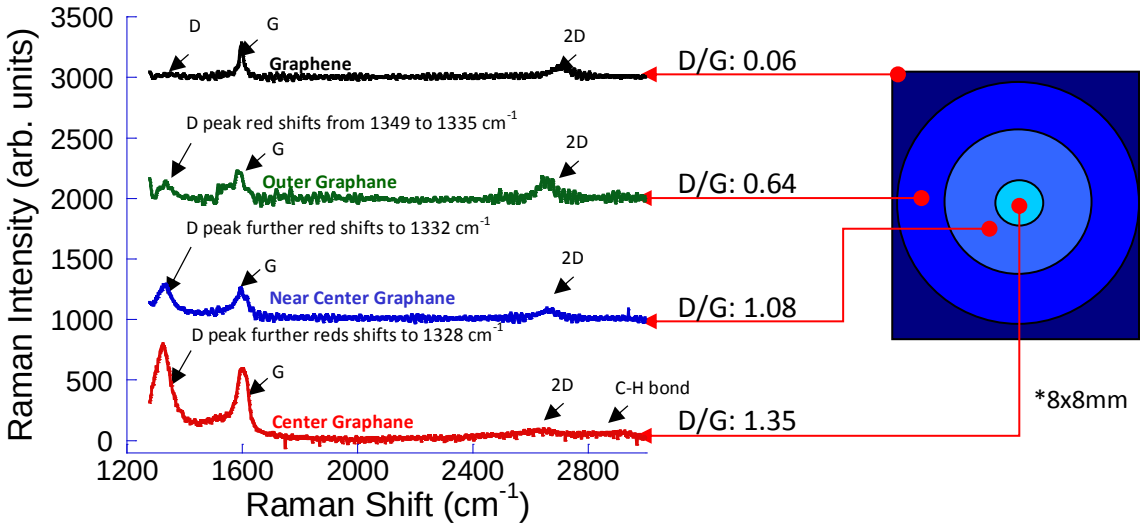

Figure 3.9 Hydrogenation gradient observed with electrochemical hydrogenation of epitaxial graphene

3.4.2 ATOMIC FORCE MICROSCOPY OF GRAPHENE/GRAPHANE

Atomic Force Microscopy (AFM) is used to characterize the surface morphology of epitaxial graphene nondestructively via tapping mode, with resolution higher than that of scanning electron microscopy. Epitaxial graphene grown on different faces and orientations of SiC result in different surface morphology. As a result, the surface of EG grown on Si-face of SiC, which is step flow mediated, appears as steps and EG grown on C-face, which is defect mediated growth appears as giraffe stripes. The incorporation of hydrogen in graphene changes the C-C bond length. There should be a noticeable change in morphology observed by AFM as the lattice constant changes to accommodate the incorporated hydrogen.

3.4.3. SCANNING TUNNELING SPECTROSCOPY OF GRAPHENE/GRAPHANE

Scanning Tunneling Spectroscopy (STS), an extension of Scanning Tunneling Microscopy (STM), uses a Pt-Ir tip to obtain information on the electron states of a sample, such as bandgap from dI/dV, or local dynamic conductance, by varying the bias voltage between the sample and the tip. STS was performed on pristine and hydrogenated EG to determine changes in bandgap. Pt-Ir tips were employed and cleaned thoroughly by electron bombardment before use. For the spectroscopy measurements the method of variable tip-sample separation was employed [19], typically using a ramp of 0.1 nm/V and with broadening parameter of 1.0 V to compute the normalized conductance (the results are only weakly dependent on these parameters). The conductance spectra were acquired using a lock-in amplifier with 50 mV modulation at a frequency of typically 1 kHz.

3.5. RAMAN SPECTROSCOPY OF HYDROGENATED GRAPHENE

As expected, there was a sharp increase in the D peak amplitude [20] of functionalized graphene (Fig. 3.7). A red shift in the D peak, from 1350cm^{-1} to 1330cm^{-1}, was also observed, likely caused by the formation of sp^3 bonds [20, 14]. The G-peak FWHM also broadens with functionalization further supporting the sp^3 hybridization of the graphene [20]. Another peak at ~2930cm^{-1} was an indication of C-H bonds [22] (Fig. 3.7). A fluorescence background, along with increased SiC substrate signal was also observed in the working area, suggesting the presence of a bandgap in the material. Such a fluorescence background was not observed in the starting EG, nor was it found in the nanocrystalline graphene on a/m plane SiC.

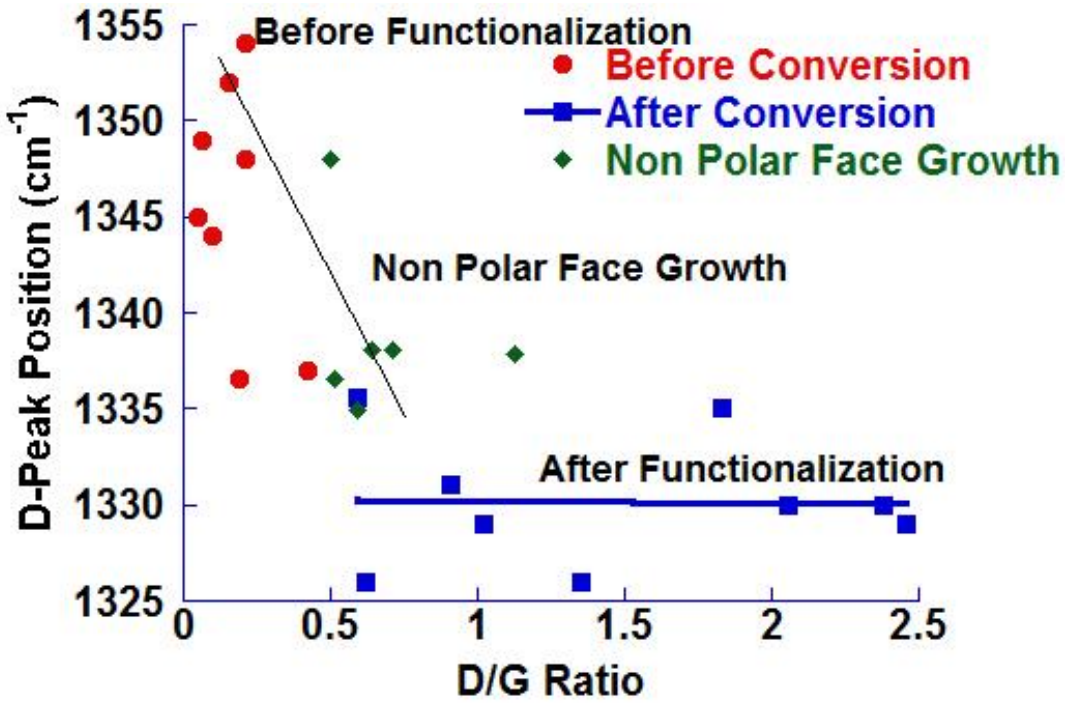

Figure 3.10 I(D)/I(G) ratio vs D-peak position of pristine EG, hydrogenated EG and nanocrystalline graphene

Figure 3.10 shows that I(D)/I(G) ratio has little effect on D-peak position in unfuctionalized graphene and non-polar face grown graphene, while functionalized samples are significantly red-shifted with respect to their pristine graphene state, with substantially larger I(D)/I(G) ratios. Despite having similarly high I(D)/I(G) ratios in the nanocrystalline a and m plane samples, D peak positions in these samples stay within the ranges of Si-face pristine graphene. Functionalization was further distinguished from damage by observing the resulting m/I(G) in functionalized graphene (Fig 3.11) , which shows that not only has functionalization occurred but also provides an estimate of the hydrogen content [22].

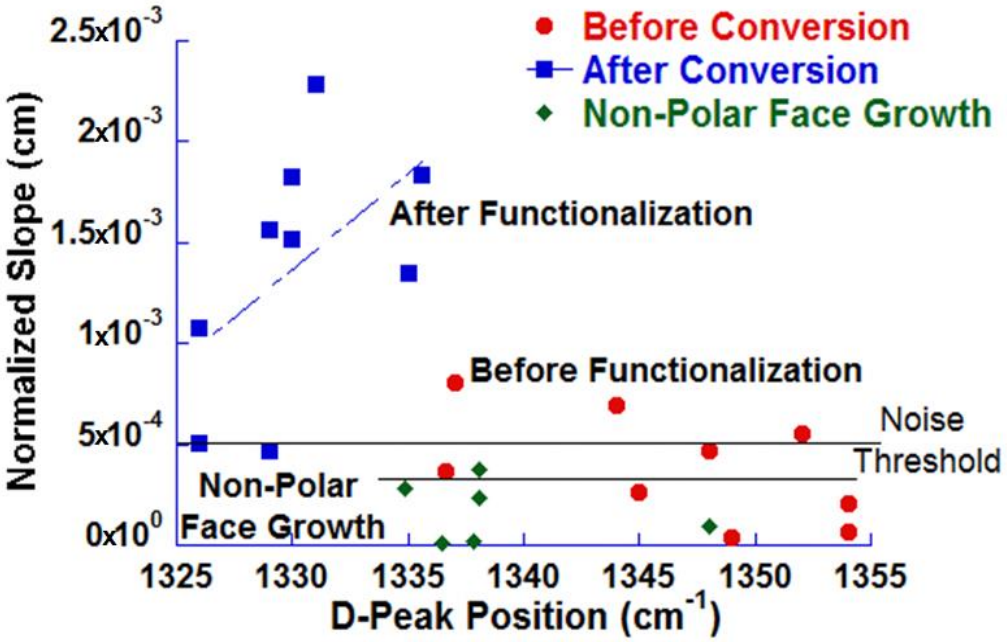

Figure 3.11 D-peak position vs. normalized slope of pristine EG, hydrogenated EG and nanocrystalline graphene

In Figure 3.11 when comparing the D-peak position and (m)/I(G), trends in the hydrogenated graphene, pristine graphene and a and m plane were very different. Much higher m/I(G) values and significantly red shifted D-peak in hydrogenated graphene

distinguish it from pristine EG. Furthermore, the D-positions seen in nanocrystalline non-polar growths have no dependence on m/I(G), a key difference between damage and hydrogenation. Among hydrogenated samples, (m)/I(G) was shown to increase with higher D-peak positions. This fluorescence background was used to approximate hydrogen content to be as high as 30-50%, which is consist with the measured thickness of 2-3ML for the sample set and the participation of approximately 1ML of hydrogen during hydrogenation (Fig. 2) [12, 23].

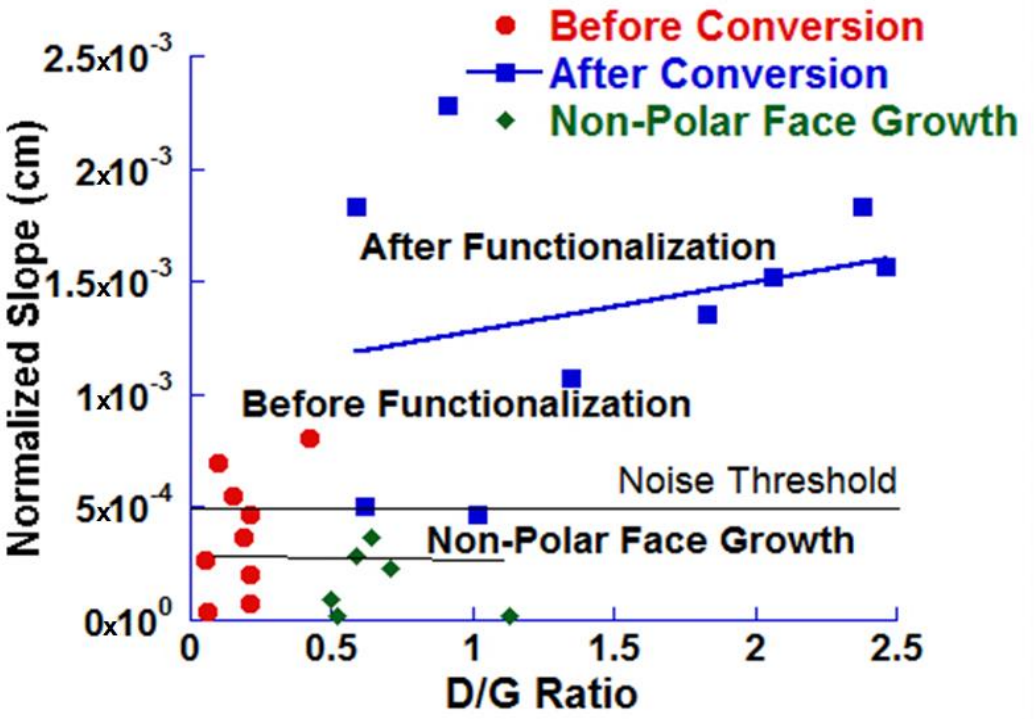

Figure 3.12 Normalized slope vs. I(D)/I(G) ratio of pristine EG, hydrogenated EG and nanocrystalline graphene

Figure 3.12 shows hydrogenated graphene (m)/I(G) increasing with rising I(D)/I(G), showing a clear correlation of hydrogen content in hydrogenated graphene with I(D)/I(G), which is now seen to arise not from disorder, but from hydrogenation.

Despite I(D)/I(G) similar to that of hydrogenated graphene, nanocrystalline graphene shows no measurable fluorescence (m/I(G)<5μm, the noise threshold). As expected, this trend is not seen in pristine EG or nanocrystalline growths as only hydrocarbons fluoresce [12]. To summarize Figures 13.10-13.12, we show evidence of hydrogenation of EG, by distinguishing the Raman signatures of hydrogenation in electrochemically treated graphene from those of damage in nanocrystalline graphene.

3.6: SURFACE MORPHOLOGY AFTER HYDROGENATION USING ATOMIC FORCE MICROSCOPY

Atomic force microscopy (tapping mode) was used to determine surface morphology changes of pristine EG to hydrogenated EG. AFM images of Si -face EG before hydrogenation show the steps which are common in EG growth on Si-face [7]. Post-hydrogenation morphologies show a slight increase in root-mean square (RMS) roughness, from 0.6 to 1.0nm on Si-face. What is interesting about the hydrogenated graphene surface is the appearance of raised streaks on the Si-face, which appear to follow the step direction. The presence of these streaks were noticed on all hydrogenated samples and suggests that a structural change has occurred in the EG such as sp^3 hybridization caused by the hydrogen incorporation. I(D)/I(G) ratio from Raman is not only used to determine quality of graphene, but as a measure of grain size in disordered/nanocrystalline graphene through the relation 4.4nm/(I(D)/I(G)) [12]. The morphology of hydrogenated EG is dramatically different from that of nanocrystalline EG, which shows small grains ~5-20nm in size, consistent with the Raman I(D)/I(G). Such grains are not seen in hydrogenated graphene. Therefore, the I(D)/I(G) in hydrogenated graphene must have a different origin.

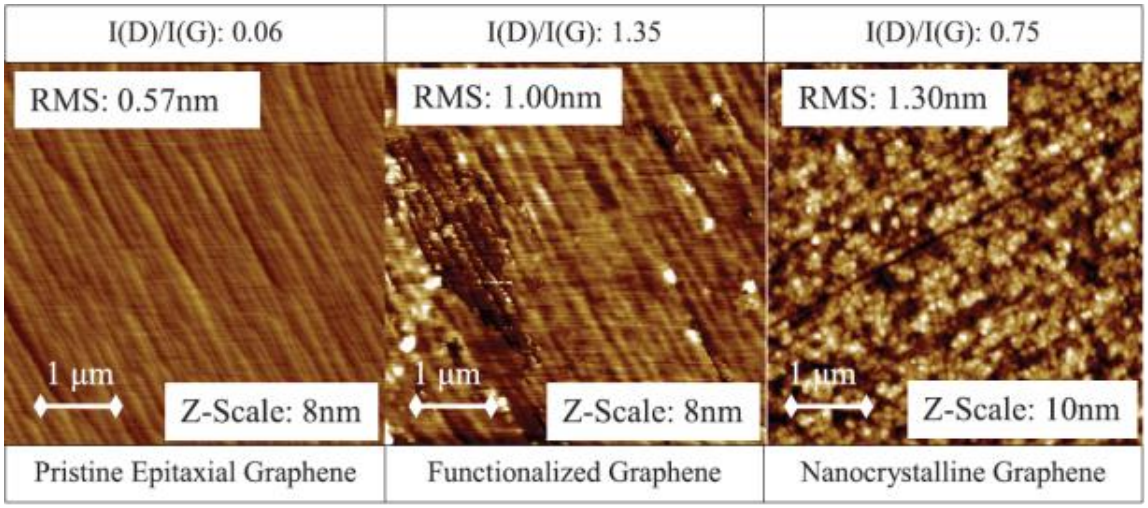

Figure 3.13 AFM of EG, hydrogenated EG and nanocrystalline graphene

3.7: SCANNING TUNNELING SPECTROSCOPY OF GRAPHENE AND HYDROGENATED GRAPHENE

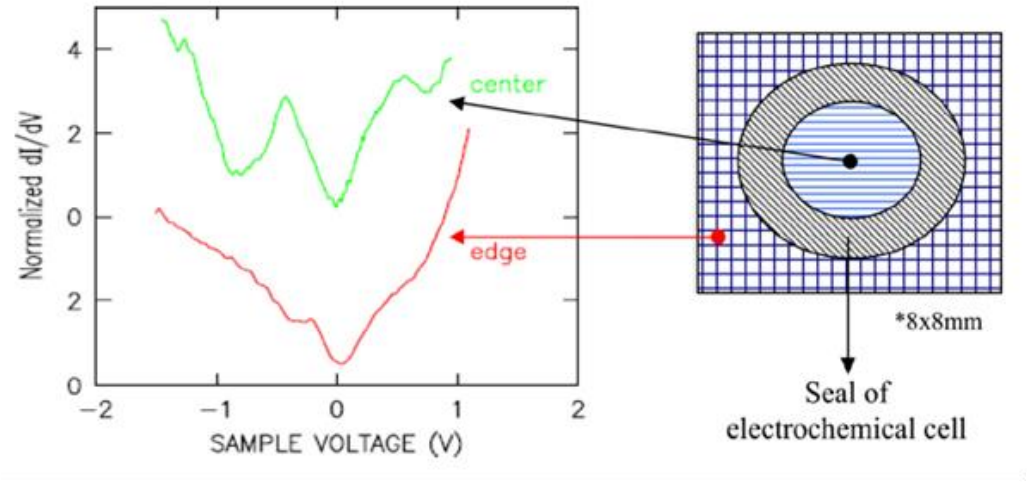

Figure 3.14 STS of pristine EG and hydrogenated EG

Measurements were performed at the edge of the sample (corresponding to pristine graphene) and at the center of the sample (corresponding to hydrogenated graphene). For both spectra, the measured conductance at 0 V is nonzero, but relatively

small, indicative of weakly metallic (semi-metallic) behavior. The main differences between the spectrum from the pristine graphene and the spectrum from the hydrogenated graphene is that the latter shows a distinct spectral peak at -0.4 V as well as a smaller peak near +0.5 V. These differences are similar to those seen between graphene and the $6\sqrt{3} \times 6\sqrt{3}$ "buffer layer" on SiC [19]. Thus it can be argued that, similar to the buffer layer, the hydrogenated graphene has covalent bonds involving sp^3 hybrid states. It should be mentioned that the spectra from the edge and center of the sample were obtained with different probe tips; nevertheless, multiple tips were employed for measurements at both positions and the differences shown in Figure 16 were reproducible over the measurement set.

3.8: INVESTIGATION OF SUBSTRATE DEPENDENCE ON HYDROGENATION

Substrate dependence was investigated by taking sets of three or more samples from each of the three wafers and functionalizing them using the described experiment. D peak position, I(D)/I(G) ratio and normalized fluorescence, slope (m)/ IG, were recorded from the pristine EG, hydrogenated graphene as well as samples grown on the a and m [8] planes of SiC which were used to show that the resulting "disorder" shown in the hydrogenated graphene, which signifies hydrogenation, were significantly different than that of damaged or nanocystalline graphite [12].

The average values for D-peak position, I(D)/I(G) ratio and slope(m)/I(G) before and after for each substrate as shown in Table 3.1. Despite being hydrogenated for the same duration, significant differences can be seen in the degree of hydrogenation between the substrates. Some possibilities for these differences could be the presence of

point defects in EG originally from the starting SiC, the slight differences in offcut angle in the 11-20 direction and/or quality of starting EG. It is suggested that hydrogenation may be due at least partially to defects. Table 3.1 shows a clear correlation in I(D)/I(G) of starting graphene with that of hydrogenated graphene. There is no such correlation between m/I(G) vs. I(D)/I(G) of EG, however, indicating that the substrate plays a role in determining the degree of hydrogenation. With clear dependence on substrate, metals were evaporated or chemically deposited in thin layers on various samples from SI3, in an attempt to enhance hydrogenation and increase the hydrogen content incorporated into the material.

Table 3.1: Average parameters before and after hydrogenation

Substrate	D-peak Position Before (cm^{-1})	D-peak Position After (cm^{-1})	I(D)/I(G) ratio Before	I(D)/I(G) ratio After	Slope (m)/I(G) Before (cm)	Slope (m)/I(G) After (cm)
SI (1 deg)	1348	1330	0.21	1.91	3.7×10^{-4}	1.4×10^{-3}
SI2 (on-axis)	1344	1332	0.17	1.32	4.2×10^{-4}	1.9×10^{-3}
SI3 (0.5deg)	1347	1328	0.13	0.82	3.7×10^{-4}	4.9×10^{-4}
a-Plane	1338		0.79		8.8×10^{-5}	
m-Plane	1340		0.58		2.5×10^{-4}	

An electrochemical process was developed with the goal of functionalizing graphene grown on SiC substrates in the efforts of enabling a bandgap in the material. This conversion was performed on EG grown on Si-face, 6H SiC substrates, with EG I(D)/I(G) ratio of <0.2. Raman showed an increase in D peak amplitude, demonstrating

surface functionalization; introduction of a peak at 2930cm^{-1}, indicating formation of C-H bonds; and D and 2D peak shifts from pristine EG to functionalized graphene, indicating likely sp^3 hybridization. Functionalized graphene showed Raman fluorescence unlike EG and nanocrystalline graphene on a/m plane, supporting the presence of C-H bonds inferred by the 2930cm^{-1} peak. AFM showed a marked difference between the morphology of nanocrystalline graphene and that of functionalized graphene, further indicating that the Raman signatures described here are indicative of functionalization, not damage. STS demonstrated the presence of localized sp^3 states, indicating that the local structure of graphene has changed from its pristine sp^2 form. Hydrogenation is further supported by hydrogen desorption by thermal anneal and electrochemical reversal which is shown in greater detail in Chapter 5.

REFERENCES

[1] W.A de Heer, C. Berger, X. Wu, P. N. First, E. H. Conrad, X. Li, T. Li, M. Sprinkle, J. Hass, M. L. Sadowski, M. Potemski, G. Martinez, Solid State Communications 143 (2007) 92-100

[2] A.K. Geim, K.S. Novoselov, Materials Science 6, 183-191 (2007)

[3] A.H. Castro Neto, F. Guiena, N.M.R. Peres, K.S. Novoselov, A.K. Geim., Rev. Mod. Phys. 81, 109-162 (2009)

[4] J. L. Tedesco, B. L. VanMil, R. L. Myers-Ward, J. M. McCrate, S. A. Kitt, P. M. Campbell, G. G. Jernigan, J. C. Culbertson, C. R. Eddy, D. K. Gaskill., Applied Physics Letters 12, 122102-122102-3(2009)

[5] Geim A. K *Science* 324, 1530 (2009)

[6] S. Stankovich et. al., Carbon 45. Vol. 7 (2007) 1558-1565

[7] B. K. Daas, O. Sabih, S. Shetu, K. M. Daniels, S. Ma, T. S. Sudarshan, MVS Chandrashekhar,. Cryst. Growth Des., 2012, 12 (7), pp 3379–3387 (2012)

[8] B. K. Daas, S. U. Omar, S. Shetu, K. M. Daniels, S. Ma, T. S. Sudarshan, MVS Chandrashekhar., Cryst. Growth Des. 12, Issue 7, 3379-3387 (2012)

[9] J. Rand. Electroanal. Chem, 35 (1972)

[10] K. Ota, S. Nishigori and N. Kamiya., J. Electroanal. Chem., 257, 205-215 (1988)

[11] C. Srinivasan and R. Saraswathi., Current Science 97, Vol. 97, No. 3 (2009)

[12] A.C. Ferrari and J.Robertson., Phys.Rev. B 61, 14095-14107 (2000)

[13] S. Shirvaraman, M.V.S. Chandrashekhar, J.J. Boeckl, M.G. Spencer., Journal of Electronic Materials,Vol. 38, No. 6 (2009)

[14] J. M. Dawlaty, S. Shirvaraman, J. Strait, P. George, M.V.S. Chandrashekhar, Farhan Rana, M.G. Spencer, D. Veksler, Y. Chen., Appl. Phys. Lett. 93, 131905 (2008)

[15] A. K. Vijh., Journal of Power Sources, Vol. 11, Issue 1-2, 171-183 (1984)

[16] D. C. Elias, R. R. Nair, T. M. G. Mohiuddin, S. V. Morozov, P. Blake, M. P. Halsall, A. C. Ferrari, D. W. Boukhvalov, M. I. Katsnelson, A. K. Geim, K. S. Novoselov., Science 30, Vol. 323, No. 5914, 610-613 (2009)

[17] B. Wang, J. R. Sparks, H. R. Gutierrez, F. Okino, Q. Hao et. al., Appl. Phys. Lett. 97, 141915 (2010)

[18] S. Ryu, M. Y. Han, J. Maultzsch. T. F. Heinz, P. Kim, M. L. Steigerwald and L. E. Brus., Nano Lett., Vol. 8, No. 12, 2008

[19] Shu Nie and R.M. Feenstra., J. Vac. Sci. Technol. A **27**, 1052 (2009)

[20] B. Verberck, B. Partoens, F. M. Peeters and B. Trauzettel., Phys. Rev. B 85, 125403

[21] R. Sprinkle, J. Hicks, A. Tejeda, A. Taleb-Ibrahimi, P. Le Fèvre, F. Bertran, H. Tinkey, M. C. Clark, P. Soukiassian, D. Martinotti, J. Hass and E. H. Conrad., J. Phys D : Appl. Phys. 43, 374006 (2010)

[22] Y. Lin and P. Avouris., Nano Lett. Vol. 8, No. 8 (2008)

[23] B. Marchon, J. Gui, K. Grannen, G. C. Rauch, J. W. Ager III, S.R.P. Silva and J. Robertson., IEEE Transactions on Magnetics, Vol. 33, No. 5 (1997)

CHAPTER 4

METAL CATALYZED ELECTROCHEMICAL SYNTHESIS OF HYDROCARBONS FROM EPITAXIAL GRAPHENE

4.1. FORMATION OF ALKANES FROM ALKENES VIA CATALYTIC METALS

Electrochemistry and other means of forming a C-H bond [1-7] are similar to the hydrogenation of π-bonds in alkenes forming alkanes in organic chemistry as shown in Figure 4.1. Traditional hydrogenation of alkenes by molecular hydrogen gas to form alkanes requires catalysis by precious transition metals, such as Pt, sometimes at high temperatures and pressures [8, 9]. These catalytic transition metals decrease the activation energy, and thus increase the rate of C-H bond formation. Platinum-group transition metals offer a facile pathway for hydrogen to adsorb and dissociate, and the resulting H atoms can then transfer directly to the alkenes adsorbed on the metal surface [10]. Edges, corners and basal planes of all metals have different catalytic activity [11-13]. As such, the effectiveness of these metals as catalysts depends directly on the size and shape of the particles [11,14] Smaller particles result in more adsorption sites for hydrogen to be adsorbed due to increase in surface area [11,12,14].

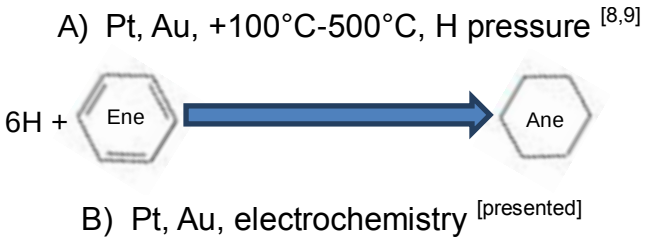

Figure 4.1. Comparison of traditional thermal chemical phase and electrochemical hydrogenation. A) In thermal chemical phase 1) hydrogen gas is introduced into the thermal chemical phase containing the alkene and the catalyst. 2) The H_2 dissociates to hydrogen ions due to the kinetics of the catalysts. 3) The kinetics of the catalysts allow for alkenes to become reactive, activation of π-bonds and 4) chemisorb H away from the catalyst resulting in 5) hydrocarbon bonds (synthesis of alkAnes). B) In electrochemical hydrogenation, bias across the electrode, graphene, and counter electrode in solution, sulfuric acid, provide the kinetics required to isolate hydrogen ions from the solution and the negative bias on the graphene allow for high density of hydrogen ions around graphene electrode. Active π-bonds in graphene allow for hydrogen to be chemisorbed similar to that in thermal chemical phase hydrogenation forming hydrocarbon bonds (synthesis of graphAne).

4.2. CATALYSIS BY PLATINUM

Despite its high cost, platinum is one of the most commonly used catalysts for hydrogenation of carbon [12, 15]. Reducing the size of the Pt nano-clusters reduces cost and results in higher catalytic activity with more atoms exposed to reactants [11]. From an electronic point of view, the catalytic activity of Pt is governed by its electron configuration. Metals in Group VIII, with the smallest number of vacant d-orbitals, can accept electrons from reactants and form, in this case, metal-hydride bonds that can easily be broken compared to other metal groups, making it a superior catalyst [17]. As Pt easily forms bonds with most molecules, adsorption selectivity is an issue in systems with multiple species, and hydrogen is not the only adsorbed species, resulting in undesired products [18].

4.3. CATALYSIS BY GOLD

Bulk gold (i.e., large Au particles) has been shown to be much less active (by two orders of magnitude) in dissociating hydrogen, due to the Au(111) surface being intrinsically inactive for this reaction [11,15]. In small clusters, however, Au has demonstrated reactivity to hydrogen in edge Au(200) and corner Au(311) [14, 15, and 16]. With decreasing particle size, Au shows tunable hydrogenation with increasing edge and corner sites compared to bulk Au [11, 14, and 15]. The H_2 dissociation rate on Au is limited by the inability of molecular hydrogen to adsorb. However, when Au is readily supplied with H atoms or ions from other transition metal spillover or acidic solutions, respectively, hydrogen atoms easily chemisorb on Au [33,34].

In electrochemical hydrogenation, a high density of H^+ is isolated from the solvent and attracted to the negatively biased EG electrode where they react with the highly reactive π-bonds to form C-H bonds. Indeed, hydrogen adsorption and reaction with EG has been shown to be possible even without the need of precious transition metals present. Since EG is negatively biased, only hydrogen ions, which are positively charged, are attracted to the surface, excluding any possibility for adsorption of other functional groups.

Electrochemistry offers the most controlled route to systematic functionalization, as the extent of the hydrogenation of graphene can be precisely controlled by changing the current level (or voltage) and time. This raises the possibility of reversible electrochemical functionalization for further fine tuning of graphane production Such tunability is not easily achievable using the other techniques described above.

Furthermore, through electrochemistry, reactions can be conducted at ambient conditions, as opposed to other techniques for graphane synthesis such as hydrogenation by in situ plasma discharge [4, 35, 36], hot tungsten filament [5] and e-beam disassociation from adsorbents [3, 37, 38]. The convenience and controllability of electrochemical hydrogenation of graphene provides a realistic approach for a tunable bandgap in graphene, though an observed dependence on the underlying SiC substrate using this technique has been previously shown [6].

4.4. ENHANCED ELECTROCHEMISTRY BY CATALYTIC METALS

As precious metals are used to increase hydrogenation of alkenes in traditional thermal catalytic hydrogenation, deposition of catalytic transition metals on EG should increase electrochemical hydrogenation, verifying that indeed hydrogen is adsorbed using this method. With most work on hydrogenation being performed on carbon and oxides [13, 16] the observed chemistries on carbon/semiconductor scaffolds could vary. In this study, enhanced electrochemical Graphene was grown as described in Chapter 2. In order to see the effect of these catalytic transition metals on the functionalization of graphene, six (6) 10 x 10mm^2 6H SiC semi-insulating samples were chosen from the same wafer used in Chapter 3, SI3, a nominally on-axis wafer, 0.5° in the 11-20 direction. Using EG, chemically derived Pt nanoparticles were formed on the graphene sample by deposition from an aqueous H_2PtCl_6 solution, drying in vacuum, and treatment with hydrogen at 200°C [30]. Using the set of six EG samples, 20 nm of either Pt or Au were evaporated on the EG surface by E-beam evaporation to act as catalysts and enhance to reactivity of graphene in a more controlled manner. The e-beam evaporator was pumped down to >1x10^{-6} at a rate of 2 Å/second. An atomic force microscopy (AFM) analysis was

performed determine the surface morphology changes of EG with catalytic metals and the functionalized EG. The images were acquired in tapping mode at a scan rate of 0.6 Hz over a 2.5 μm^2 area.

4.5. ENHANCED HYDROGENATION BY AQUEOUS PLATINUM NANOPARTICLES

The Raman spectra of the functionalized Pt nanoparticle catalyzed graphene (Figure 4.2) revealed a very large I(D)/I(G) ratio <5 and a narrow FWHM of 33 cm^{-1} FWHM, showing an extremely high sp^3 content present in the material. The sharpness of the peak indicates the lack of damage to the graphene surface. The D and 2D peak red shifted, likely caused by the formation of sp^3 bonds. The G and 2D peak full width half maximum (FWHM) broadens, further supporting the sp^3 hybridization of graphene and the C-H bond peak at ~2930 cm^{-1} further supports successful functionalization. A very prominent D' prime shoulder peak on the G peak indicating distortion of the ideal graphene lattice further suggested that changes in the C-C bond length have taken place. Higher current was observed in the I vs. t curves during functionalization, which is directly observed in the increased levels of I(D)/I(G) and fluorescence slope. A hydrogen content of 43% was extracted from the fluorescence background. While this method is promising, it lacks reproducibility and uniformity due to changes in conductivity and reactivity of graphene due to the aqueous nature and clustering of the nanoparticles causing a large variability between the four samples hydrogenated. 50% of samples showed little to no hydrogenation, increase in sp^3 content, based on I(D)/I(G) ratio, increasing to 0.17 and 0.44 from starting I(D)/I(G) ratio of 0.14. This is compared to the

50% of samples that showed prominent increases in sp^3 content with increases in I(D)/I(G) ratio of 1.1 and the result shown in Figure 4.2 of 5.

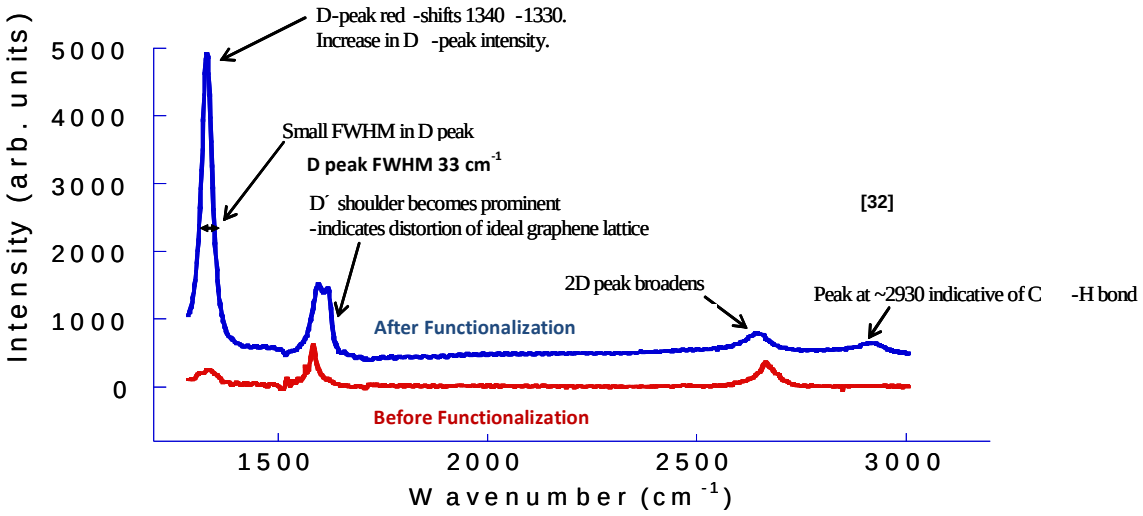

Figure 4.2 Typical Raman spectra of hydrogenation with and without chemically deposited Pt nanoparticles

Raman confirmed that no damage occurred to the graphene during deposition and that the material was electrochemically functionalized successfully. However, a more controlled, non-aqueous deposition of catalytic metals was needed to make this functionalization more reproducible, since aqueous based solutions can change the doping of graphene. Similar to water reactions observed with single wall carbon nanotubes (SWCNT), water results in p-type doping of graphene, changing its conductivity, and ultimately affecting reactivity reliability [31].

4.6. ENHANCED HYDROGENATION BY ELECTRON BEAM EVAPORATION OF PLATINUM AND GOLD NANOPARTICLES

To better control the deposition of metal and increase reproducibility, 20 nm of either Pt or Au were e-beam evaporated on the graphene surface. Raman spectroscopy

was used to confirm no changes to the material quality of the EG had occurred after evaporation of metals. Figure 4.3 shows the AFM images, 2.5x2.5μm scale, of pristine graphene, as well as Pt- and Au-coated graphene before and after functionalization. Before metal deposition, the steps associated with graphene growth on Si-face SiC are shown with an average RMS roughness of **0.4** nm. After metal deposition the RMS roughness increases to an average of **0.6** nm for Pt and **3.7** nm for Au and the graphene steps observed before metal deposition are not visible. The evaporated metals appear to be well dispersed according to AFM of these films before electrochemical hydrogenation.

However, after hydrogenation the metal particles appear to agglomerate together, exposing the underlying steps of the graphene surface. These metals also appear to partially lift off during functionalization, more so with evaporated Pt than with Au, according to AFM with RMS roughness of 4.2nm and 2.6nm for Au and Pt respectively with areas in the Pt deposited sample showing the underlying graphene with an RMS roughness of 0.4 nm. This could change the concentration and overall geometry of the catalyst, affecting reactivity. Despite the lower reactivity of Au, the enhanced hydrogenation seen with this metal could simply be more metal remaining during electrochemical hydrogenation and more hydrogen adsorbing due to the higher concentration of adsorption sites compared to Pt. The adhesion of metal to graphene needs to be investigated as changes in geometry during functionalization could affect the reactivity and overall effectiveness of the catalytic metal.

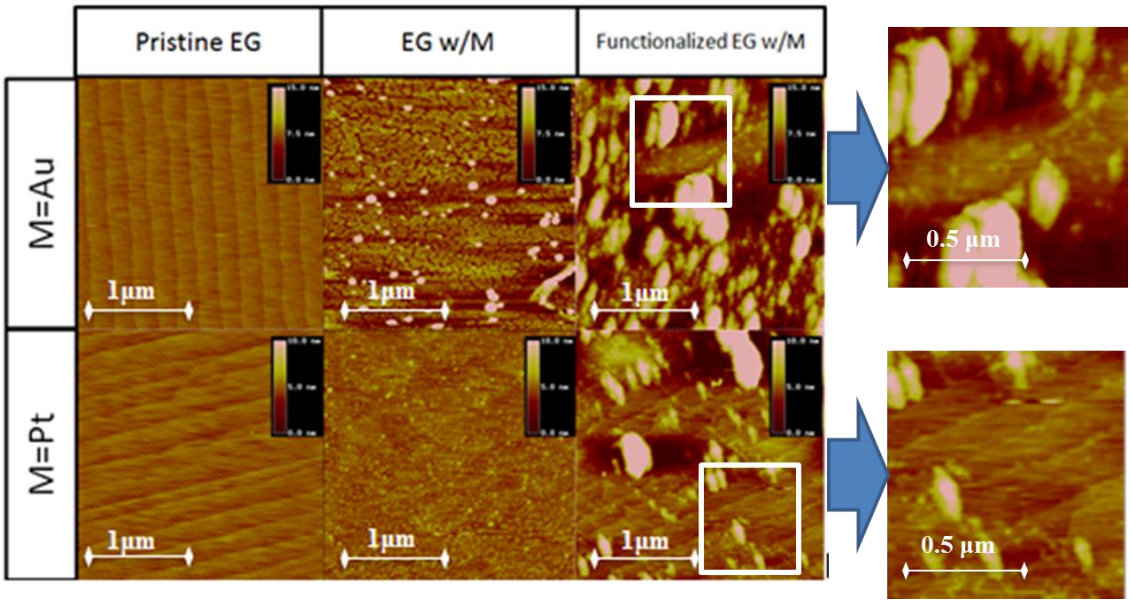

Figure 4.3 AFM of epitaxial graphene without evaporated metals, after evaporated metal deposition showing conformal evaporated metal and after electrochemical hydrogenation showing clustering of nanoparticles revealing underlying EG layers suggesting lift off of catalytic metals

Functionalization of metal catalyzed EG revealed increases in functionalization as evident by marked increases in I(D)/I(G) ratio, shifts in D, G and 2D peaks (lines represent peak position of unfunctionalized EG) and emergence of C-H peaks for typical Au and Pt enhanced EG. These data are shown in Figure 4.4 and Table 4.1.

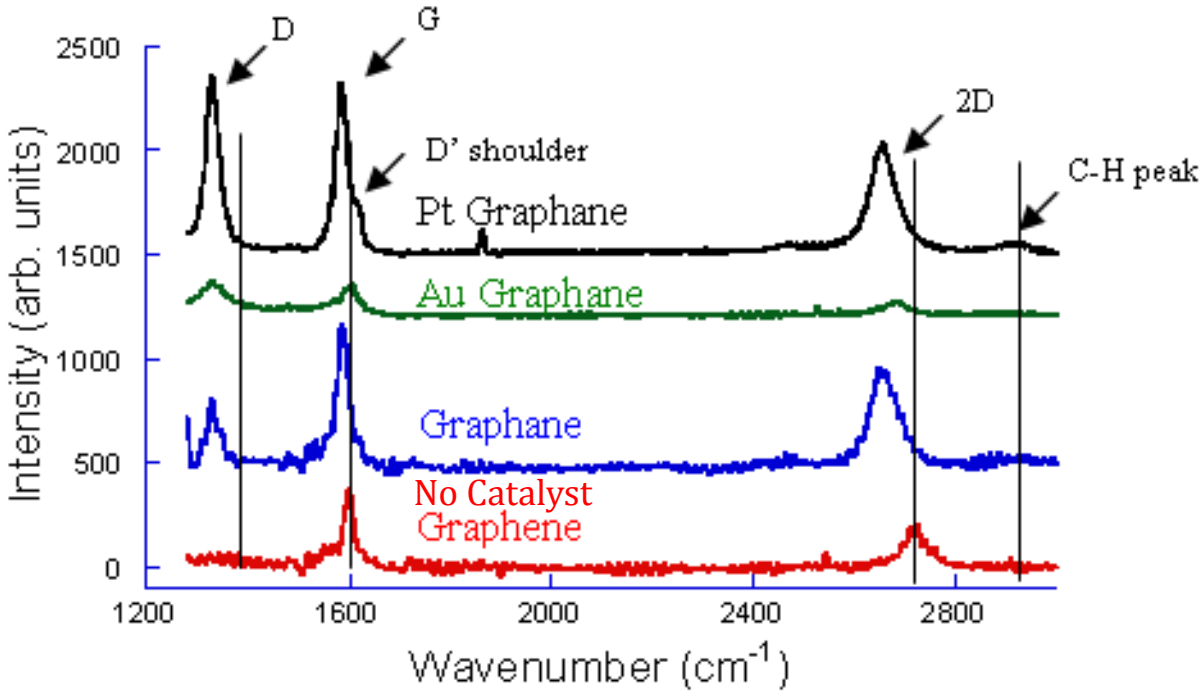

Figure 4.4 Raman spectra of evaporated metal enhanced functionalized graphene showing increase in I(D)/I(G) ratio compared to functionalization on pristine graphene

Table 4.1: Average parameters showing enhanced reactivity after evaporation of metal catalysis

Substrate	D Position Before (cm^{-1})	D Position After (cm^{-1})	I(D)/I(G) Ratio Before	I(D)/I(G) Ratio After	Slope (m)/I(G) Before(μm)	Slope (m)/I(G) After (μm)	Calculated H content
SI3(0.5°)	1347	1328	0.13	0.82	Unmeasureable	4.9	33±0.5
SI3 Pt Avg	1342	1330	0.22	1.05	Unmeasureable	7.9	37±1.1
SI3 Au Avg	1364	1330	0.09	1.24	Unmeasureable	17.7	42.4±2.3
SI3 Pt Nano Avg*	1340	1330	0.14	1.7	Unmeasureable	9.1	38±4.8

*Average offset by outlier

Figure 4.5 shows hydrogen content (%) vs. hydrogen cluster density, where hydrogen content % is extracted from Figure 4.3, hydrogen content (%) vs. normalized

slope of Marchon et al. [29]and hydrogen cluster density calculated as a function of I(D)/I(G) ratio, of the six samples after hydrogenation. The samples before hydrogenation, which are also represented on the graph as starting pristine epitaxial graphene, are of good quality. The I(D)/I(G) <0.22 and fluorescence background (m/I(G) <5) below the noise threshold of the Raman spectra indicate zero H-content. Samples functionalized with no catalyst showed an increase in the I(D)/I(G) ratio and an increase in fluorescence background greater than the noise threshold indicating an increase in sp^3 content as well as hydrogen content. The average hydrogen cluster density observed, 0.7-1.6x10^{11}, is similar to the average electron/hole puddle density from charge impurities (~1-3x10^{11}) [39,40] and defect density (~10^{10}) [41] suggesting that these sites may play a role in hydrogen adsorption on epitaxial graphene.

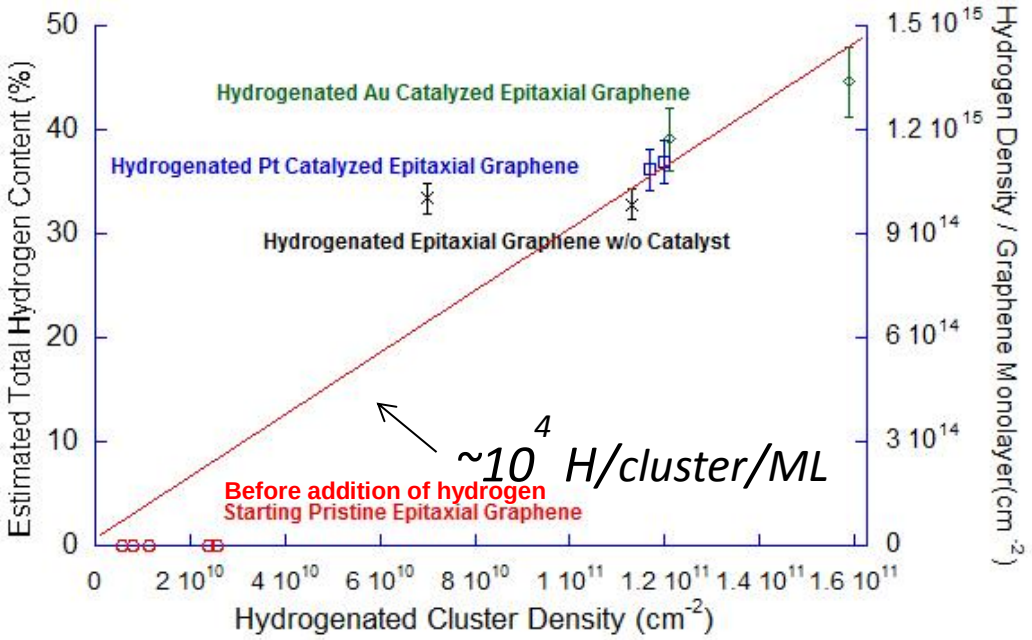

Figure 4.5 Estimated hydrogen content (by Raman) after electrochemical hydrogenation of ~2ML epitaxial graphene films on 6H SiC with and without precious metal (Pt or Au) catalysts. The presence of both Au and Pt catalyst show increases in hydrogenation beyond epitaxial graphene without catalyst.

From the Raman spectra, the hydrogen cluster size, region of the graphene functionalized with hydrogen, was estimated to be ~28.5nm with ~10^4 hydrogen atoms per cluster as shown in Figure 4.6. The intrinsic electron/hole puddle density of graphene, 10^{11} cm^{-2}, was shown to be around the observed hydrogen cluster density, ~10^{11}, suggesting impurities and ripples present in the graphene lattice play a role in hydrogenation. Space between hydrogenated clusters was calculated to be <30nm, decreasing with decreasing density of hydrogenated clusters.

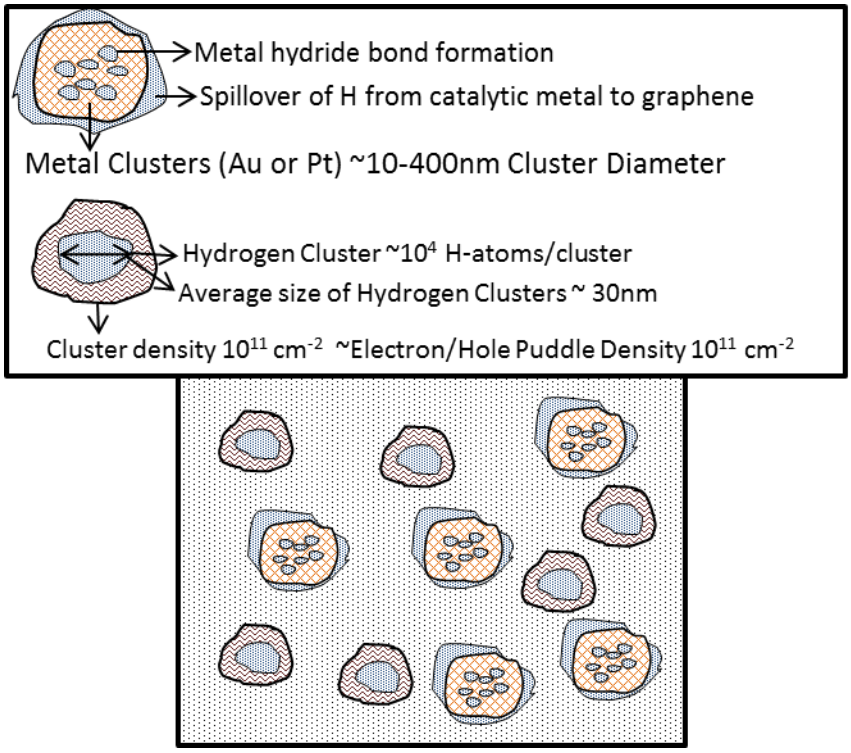

Figure 4.6 Diagram showing random distribution of hydrogen spillover and adsorption on graphene from metal hydride formation and hydrogen adsorption on graphene from possible interactions with electron/hole puddles and defects.

Functionalization with catalytic metals show improvements in hydrogenation with increases in fluorescence and I(D)/I(G) ratio compared to epitaxial graphene without catalyst. Counter to what the literature suggests [11], hydrogen content on average was shown to be higher in Au enhanced hydrogenation than Pt some reasons Au would perform better than Pt:

1) Cluster density geometry favoring Au more than Pt with the presence of more edges in metal clusters allowing for greater hydrogenation [11, 12, 15, and 16].
2) Au has shown to have much greater selectivity to adsorbed species than Pt, particularly with H [18,19]

3) Observed lift of catalyzed metal after electrochemical hydrogenation as shown by AFM in Figure 4.3.

Despite this, the different dispersions observed of Pt and Au as shown by AFM makes it impossible to determine if these effects are directly involved in observed enhanced hydrogenation in graphene.

4.7. SUMMARY OF METAL CATALYZED HYDROGENATION

The present study shows enhanced electrochemical hydrogenation of epitaxial graphene by chemically deposited and evaporated metals to reduce activation energy and improve hydrogen incorporation in graphene. The introduction of catalytic metals has shown to improve electrochemical functionalization with H-content as much as 42% seen with aqueous Pt nanoparticles and evaporated Au. This opens up potential for composite carbon on semiconductor scaffolds, as well as contact in fuel cells for electricity generation. Contrary to what is typically observed in literature, gold on EG demonstrated higher catalytic activity than platinum. One possible reason for the difference in hydrogen incorporation could be due to the weak adsorption gold has with hydrogen, allowing it to be adsorbed by graphene much easier than strongly adsorbed hydrogen on platinum. How well the metals adhere to the EG surface throughout functionalization, particle size, as well as the geometry of the metal on graphene can also have an effect on catalytic activity.

REFERENCES

[1] J. O. Sofo, A.S. Chaudhari, G. D. Barber., Physical Review B 75, 153401 (2007)

[2] R. Zan, Q. M. Ramasse, R. Jalil and U. Banger ,. Atomic Structure of Graphene and h-BN Layers and Their Interactions with Metals, Advances in Graphene Science, Dr. M. Aliofkhazraei (Ed.), ISBN: 978-953-51-1182-5, InTech, DOI: 10.5772/56640. (2013)

[3] S. Ryu, M. Y. Han, J. Maultzsch. T. F. Heinz, P. Kim, M. L. Steigerwald and L. E. Brus., Nano Lett., Vol. 8, No. 12, 2008

[4] D. C. Elias, R. R. Nair, T. M. G. Mohiuddin, S. V. Morozov, P. Blake, M. P. Halsall, A. C. Ferrari, D. W. Boukhvalov, M. I. Katsnelson, A. K. Geim, K. S. Novoselov.**,** Science 30, Vol. 323, No. 5914, 610-613 (2009)

[5] C. Riedl, C. Coletti, T. Iwasaki, A. A. Zakharov and U. Starke., PRL 103, 246804 (2009)

[6] K. M. Daniels, B. K. Daas, N. Srivastava, C. Willams, R. M. Feenstra, T. S. Sudarshan, MVS Chandrashekhar., J. Appl. Phys. 111, 114306 (2012)

[7] A. C. Dillon, M. J. Heben., Appl. Phys. A 72, 133-142 (2001)

[8] P. Maity, S. Basu, S. Bhaduri, G. K. Lahiri., Advanced Synthesis & Catalysis 349, Issue 11-12, 1955-1962 (2007)

[9] A. S. Hussey, G. W. Keulks, G. P. Nowack, R. H. Baker., Journal of Organic Chemistry 33, No. 2, 610-616 (1986)

[10] C. Nwosu.,Journal of Technical Science and Technologies, 1(2):25-28, (2012)

[11] K. Okazaki-Maeda, T. Akita, S. Tanaka and M. Kohyama., Materials Transactions, Vol. 49, No. 11, 2441-2444 (2008)

[12] G. A. Somorjai et al., Nature Vol. 258 (1975)

[13] E. Bus, J. T. Miller, J. A. van Bokhoven., J. Phys. Chem. B 109, No. 30, 14581-14587 (2005)

[14] M. Haruta.,Catalysis Today 36, 153-166 (1997)

[15] A. S. Hussey, G. W. Keulks, G. P. Nowack, R. H. Baker., Journal of Organic Chemistry 33, No. 2, 610-616 (1986)

[16] C. Kartusch and J. A. van Bokhoven., Gold Bulletin 42, No. 4, 343-348 (2009)

[17] M. K. Oudenhuijzen, J. H. Bitter, and D. C. Koningsberger., J. Phys. Chem. B 105, 4616-4622 (2001)

[18] P. Claus., Applied Catalysis A : General 291 (2005) 222-229

[19] T. Mitsudome and K. Kaneda., Gold nanoparticle catalysts for selective hydrogenations., Green Chem. Advance Artlcle (2013) DOI:10.1039/C3GC41360H

[20] D. J. Gorin, F. D. Toste., Nature 446, 395-403 (2007)

[21] B. K. Daas, K. Daniels, S. Shetu, T. S. Sudarshan, and M. V. S. Chandrashekhar, Mater. Sci. Forum **717–720**, 633–636 (2012).

[22] J. Rand, Electroanal. Chem **35**, 209–218 (1972).

[23] K. Ota, S. Nishigori, and N. Kamiya, J. Electroanal. Chem. **257**, 205–215 (1988).

[24] C. Srinivasan and R. Saraswathi., Current Science 97, Vol. 97, No. 3 (2009)

[25] C. Casiraghi, A. C. Ferrari, and J. Robertson., Physical Review B **72**, 085401 (2005)

[26] J. Schwan, S. Ulrich, V. Batori, H. Ehrhardt, S. R. P. Silva., J.Appl.Phys.,Vol.80,No.1(1996)

[27] A.C. Ferrari and J.Robertson., Phys.Rev. B 61, 14095-14107 (2000)

[28] B. Wang, J. R. Sparks, H. R. Gutierrez, F. Okino, Q. Hao et. al., Appl. Phys. Lett. 97, 141915 (2010)

[29] B. Marchon, J. Gui, K. Grannen, G. C. Rauch, J. W. Ager III, S. R. P.Silva, and J. Robertson, IEEE Trans. Magn. 33(5), 3148–3150 (1997)

[30] A.Siani, K. R. Wigal, O.S Alexeev, M.D Amiridis., Journal of Catalysis 257 (2008) 5–15

[31] A. Tiberj et al.,Sci. Rep. 3, 2355 (2013)

[32] Cançado et al., *Nano Lett.*, **2011**, 11 (8), pp 3190–3196

[33] B. J. Wood and H. Wise., Journal of Catalysis 5, 135-145 (1966)

[34] M. Lazar, C. Ducu, V. Almasan, N. Aldea, B. Barz, P. Marginean, C. Sutan, V. Malinnovschi, Rom. Journ. Phys. Vol. 51, No. 1-2, 299-304 (2006)

[35] B. Dren, D. Hug, L. Marot, R. Pawlak, M. Kisiel, R. Steiner, D. M. Zumbühl and E. Meyer., Bellstein J. Nanotechnol. 3, 852-859 (2012)

[36] M. Woitaszek, N. Tombros, A. Caretta, P. H. M. van Loosdrecht and B. J. van Wees., J. Appl. Phys. 110, 063715 (2011)

[37] J.D. Jones, K. K. Mahajan, W. H Williams, P. A. Ecton, Y. Mo, J. M. Perez., Carbon 48, Issue 8, 2335-2340 (2010)

[38] M. Pumera and C. H. A. Wong., Chem. Soc. Rev 42, 5987 (2013)

[39] A.E. Curtin. *Kelvin Probe Microscopy Studies of Epitaxial Graphene on SiC(0001)*. Dissertation, University of Maryland, Digital Repository at the University of Maryland, 2011. (http://hdl.handle.net/1903/12004)

[40] S. Adam, S. Jung, N. N. Klimov, N. B. Zhitenev, J. A. Stroscio and M. D. Stiles., Phys. Rev. B 84, 235421 (2011)

[41] J. Hwang, C. Kuo, L. Chen, K, Chen., Nanotechnology **21,** 465705(2010)

CHAPTER 5

THERMAL AND ELECTROCHEMICAL HYDROGEN REMOVAL

While these Raman signatures are compelling evidence of successful hydrogenation, they can also be interpreted on the basis of lattice damage, which would provide similar changes in the Raman spectrum [1]. Therefore, to provide further evidence apart from substrate dependence, a reversal of hydrogenation back to EG was performed by high temperature thermal anneal [2-6]. This reversal is possible due to low bonding energy of only 0.4eV per bonded hydrogen, allowing for hydrogenation of graphene to be thermally reversible [7]. For proof of concept, thermal anneal was performed on hydrogenated samples to remove hydrogen.

5.1: DESORPTION OF HYDROGEN BY THERMAL ANNEAL

Hydrogenated graphene was annealed in vacuum for at 1000°C. The Raman spectra of the area (Fig.5.1) after reversal clearly shows the disappearance of the C-H peak at ~2930cm-1 indicating desorption of hydrogen in the material. After the 4 hour anneal, however, an I(D)/I(G) ratio of ~ 1 indicated that the material remained partially hydrogenated. With hydrogen still present, a 50 hour anneal was performed to ensure that hydrogen was desorbed from graphene.

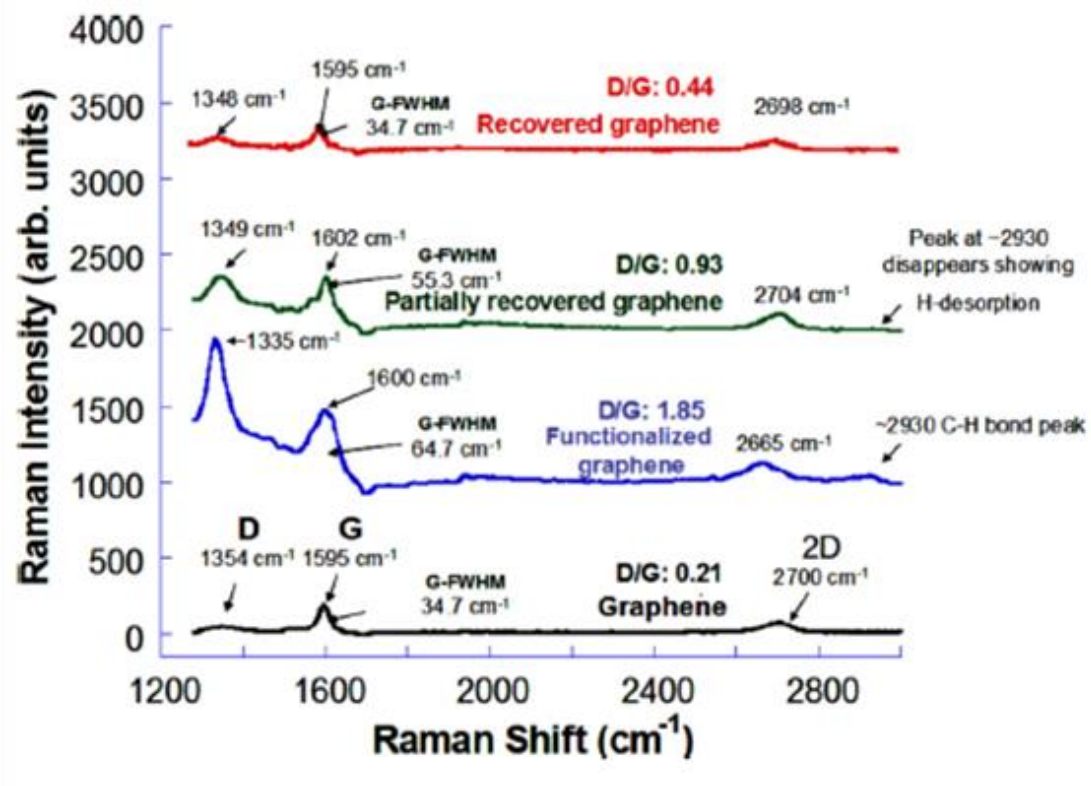

Figure 5.1 Raman spectra showing thermal anneal of hydrogenated EG

After the 50 hour anneal, the D peak shifted back to pre-conversion state at 1340 cm^{-1} and the fluorescence background was no longer present. While the D and 2D peaks shifted back to pre-conversion positions and the G-peak FWHM decreased, the resulting I(D)/I(G) ratio of 0.4, up from the starting EG at 0.1, was most likely caused by the strain induced during the hydrogenation and reversal [1]. This strain has its origin in the difference in atomic structure between graphene and hydrogenated graphene as discussed previously [6]. Unfunctionalized EG samples grown on Si-face, a and m planes, with varying I(D)/I(G) ratios were also annealed to eliminate the possibility of thermal "healing" of disorder. They were subjected to a similar 72 hour thermal anneal at 1000°C. As shown in Table 5.1, I(D)/I(G) ratio before and after anneals were identical in unfunctionalized EG but substantially reduced in hydrogenated graphene. This clearly

shows that the decrease in I(D)/I(G) is due to the desorption of hydrogen (or other functional groups) in hydrogenated graphene, and not by self-healing of disorder.

Table 5.1: Thermal anneal of hydrogenated EG with nanocrystalline graphene as control

Sample	Pristine EG I(D)/I(G) Ratio	After Electrochemical Hydrogenation I(D)/I(G) Ratio	After Thermal Anneal I(D)/I(G) Ratio
Si-face EG (Funct.)	0.21	1.85	0.44
Si-face EG	0.10		0.10
a-Plane EG	0.64		0.63
m-Plane EG	0.71		0.71

5.2: ELECTROCHEMICAL REVERSAL OF HYDROGENATION

While thermal reversibility does distinguish hydrogenation from damage, it doesn't, however, offer a practical means for hydrogen desorption in applications such as hydrogen storage. For microbial fuel cells and solid state hydrogen storage, graphene must be able to bond and release hydrogen at much lower temperatures (>100 °C) to be energy efficient. Other means of graphene hydrogenation shown in Chapter 2 offer only one way hydrogenation, with thermal anneal needed to remove the hydrogen incorporated

[2-6]. Hydrogen desorption by potential reversal of the electrochemical cell is shown, demonstrating a practical means for hydrogen desorption, with application to carbon-hydride batteries.

5.2.1 CYCLIC VOLTAMMETRY

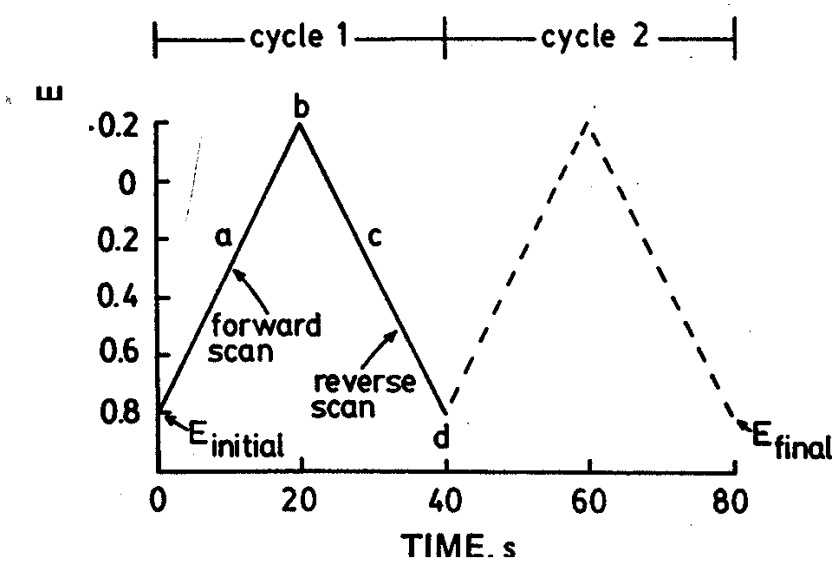

Figure 5.2 Potential sweep used in cyclic voltammetry over time

Cyclic voltammetry (CV) is an electrochemical technique where the energy potential of the working electrode is swept, as shown in Figure 5.2 and the resulting current is measured. In doing so, the potential(s) of oxidation and reduction are displayed as extrema points on a cyclic voltammogram as. The voltammogram gives information on oxidation and reduction, electron transfer mechanisms as well as adsorption processes between the working electrode and the analyte [8].

5.2.2 EXPERIMENTAL SETUP

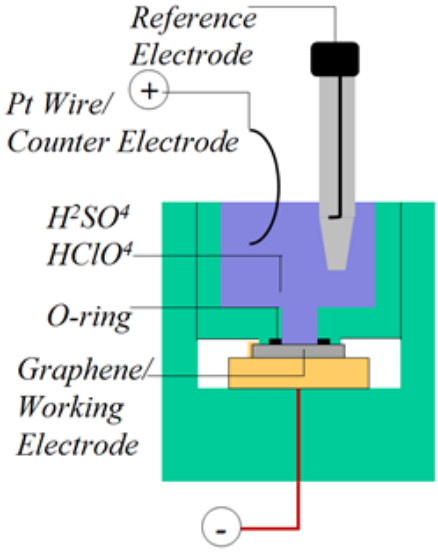

Figure 5.3 Three terminal electrochemical cell with reference electrode to ensure accuracy and repeatability of the measurement

To ensure accurate oxidation and reduction potentials, the electrochemical cell was upgraded to a three terminal system as shown in Figure 5.3, with the addition of a reference electrode and the use of a potentiostat. . A potentiostat (Series GTM 300, Gamry Instruments, Warminster, PA, USA) was used for potential holds and CV measurements. With the use of H_2SO_4 electrolyte, a mercury/mercurous sulfate ($Hg/HgSO_4$) reference electrode in saturated potassium sulfate (K_2SO_4), 0.64V versus normal hydrogen electrode, was used as dilute and concentrated H_2SO_4 does not react with Hg.

5.2.2 DEMONSTRATION OF HYDROGEN DESOPRITON BY POTENTAL REVERSAL

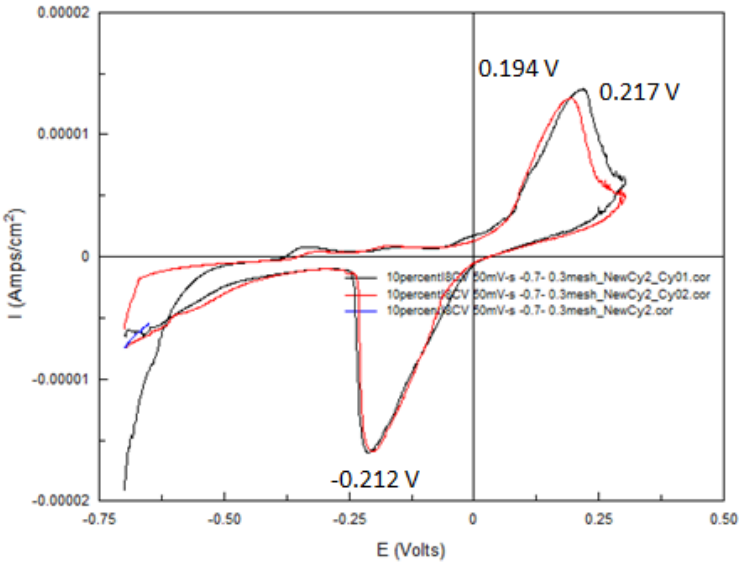

Figure 5.4 Cyclic voltagram of electrochemical cell with graphene as the working electrode.

In the electrochemical hydrogen reversal experiment oxidation (0.217 V vs. $Hg/HgSO_4$ [0.64 vs. NHE]) and reduction (-0.212 V vs. $Hg/HgSO_4$ [0.64 V vs. NHE]) potentials were obtained by CV as shown in Figure 5.4. Using these potentials, samples were first held above the hydrogen loading potential observed from CV at -0.3V versus reference to ensure hydrogenation, confirmed with Raman. Through Raman, as shown in Figure 5.5, an increase in I(D)/I(G), from 0.15 to 0.37 and blue shifts in peak positions was observed after the first hydrogenation. A small fluorescence background was also observed after functionalization. The samples were then held above the hydrogen unloading potential at 0.3V and checked again, Raman confirming removal of hydrogen.

Dehydrogenation of graphene showed decrease in I(D)/I(G), 0.167 close to that of pristine EG at 0.146, though G and 2D peaks were significantly blue shifted beyond

pristine EG suggesting bonding with another functional group. This is further supported by the addition of a fluorescence differing from that observed with hydrogenated EG and similar to spectra observed with graphene oxide. Sulfur groups from the acid are believed to be responsible for this behavior, as SO_4^{-2} ions are known to passivate C-surfaces in hydrocarbon polymers. The 2nd hydrogenation of the sample supports this claim with increase in I(D)/I(G) to 0.326, less than that of the first hydrogenation, suggesting energy was required to remove functional groups from the oxidation cycle before hydrogenation of the sample could take place.

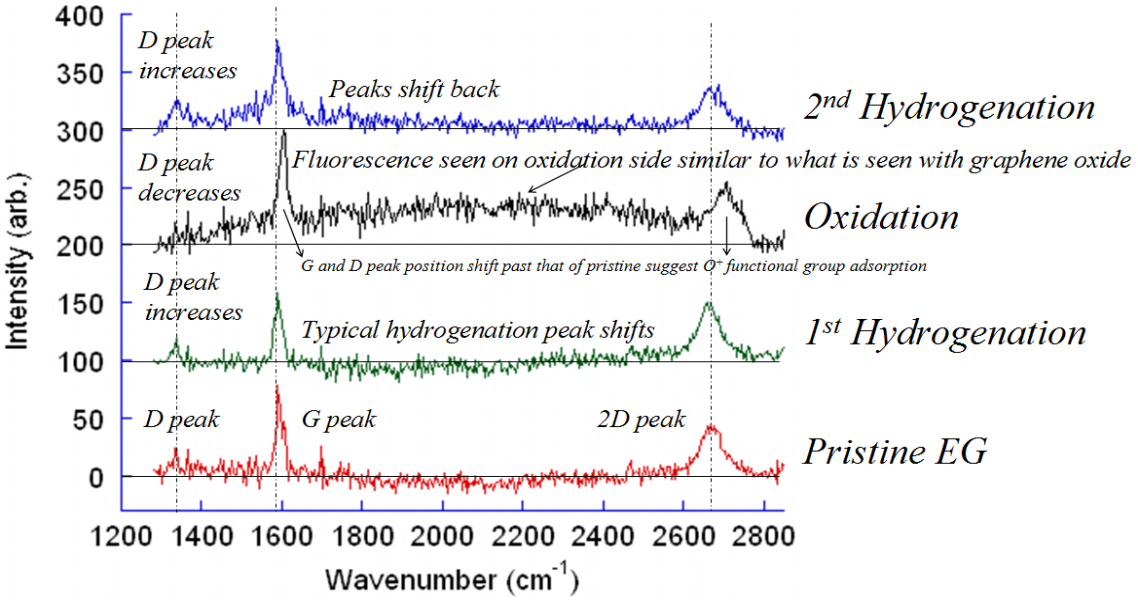

Figure 5.5 Raman spectra of electrochemical cycling of hydrogen on EG.

Detailed values obtained with Raman are shown in Table 5.2. G peak width was observed to increase after each cycle, suggesting damage/strain in the lattice caused by the changing C-C bond length after each cycle. Changes in I(D)/I(G) ratio shows clear hydrogen adsorption and desorption with a decrease in functionalization shown after

hydrogen unloading due to the addition of non-hydrogen functional groups. These results show that graphene hydrogenation is reversible electrochemically and history dependent. This process demonstrates a new pathway to hydrocarbon bond formation for synthesis of advanced organic/inorganic carbon-based compounds.

TABLE 5.2. Raman Spectra Data from Hydrogen Cycling Experiment

Cycles	**D peak position (cm^{-1})**	**G peak position (cm^{-1})**	**2D peak position (cm^{-1})**	**I(D)/I(G)**	**D peak width (cm^{-1})**	**G peak width (cm^{-1})**	**2D peak width (cm^{-1})**
Pristine EG	1339	1593	2671	0.15	41.8	18.7	67.1
1^{st} H-Loading	1335	1591	2663	0.37	25.3	21.9	63.3
H- Unloading	1345	1604	2705	0.17	86.2	22.8	83.7
2^{nd} H-Loading	1339	1590	2669	0.33	45.6	26.6	81.3

REFERENCES

[1] A.C. Ferrari and J.Robertson., Phys.Rev. B 61, 14095-14107 (2000)

[2] S. Ryu, M. Y. Han, J. Maultzsch. T. F. Heinz, P. Kim, M. L. Steigerwald and L. E. Brus., Nano Lett., Vol. 8, No. 12 (2008)

[3] M. Wojtaszek, N. Tombros, A. Caretta, P. H. M. van Loosdrecht, B. J. van Wess J. Appl. Phys. 110, 063715 (2011)

[4] R. Balog, B. Jørgensen, J. Wells, E. Lægsaard, P. Hofmann, F. Besenbacher, L. Hornekær., J. Am. Chem. Soc. 131, 8744-8755 (2009)

[5] J. D. Jones, K. K. Mahajan, W. H. Williams, P. A. Ecton, Y. Mo, J. M. Perez., Carbon 48, Issue 8, 2335-2340 (2010)

[6] Jorge O. Sofo, Ajay S. Chaudhari, Greg D. Barber., Physical Review B 75, 153401 (2007)

[7] D.W. Boukhvalov and M.I. Katsnelson., J.Phys.:Condes. Matter 21, 344205 (2009)

[8] P. T. Kissinger and W. R. Heineman., J. Chem. Educ. 60, Issue 9, 702 (1983)

CHAPTER 6

MECHANISM OF ELECTROCHEMCAL HYDROGENATION

In this chapter, we investigate mechanisms of hydrogenation as observed by cyclic voltammetry (CV) and electrochemical impedance spectroscopy (EIS). Through observations in hydrogen adsorption, the reactivity of carbon electrodes can be better understood. Degree of hydrogenation was suspected to be either dependent on the underlying SiC, more specifically on the off-cut angle in the 11-20 direction, or on the quality of starting EG, where hydrogenation may be due at least partially to defects [1]. To further understand this dependence, the electrochemical characteristics of these electrodes are studied. To test the electrochemical characteristics of the graphene electrodes and further understand the nature of graphene for its use as an electrode material, Raman spectroscopy, cyclic voltammetry and electrochemical impedance spectroscopy will be used.

6.1. ELECTROCHEMICAL IMPEDANCE SPECTROSCOPY

Electrochemical Impedance Spectroscopy (EIS) uses the frequency response of an electrochemical system to obtain detailed information on the kinetics of electrochemical cells, or in our case, the kinetics and reactivity of hydrogen on graphene. Electrochemical cells are not linear so in this technique we input a small AC signal with the form

$$E(t) = E_0 \cos(2\pi f t) \quad (1)$$

,where E(t) is the potential as a function of time, E_0 is the signal amplitude and f is the frequency, is applied to an electrochemical cell and the output is measured. By imputing a small enough signal, as shown in Figure 6.1, the electrochemical system can become pseudo-linear with linear output,

$$I(t) = I_0 \cos(2\pi f t - \emptyset) \quad (2)$$

that changes amplitude, I_0, and phase, φ.

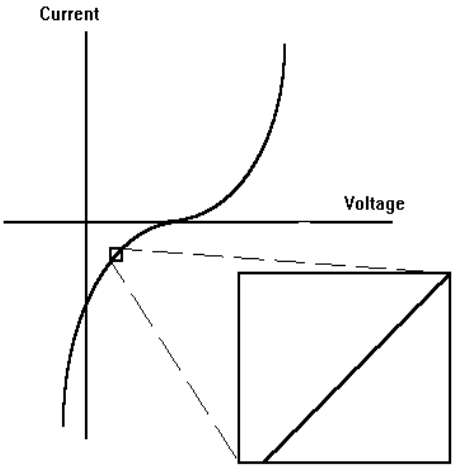

Figure 6.1 Psuedo linear response to small excitation signal

With input and output known, we treat the cell as transfer function, with each component used in the model signifying some physical electrochemical behavior occurring in the cell (i.e. adsorption or diffusion of ions). This impedance is represented by

$$Z(t) = \frac{E(t)}{I(t)} = \frac{E_0 \cos(2\pi f t)}{I_0 \cos(2\pi f t - \emptyset)} = Z_0 \frac{\cos(2\pi f t)}{\cos(2\pi f t - \emptyset)} \quad (3)$$

which can be expressed as a complex function using Euler's formula resulting in

$$Z = \frac{E}{I} = Z_0(\cos\emptyset + i\, sin\emptyset) \quad (4)$$

composed of real and imaginary impedance. From this expression, a Nyquist plot can be made from the real and imaginary parts of the impedance, giving information on electrochemical processes happening in the cell.

EIS is used to not only acquire information regarding the electrolyte/electrode interface but kinetics and reactions that take place with the electrode [2].The input frequency is swept to observe the diffusion and adsorption processes that occur within the cell, with conduction and reactions occurring at higher frequencies and diffusion occurring at lower frequencies. EIS data is analyzed by fitting to an equivalent circuit model. To be useful, an accurate model must be built with bearings to the physical electrochemistry of the system. The equivalent circuit model is generally made up of elements such as capacitors and resistors with the exception of a few elements such as constant phase element (CPE) and Warburg (W) elements used to model surface roughness/non uniform surface reaction sites and diffusion in the electrode [3]. To determine the material dependence on electrochemical hydrogenation four different EG samples (Si-face EG [~2ML], C-face EG [~10ML], M-plane EG [~25ML] and defective Si-face EG [>50ML]) and a smooth graphite disk [>500ML] were characterized by Raman spectroscopy, CV and EIS.

6.2. EIS EXPERIMENTAL SETUP

Growth of EG was prepared by thermal decomposition of Si from SiC from different substrates in vacuo , $<10^{-5}$ Torr, using an RF furnace previously described in more detail [30]. 10 x 10mm^2 6H SiC semi-insulating samples were chemical-mechanical

polished (CMP) and thoroughly cleaned using standard RCA clean (Trichloroethylene [TCE], acetone, methanol) and HF to remove any native oxide.

Raman spectroscopy was used to determine the defect density of grown EG. Raman was performed using a micro-Raman setup with laser excitation wavelength at 632nm and a spot size of ~2 μm. The Raman system was calibrated using the known Si peak at 520.7 cm^{-1}. Reference blank SiC substrate spectra were scaled appropriately and subtracted from the EG/SiC spectra to show only the graphene peaks [4]. Defect density of each sample was calculated using the relation n_D (cm^{-2})=(1.8 x 10^{22}/(λ^4))*(I(D)/I(G)), where λ is the excitation wavelength of the Raman and I(D)/I(G) is the ratio between the peak intensity of the D and G peak [5].

Electrochemical measurements were carried out in 1.84 M $HClO_4$ using a three electrode home-built electrochemical cell where a 99.6% Pt wire and exposed EG (approximately a 4mm diameter circular area) were used as the anode and cathode, respectively with a Ag/AgCl reference (0.198 V vs. NHE) electrode. A potentiostat (Series GTM 300, Gamry Instruments, Warminster, PA, USA) was used for CV and EIS measurements. CV was performed to determine oxidation and reduction potentials at a scan rate of 50mV s^{-1}. Spectra from EIS were measured over frequencies ranging from 300 kHz down to 0.1 Hz as a function of time and potential with a perturbation signal of 10 mV. Since system stability is important for obtain accurate data, impedance measurements were taken after reaching a system steady state after holding the potential constant.

6.3. EIS OF ELECTROCHEMICAL CELL

Figures 6.2-6.5 show CV and EIS data obtained from various carbon materials, bulk graphite, C-face graphene, Si-face graphene and defective Si-face graphene. Oxidation and hydrogenation peaks observed in the CV of the graphite disk, Figure 6.2, were not well defined, most likely due to layer inaccessibility to the solution and subsequent hydrogen ions. Defects in the material could mediate this high diffusion, supplying sites for hydrogen to easily penetrate. To test this hypothesis further, we look at a sample with very low defect density.

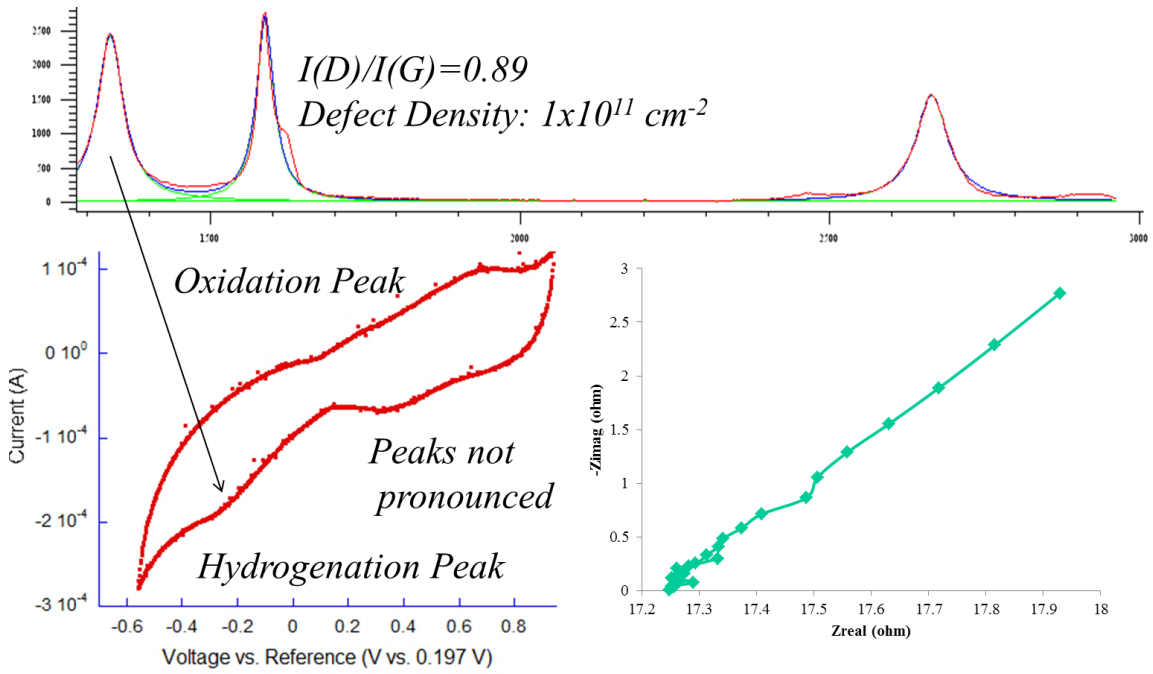

Figure 6.2. Raman, CV and EIS data of a smooth graphite disk.

C-face EG, Figure 6.3, showed an absence of hydrogenation peak most likely due to the lack of point defects in the material as I(D)/I(G)~0. This suggests that grain boundaries in the material are not as electrochemically active as vacancies as previously thought and that functionalization is dependent instead on the presences of point defects

in the material. This is further supported by a straight line in the high frequency regime in the EIS nyquist plot showing surface adsorption of hydrogen to the graphene electrode but little charge transfer, or C-H bonding, similarly observed with closed carbon nanotubes [6]. The large charge transfer resistance observed in EIS showed the system as being kinetically slow, likely due to inaccessibility of hydrogen ions through the chemically unreactive basal plane of graphene The Nyquist plot supports this, showing little charge transfer in the high frequency regime.

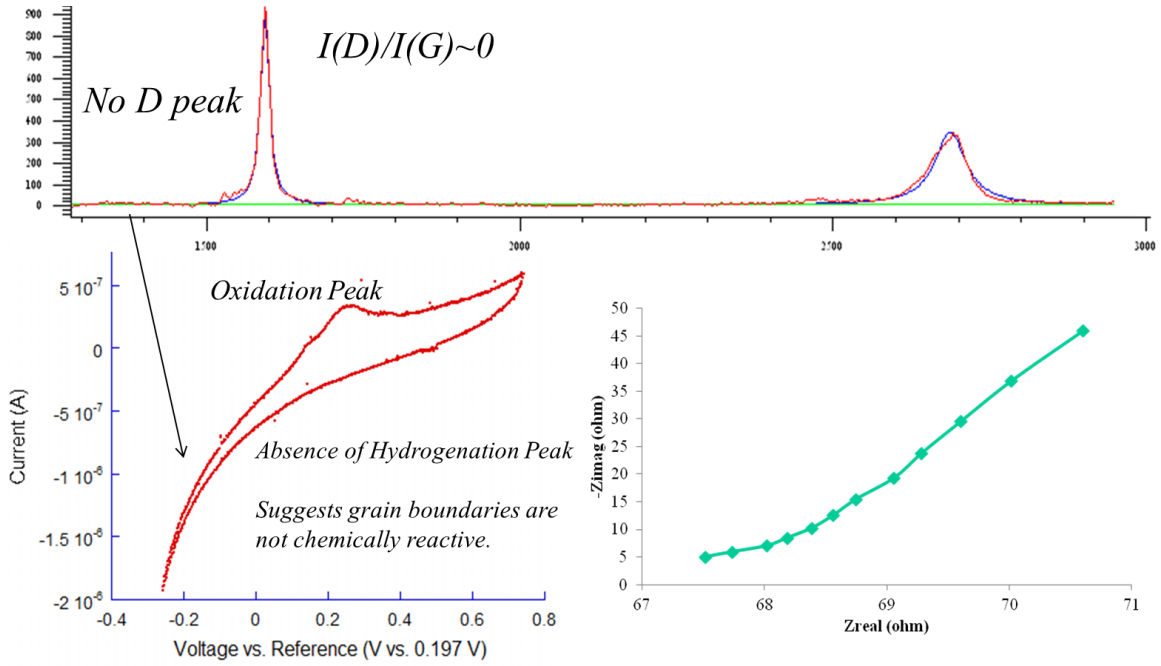

Figure 6.3. Raman, CV and EIS data of C-face EG.

Si-face EG, Figure 6.4, showed a sharp hydrogenation peak most likely due to point defects present in the material, I(D)/I(G)~0.08. This is further supported by the plateau observed in the high frequency regime in the EIS Nyquist plot showing charge transfer to the graphene electrode. The large charge transfer resistance shown in the EIS however, shows the system is kinetically slow.

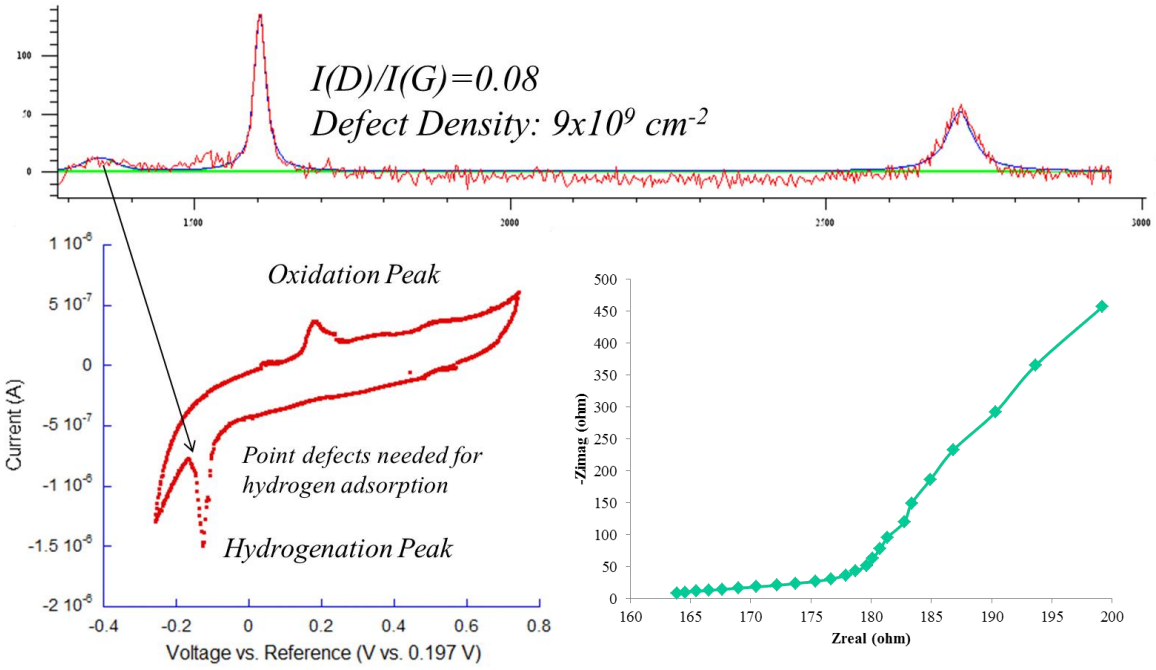

Figure 6.4. Raman, CV and EIS data of Si-face EG.

Defective Si-face EG, Figure 6.5, further supports dependence on the presence of defects present in the material, as the system revealed a semicircle in the high frequency regime. The diameter of the semicircle revealed a kinetically fast system with ample sites for hydrogen to diffuse and adsorb within the graphene lattice. This data suggests that there may not be a substrate to substrate dependence in electrochemical functionalization but a dependence on the quality of the EG film grown on it, with more defective EG ideal for electrochemical hydrogenation. To obtain quantitative information regarding the EIS data, an electrochemical model was designed to accurately model the resistive and capacitive nature of the electrochemical cell.

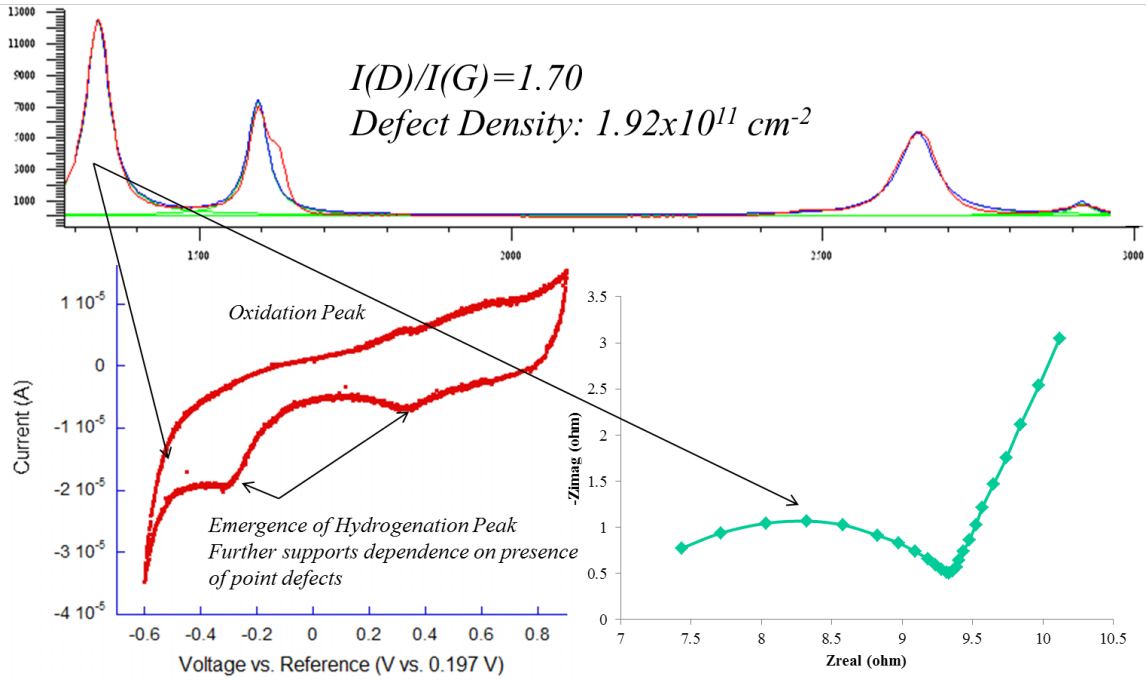

Figure 6.5. Raman, CV and EIS data of defective Si-face EG.

6.4. ELECTROCHEMICAL MODEL

Based on oxidation and reduction points observed in CV, we suspect hydrogen to be the only adsorbed species in the system. For a single adsorbed species, in our case hydrogen, we modeled the electrochemical cell from the equivalent circuit for the case of one adsorbed species [7]. A Warburg element was added to take into account diffusion of ions in the electrolyte through the graphene lattice.

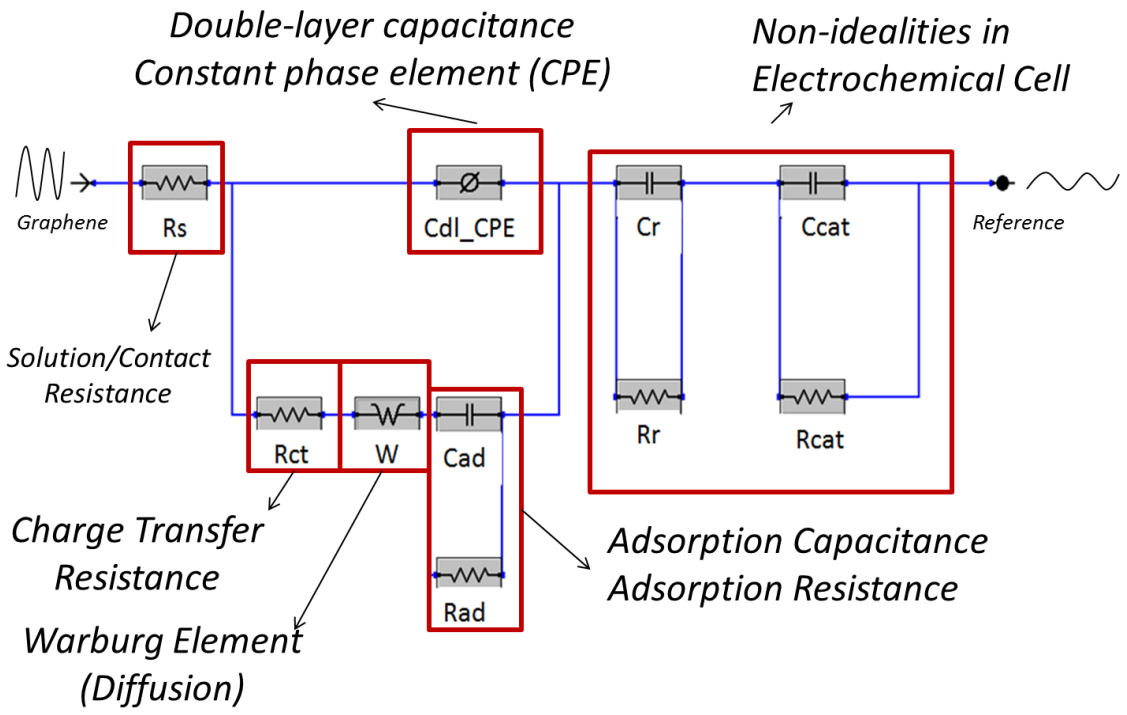

Figure 6.6 Electrochemical Impedance Model for graphene electrochemical cell

In the electrochemical impedance model in Figure 6.6 R_s represents the solution resistance; C_{dl_CPE} is the double layer capacitance as a constant phase element to account for surface roughness and nonuniform distribution of reaction sites in the electrode; R_{ct} is the charge transfer resistance; W is the Warburg element; R_{ad} is the resistance formed by adsorbed species on the working electrode; C_{ad} represents the adsorption pseudocapacitance of the adsorbed species; R_r, R_{cat}, C_r, C_{cat} represent non-idealities in the electrochemical cell manifested as additional time constants in the electrochemical reaction [8]. As shown in Figure 6.7, 6.8 and 6.9, the bode plot and Nyquist plot agrees with this model.

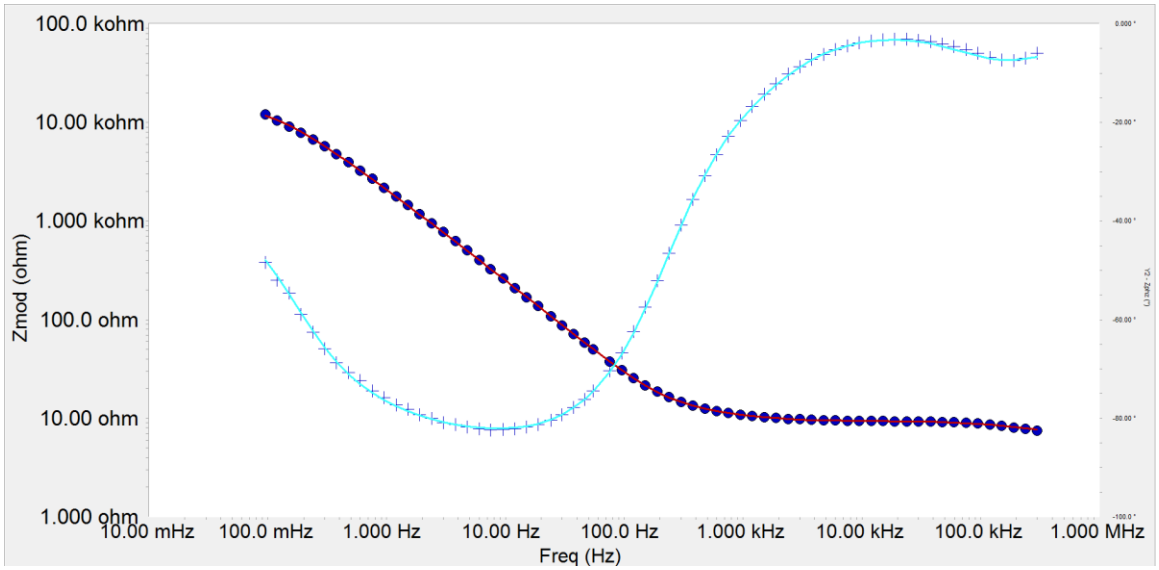

Figure 6.7 Bode Plot of defective Si-face graphene with impedance model fit

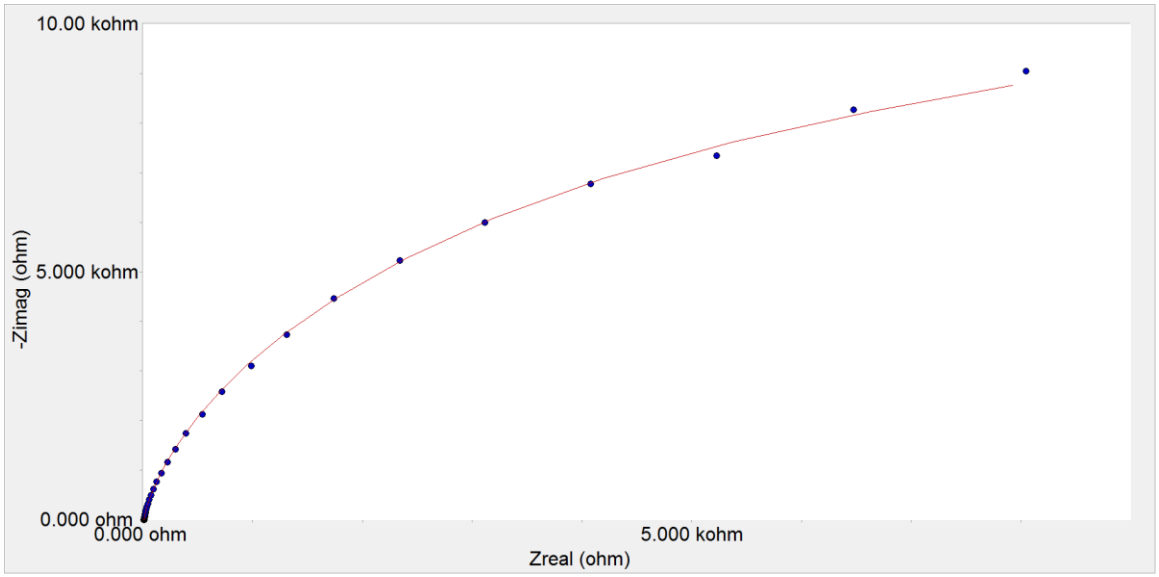

Figure 6.8 Full Nyquist plot of defective Si-face graphene with impedance model fit

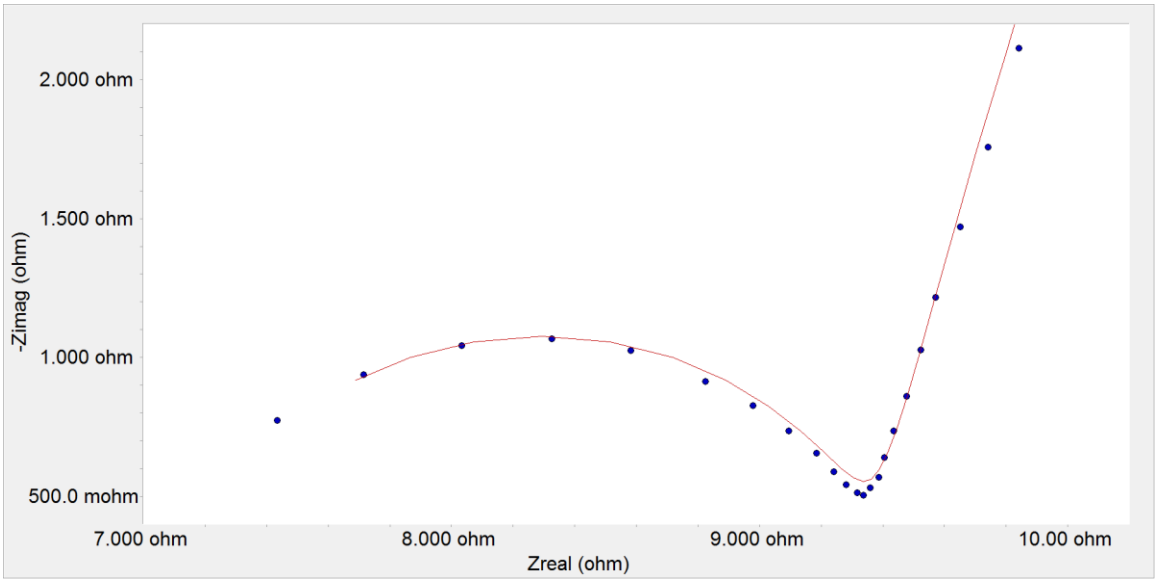

Figure 6.9 High frequency Nyquist range of defective Si-face graphene with impedance model fit

6.5. EIS MODEL ANALYSIS

The resulting charge transfer and adsorption resistance obtained from the EIS model fit was plotted as a function of electrode defect density, Figure 6.10. A dependence on charge transfer and adsorption and defect density is established, with increasing defect density resulting in decreases in both resistances. This can be attributed to better ion diffusion through defects over pristine EG resulting in additional sites for hydrogen to adsorb and form C-H bonds as compared to the inert basal plane of EG.

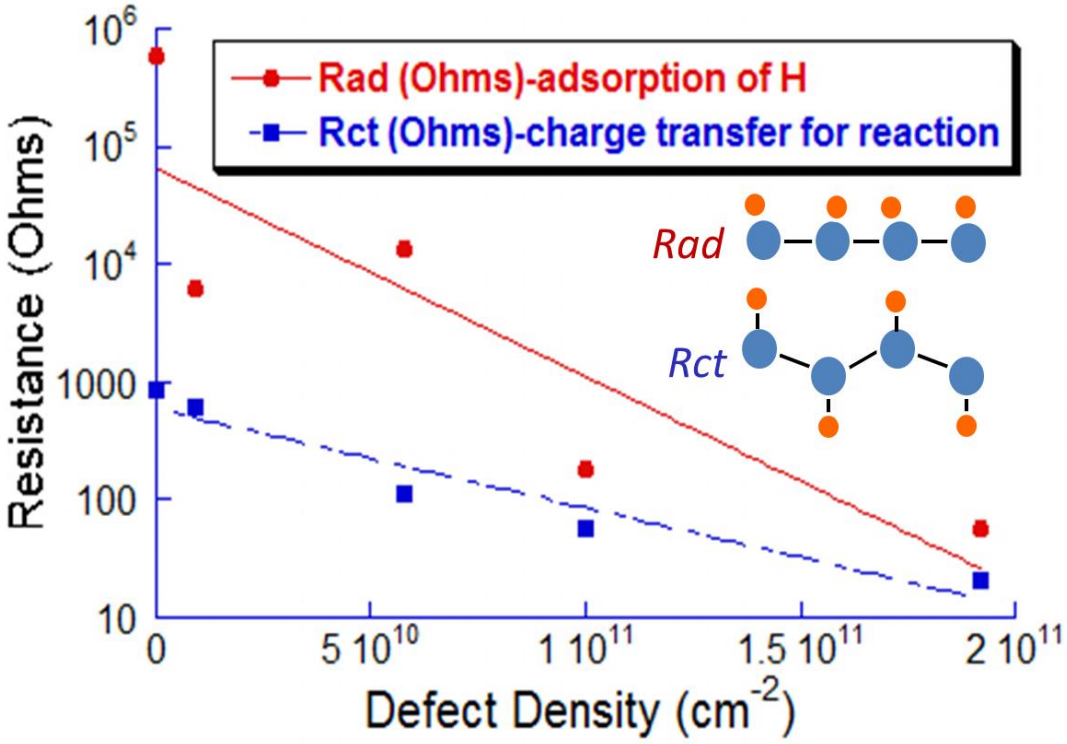

Figure 6.10 Adsorption and charge transfer resistance extracted from EIS impedance model

This hypothesis is further supported by increases in Warburg impedance suggesting higher diffusion in more defective electrodes in Figure 6.11. Additional adsorption sites for hydrogen are supported by increases in double layer capacitance with increasing defect density as shown in Figure 6.12. With more ions on the electrode as shown with the Warburg and double layer capacitance, one would expect the resulting adsorption capacitance to also increase with defect density.

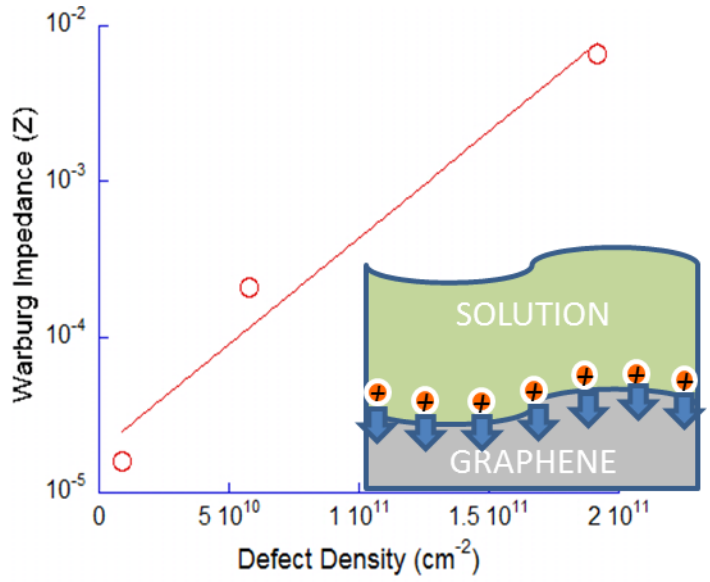

Figure 6.11 Warburg impedance normalized to a single graphene monolayer with diagram of ion diffusion into graphene

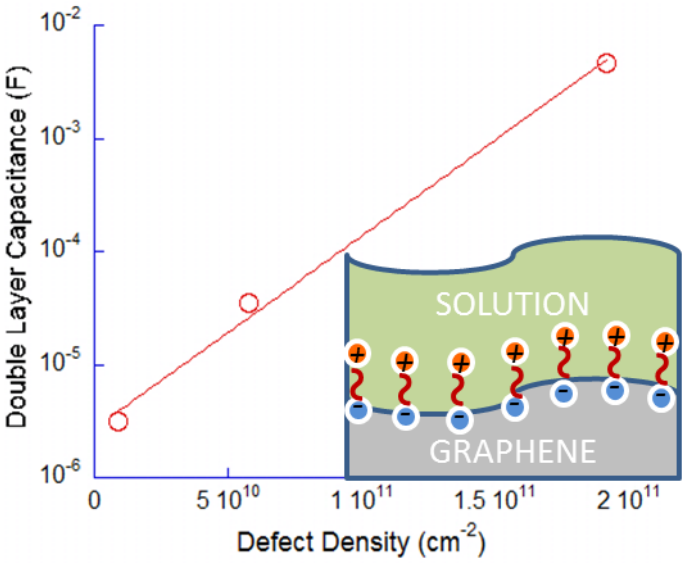

Figure 6.12 Double layer capacitance normalized to a single graphene monolayer with diagram of charges separated by small space on the order of angstroms

The pseudocapacitance represents the capacitance formed by adsorption of ions on the electrode surface. As shown in Figure 6.13, an increase in adsorption capacitance is observed at a small increase in defect density. When defect density is increased further, pseudocapacitance decreases exponentially. This is caused by an increase in internal surface area greater than the external surface area, where defects at as micropores allowing ions access to underlying monolayers of graphene. This, however, results in an increased contribution from double layer capacitance as observed in Figure 6.12[9]. To see this effect further, total capacitance of the electrochemical cell, capacitance derived from CV and specific capacitance was calculated.

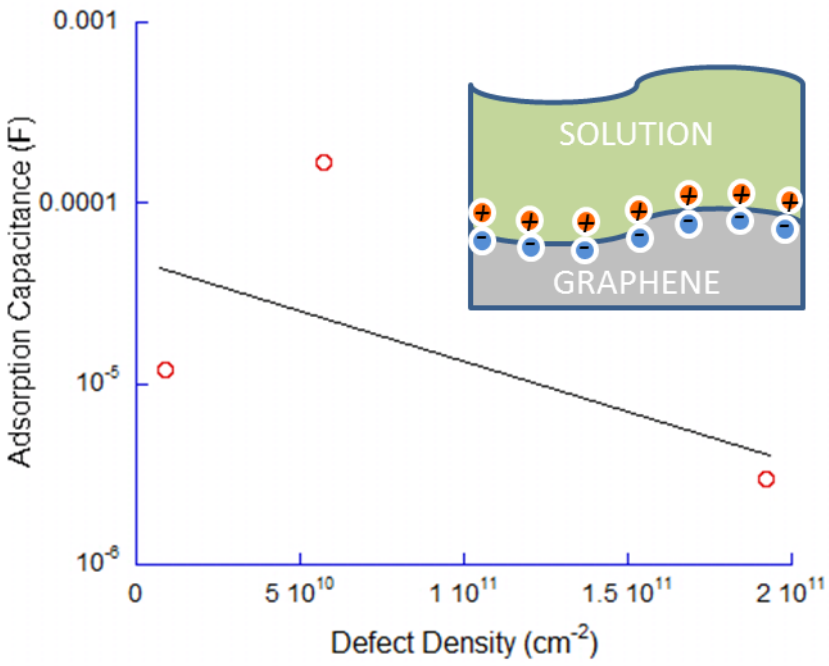

Figure 6.13 Adsorption capacitance normalized to a single graphene monolayer with diagram of adsorbed charges forming a pseudocapacitance

6.6. SPECIFIC CAPACITANCE

Specific capacitance, or capacitance per unit weight, was calculated by integrating under the curve obtained from cyclic voltammetry for each electrode, then dividing by the scan rate and the electrode weight [10]. Since graphene is grown on an insulating SiC substrate, only the weight of the graphene is considered. Capacitance obtained from cyclic voltammetry was found to be in close agreement with the effective capacitance of the electrodes obtained from fits of the EIS model data for electrode. As observed in Table 6.1, specific capacitance increases with increasing defect density, further evidence that graphene's performance as an electrode and the degree of hydrogenation electrochemically are dependent on defect density.

Table 6.1. Effective, Integrated and Specific Capacitance of Graphene Electrodes

	Defect Density (cm^{-2})	Effective Capacitance [EIS] (F)	Integrated Capacitance [CV] (F)	Specific Capacitance (F/g)	~# of ML
C face	$1.1x10^{2}$	$1.3x10^{-5}$	$9.4x10^{-6}$	142	10
Si face	$9.0x10^{9}$	$1.1x10^{-5}$	$9.5x10^{-6}$	504	2
M plane	$5.8x10^{10}$	$1.2x10^{-5}$	$9.7x10^{-5}$	926	25
Defective Si face	$1.9x10^{11}$	$3.3x10^{-4}$	$3.7x10^{-4}$	1510	50

6.7. SUMMARY

The hydrogen adsorption and electrochemical properties of epitaxial graphene (EG) grown on silicon carbide (SiC) were shown. According to CV and EIS, electrochemical activity is dependent on the defect density of EG suggesting a dependence on point defects in the material for successful hydrogenation. Defects in graphene mediate charge transfer by increasing diffusion of hydrogen ions through graphene hydrogen adsorption by supplying sites for hydrogen to easily penetrate the graphene lattice resulting in high

diffusion of hydrogen ions while providing sites for hydrogen to easily adsorb as shown by an increase in capacitance and decrease in charge transfer and adsorption resistances with increasing defect density in the electrodes. Charge transfer is associated with increased diffusion of hydrogen ions though defects in epitaxial graphene through pristine graphene and is further supported by the decrease in psuedocapacitance as concentration of ions inside the graphene layers exceed ions adsorbed on the graphene surface. Engineering defects EG layers presents a new pathway to the formation of hydrocarbons and its use in supercapacitors, batteries and fuel cell electrodes.

REFERENCES

[1] K.M. Daniels, B. K. Daas, N. Srivastava, C. Williams, R. M. Feenstra, T. S. Sudarshan, MVS Chandrashekhar., Journal of Applied Physics 111, 114306 (2012)

[2] O. M. S. Filipe, C. M. A. Brett., Electroanalysis 16, No. 12, 994-1001 (2004)

[3] A. J. Bard, L. R. Faulkner., *Electrochemical Methods: Fundamentals and Applications*. 2000. Print

[4] A.C. Ferrari and J.Robertson., Phys.Rev. B 61, 14095-14107 (2000)

[5] L. G. Cançado, A. Jorio, E. H. M. Ferreira, F. Stavale, C. A. Achete, R. B. Capaz, M. V. O. Joutinho, A. Lombardo, T. S. Kulmala, A. C. Ferrari., Nano Letters 11, 3190-3196 (2011)

[6] Z. Yang, H. Wu., Chemical Physics Letters 343, 235-240 (2001)

[7] A. Lasia., Modern Aspects of Electrochemistry 35, 1-49 (2002)

[8] V. D. Jović, B. M Jović., Journal of Electroanalytical Chemistry 541, 1-11 (2003)

[9] C. Lin, B. N. Popov, H. J. Ploehn., Journal of The Electrochemical Society, 149, Issue. 2, A167-A175 (2002)

[10] J. W. Lee, T. Ahn, D. Soundararaian, J. M. Ko, J. Kim., Chem. Communications 47, 6305-6307 (2011)

CHAPTER 7

BIOSENSING APPLICATIONS OF EPITAXIAL GRAPHENE

7.1 BACTERIA AND BIOFILM SENSING: BACKGROUND AND CURRENT METHODS

Bacterial pathogens, ~1μm in size, are found in a variety of places in our environment, from bodies of water we drink to the soil we grow crops and raise livestock. We carry over 150 different types of bacteria with us on and in our person, though for the most part they are beneficial. With that being said there are a number of strains of bacteria that can cause illness and some that are fatal. For instance the O157:H7 strain of *E. coli* can produce large amounts of toxins in the intestines that can cause death [1]. Even in small quantities of these types of bacteria, serious damage can still occur, further supporting the need for fast, sensitive and selective testing. Bacteria are detectable by their distinctive sequences of nucleic acid. To detect these pathogens, the standard method is colony counting. But with the time of 72 hours to positively confirm pathogen, other methods have been developed [1].

Enzyme-Linked Immunosorbent Assay (ELISA) is just one type of immunological based detection that uses antigen-antibody bindings as its method of pathogen recognition. The shortcoming of all immuno forms of detection is the need to completely understand antibody/pathogen reaction to ensure the correct pathogen is detected. This not only is an issue for unknown pathogens but if the pathogen has a low

affinity to the antibody then it also suffers from low sensitivity. Another issue is the inability to detect pathogens in real-time when it is present in low concentrations, further delaying detection time. When detecting low concentrations, down to the single cell of a pathogen using traditional techniques, polymerase chain reaction is ideal [2, 3].

Polymerase Chain Reaction (PCR) is a type of nucleic acid amplification that detects a single copy of a targeted DNA sequence and amplifies it. By amplifying the DNA of a targeted pathogen, false-positives are greatly reduced. PCR is also less time consuming only taking from 5 to 24 hours to produce detectable results. The problem arises that dead and live cells have DNA that is always present meaning in typical PCR it is not possible to discern the difference between the two [2]. While PCR has sped up testing time tremendously it suffers from the complexity of the test, which require skilled workers further adding to its expense. With the traditional methods of detection complicated and/or time consuming, a real-time biosensor with the ability to monitor bacterial activity through changes in electrical resistance of epitaxial graphene (EG).

The high surface area of EG allow for its usage as a sensitive, real-time technique for sensing bacterial activity without the need of taking bacteria cultures or using standard laboratory techniques such as ELISA and PCR, all requiring time and skilled workers. Similar with molecule sensing, graphene has shown specific π- π and non-specific hydrophobicity induced interactions with biological relevant macromolecules [4,5,6]. The high parallel conductivity of graphene as well as its strong physicochemical interactions with biomacromolecules allows for monitoring activity bacterium, and its secreted matrix of mucilaginous extracellular polymers (EPS), as bacteria typically form what is known as a biofilm, a form of protection mode of growth for bacteria that can

form on biotic surfaces, organic life, and abiotic surfaces such as epitaxial graphene as shown in Figure 7.1 [7].

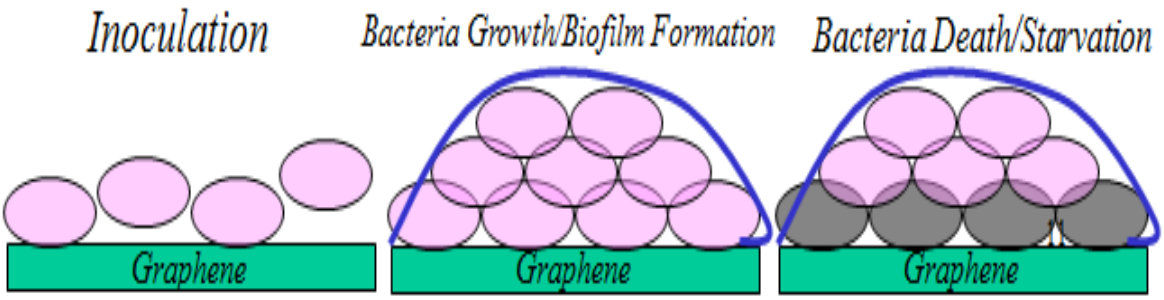

Figure 7.1 Illistrations of inoculation, growth and decay phase of bacteria on graphene

In the initial inoculation phase free-floating bacteria are governed by weak van der Waals forces, where adhesion to the surface is temporary. In this phase the conductivity of the graphene should change suddenly as cells attach and detach from the surface. As the bacteria grow adhesion becomes permanent and colonies start forming on the surface. From these colonies cells disperse and biofilm is formed. As cells disperse graphene conductivity should change before reaching a saturation point, where the biofilm fully covers the sample. As bacteria die, from antibacterial treatment of contaminated water for example, conductivity observed should return to pre-inoculation values.

7.2 Fabrication and Experimental Setup of Graphene Biosensor

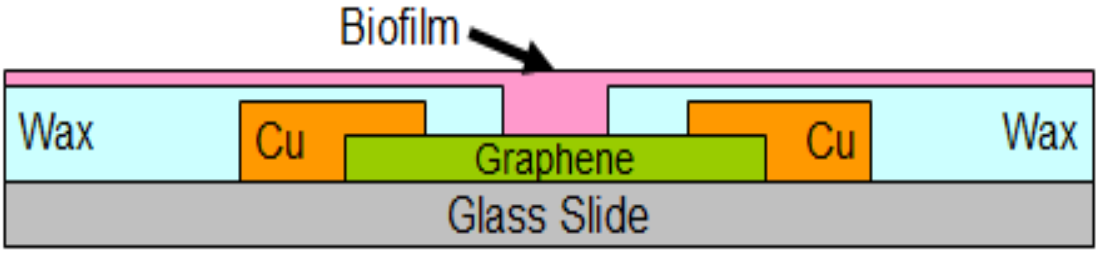

Figure 7.2 Schematic of graphene biosensor with graphene exposed to bacteria.

On-axis, semi-insulating, 6H-SiC substrate was used to form EG on the silicon face at ~1400°C in vacuum. A slide containing a 1cm x 1cm piece of EG with two copper contacts was sealed leaving approximately 0.5cm x 0.5cm of EG exposed, as shown in Figure 7.2, to be placed in the aqueous media. The organism used in this initial experiment was *Escherichia coli* strain 25922. The surface charge of the bacteria was measured at -36.27±4.95mV using a Brookhaven ZetaPALS electrophoresis technique.

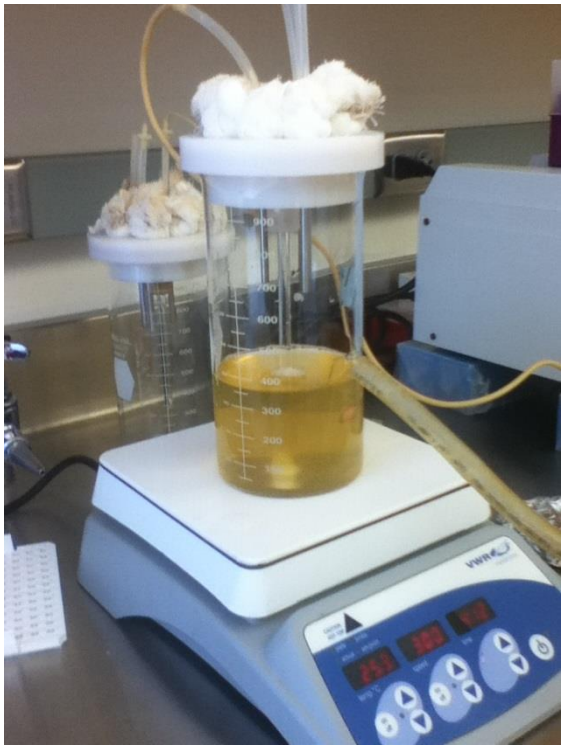

Figure 7.3 CDC Biofilm Reactor used to grow biofilm

The reactor used to grow the biofilm is a CDC Biofilm Reactor made by BioSurface Technologies Corporation (Bozeman, MT) as shown in Figure 7.3. The reactor was stirred 400 rpm in room temperature with a flow rate of 0.1 mL/min. The media used was "K12 Growth Medium" which consisted of 37 g/L EC Media (EMD Chemicals, Gibbstown, NJ), in deionized water. Resistance of EG was measured prior to

inoculation in media to exclude media contributions to change in conductivity. The system was then inoculated with ~3 mL of *E. coli* and resistance measured for 7 days throughout the growth of the biofilm.

Optical microscopy used to verify biocompatibility of bacterial on EG. Raman spectroscopy was performed using a micro-Raman setup with laser excitation wavelength at 632nm and a spot size of ~2 μm to verify quality of EG before and after biofilm growth. The Raman system was calibrated using the known Si peak at 520.7 cm^{-1}. Reference blank SiC substrate spectra were scaled appropriately and subtracted from the EG/SiC spectra to show only graphene phonon peaks. Confocal microscopy was used to observe the number of live and dead cells throughout the growth of the biofilm on EG using fluorescent dies and laser excitation wavelength of 488, with intact membranes displaying green fluorescence and bacteria with ruptured membranes fluorescing red.

7.3 Real Time Detection of Bacteria by Changes in EG Conductivity

The graphene sensor was placed into the growth media without bacteria to exclude its contribution to changes in conductivity. Electrical resistance was unchanged after placing it in media with a baseline of 2.3kΩ measured across the graphene layer prior to inoculation. The system was then inoculated with ~3mL of *E. coli* with the sensor showing an immediate response to the presence of bacteria after inoculation, picking up minute traces of the pathogen prior to the formation of a biofilm, showing an 8% increase in electrical resistance in less than 5 minutes as shown in Figure 7.4.

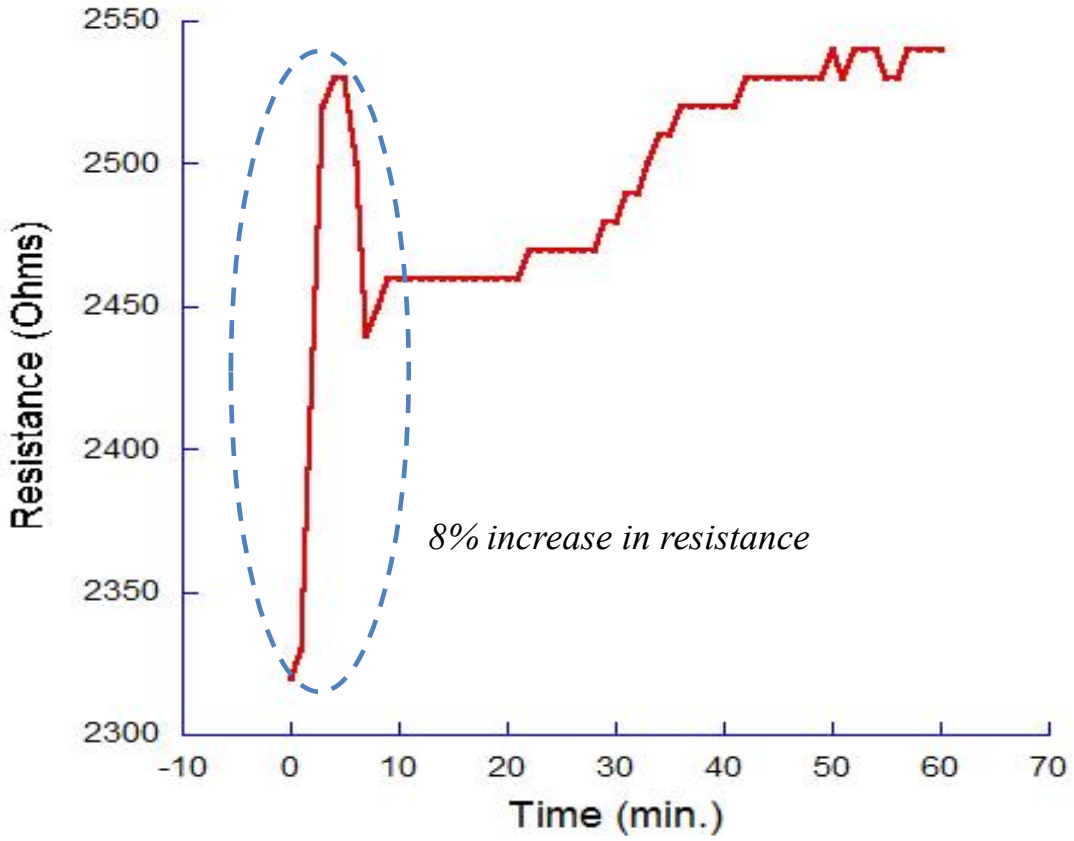

Figure7.4 Real-time sensing of bacteria interaction with graphene sensor showing immediate changes in electrical resistance after inoculation.

Once a biofilm is formed, graphene furthers its ability to track the growth of bacteria with increases in electrical resistances correlating directly with the growing presence of bacteria. Graphene resistance increased before leveling off corresponding to the saturation growth phase of the bacteria as shown in Figure 7.5. The major contributor of this conductivity change is changes in doping of graphene due to cellular interactions. Localized changes in pH caused by clumps of cells and the waste they produce (acetic acid) in the biofilm are also a contributor to changes in conductivity.

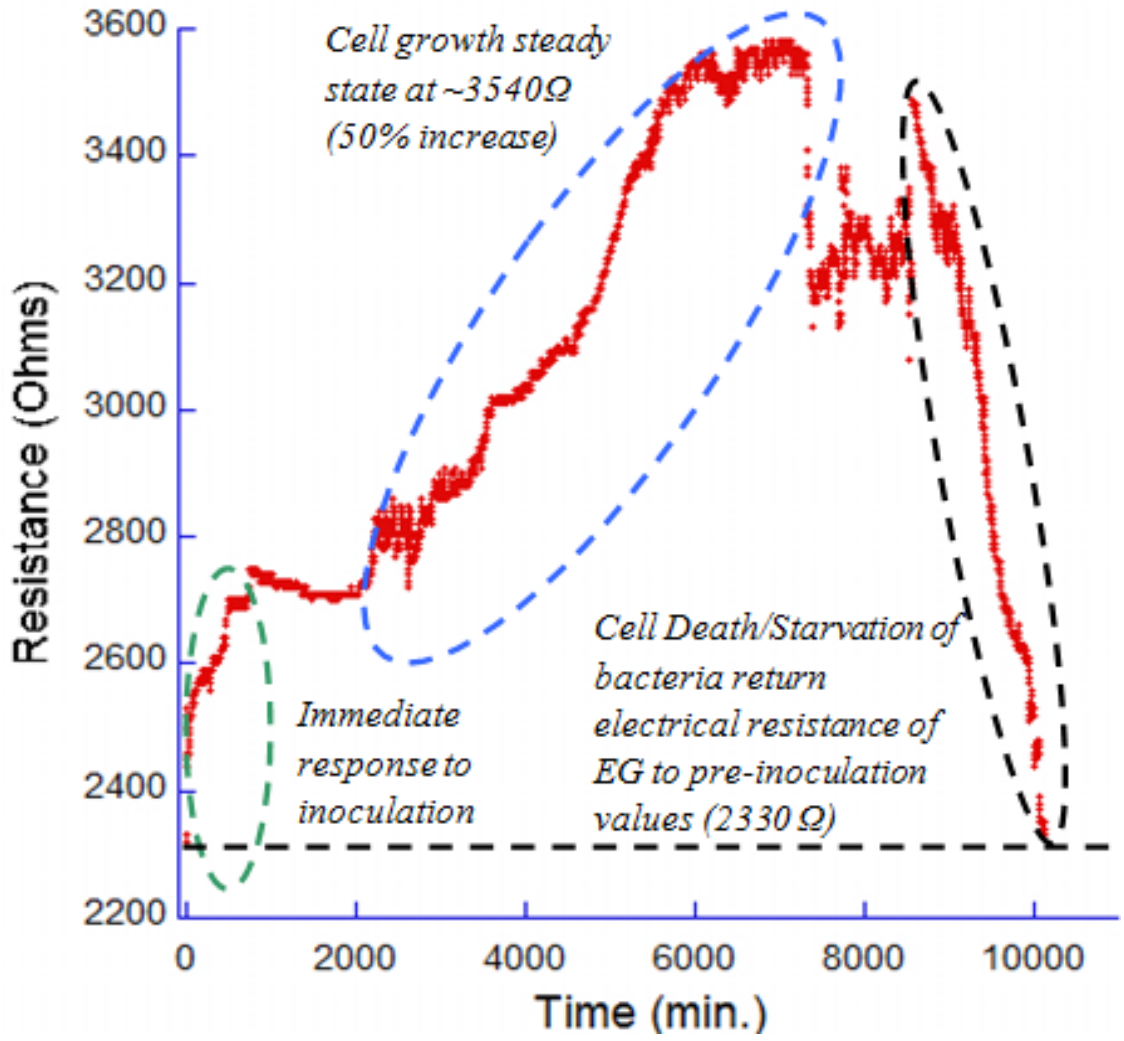

Figure 7.5 Growth of *E. coli* measured by changes in electrical resistance of epitaxial graphene biosensor.

As the growth of the *E.coli* became limited by the size of growth reactor and limited food supply, starvation and death of bacteria occurred. In death *E.coli* is no longer able to significantly contribute to the conductivity of graphene in death as shown in Figure 4, with a steady decline in electrical resistivity back to pre-inoculation values. Decrease in electrical resistance was directly correlated to substantial death of bacteria on the sensor confirmed by confocal microscopy as shown in Figure 7.7. The electrical resistance of graphene change directly with bacterial activity on the surface,

demonstrating its use as a sensitive, real-time sensor to the presence of bacteria and its metabolic processes.

7.4 Verifying Biocompatability by Optical and Confocal microscopy

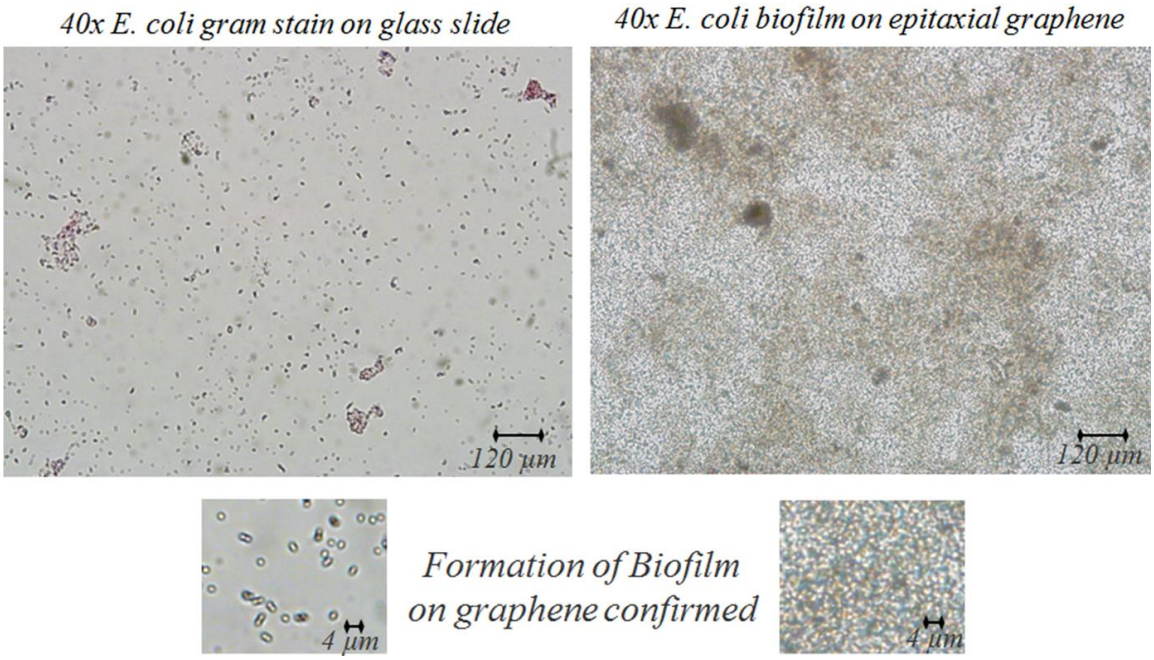

Figure 7.6 Gram stain of *E.coli cells* on glass slide and formation of *E.coli* biofilm on epitaxial graphene

Formation of *E.coli* biofilm on epitaxial graphene was verified with optical microscopy showing gram stained biofilm formation on EG surface as shown in Figure 7.6. To demonstrate bacteria biocompatibility with graphene, bacteria was stained with fluorochromes, a fluorescent die that absorbs photons in the UV spectra (200-800nm) and releases photons after light excitation, and observed with a confocal microscope. As shown in Figure 7.7, E.*coli* was stained with fluorescein isothiocyanate (FITC), green for living cells and 4',6-diamidino-2-phenylindole (DAPI) , red for dead cells.

Initial formation of biofilm is observed 24 hours after inoculation corresponding directly to the initial increase in electrical resistance. Dead cells are observed in what appears to be a tear in the graphene layers suggesting toxicity at sharp edges as seen with carbon nanotubes (CNTs). As the biofilm becomes more uniform as shown 144 hours after inoculation, edges appear to not have any effect on the formation of the biofilm. This is apparent by the increase in electrical resistance observed in Figure 7.5. Cell death that was attributed to the decrease in electrical resistance to pre-inoculation was confirmed by mass cell death observed by confocal microscopy.

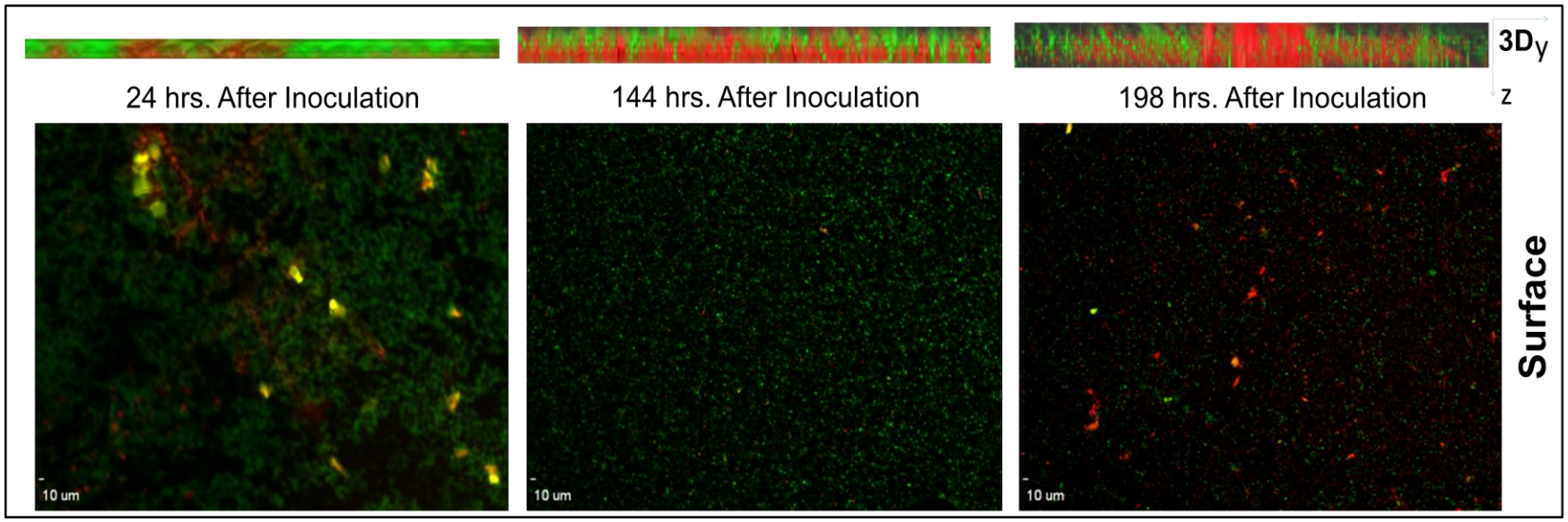

Figure 7.7 Confocal microscopy of bacteria growth on epitaxial graphene

7.5 Summary of Graphene Biosensor

It may be possible to differentiate different rates of change in electrical resistance with different types of bacteria and surface charges, leading to the possibility of a bio-detector capable of differentiating pathogen type simply by changes in conductivity of the graphene. Efforts of treating the water source could also be monitored using this sensor as death of bacteria can be monitored by decreasing of electrical resistance and could be used as a guide as to whether water treatment is effective as well as when it is safe to drink. This sensor has demonstrated the ability to monitor bacterial activity through the measurement of graphene electrical resistance, which is not possible in bulk graphite and allows for its usage as a sensitive, real-time technique for sensing bacterial activity.

REFERENCES

[1] D. Ivnitski, I. Abdel-Hamid, P. Atanasov, E. Wilkins, "Biosensors for detection of pathogenic bacteria," Biosensors & Bioelectronics 14, 1999, pp. 599-624.

[2] O. Lazcka, F. Campo, F. X. Munoz, "Pathogen detection: a perspective of traditional methods and biosensors," Biosensors and Bioelectronics 22, 2007, pp. 1205–1217.

[3] V. Velusamy, K. Arshak, O. Korostynska, K. Oliwa, C. Adley, "An overview of foodborne pathogen detection: In the perspective of biosensors," Biotechnology Advances 28, 2010, pp. 232-254

[4] R. Sharma, J. H. Baik, C. J. Perera, M. S. Strano, "Anomalously large reactivity of single graphene layers and edges toward electron transfer chemistries," Nano Letters 10, 2010, pp. 398-405.

[5] N.Varghese, U.Mogera, A.Govindaraj, A.Das,P.K.Maiti, A.K.Sood, C.N.R.Rao, " Binding of DNA nucleobases and nuleosides with graphene," Chem. Phys. Chem. 10, 2009, pp. 206–210.

[6] G.B.McGaughey, M.Gagne, A.K.Rappe, "Π-Stacking interactions alive and well in proteins," J.Biol.Chem. 273, 1998, pp. 15458–15463.

[7] A.W. Decho, "Microbial biofilms in intertidal systems: an overview," Continental Shelf Research, Volume 20, Issues 10-11, 2000, pp.1257-1273

CHAPTER 8

CONCLUSION

The research presented in this dissertation focuses on the reactivity and biocompatibility of graphene, towards the application of microbial fuel cells. Though this work, chemical and biological reactivity of graphene were reviewed. We explored work in molecular absorption/adsorption and sensing on epitaxial graphene. Previous work in hydrogenation of graphene for hydrogen storage applications and bandgap engineering is then explored in detail. As most of these methods are in situ and require thermal annealing to desorb adsorbed hydrogen, an ex situ electrochemical means was developed as a less expensive and possibly reversible means of hydrogen incorporation into graphene.

A home-built electrochemical cell was designed and built to test hypothesis of hydrogen adsorption via electrochemistry. Positive hydrogen ions in dilute acidic solution are attracted to negatively biased EG where they are adsorbed and form C-H bonds with graphene. Hydrogen adsorption by electrochemistry was proven by a detailed study using Raman spectroscopy, Atomic Force Microscopy (AFM) and Scanning Tunneling Spectroscopy (STS). Increases in sp^3 content, adsorption of hydrogen on the π-bonds of sp^2 bonded graphene, was observed by increases in D peak intensity in the Raman spectra and a fluorescence background was observed in hydrogenated material, which is only observed in hydrocarbons. Stress and strain caused by changes in C-C bond length, from

1.42 Å to 1.54 Å, was observed not only by peak shifts in the Raman spectra but strain in the graphene layer observed by AFM. Evidence of localized states was also observed by STS, revealing that hydrogenation is not continuous throughout the layer but in clusters. Possible substrate/sample dependence was also observed.

To overcome this substrate/sample dependence, catalytic metals, Gold (Au) and Platinum (Pt) were deposited on the surface and concentration of hydrogen adsorbed on graphene increased beyond that of hydrogenated EG without catalyst as catalytic metals lower activation energy and offer additional pathways for hydrogen to adsorb. Samples with gold nanoparticles were shown to have higher hydrogen adsorption than those with platinum nanoparticles despite having lower catalytic activity than Pt by two orders of magnitude. This could simply be due to nanoparticles adhesion or size during hydrogenation.

Hydrogen desorption from electrochemically hydrogenated samples was demonstrated, proving hydrogenation of graphene over damage. Electrochemical reversibility was shown, revealing history dependence and lattice strain after each cycle as observed by Raman. Mechanism of hydrogen adsorption of epitaxial graphene was observed to be dependent on defects in EG as observed by cyclic voltammetry, electrochemical impedance spectroscopy and Raman and an impedance model of the electrochemical cell was derived from EIS measurements.

Lastly, biocompatibility of epitaxial graphene was demonstrated by fluorescence confocal microscopy. EG bacteria sensor was fabricated with sensor responding

electrically in real-time with bacteria and biofilm growth via changes in material resistance.

REFERENCES

[1] M.Zhou et al., Journal of Chemical Technology & Biotechnology 88.4, 508-518 (2013)

[2] R. S. Dhillon and G. von Wuehlisch., Biomass and Bioenergy 48, 75-89 (2013)

[3] P. McKendry., Bioresource Technology 83.1, 37-46 (2002)

[4] Z. Du, H. Li and T. Gu., Biotechnology Advances 25.5, 464-482 (2007)

[5] D. Jiang and B. Li., Biochemical Engineering Journal 47.1–3, 31-37 (2009)

[6] Feng et. al., Journal of Power Sources 195.7, 1841-1844 (2010)

[7] D. R. Lovley and K. P. Nevin., "Electricity Production with Electricigens." (2008): 295–306.

[8] A. ElMekawy et al. Bioresource Technology 142, 672-682 (2013)

[9] K. Rabaey and W. Verstraete., Trends in Biotechnology 23.6, 291-298 (2005)

[10] V.B. Oliveira et al., Biochemical Engineering Journal 73, 53-64 (2013)

[11] D.R. Lovely., Nature Reviews Microbiology 4.7 497-508 (2006)

[12] B.E. Logan., Nature Reviews Microbiology 7.5, 375-381 (2009)

[13] A. C. Brownson and C. E. Banks., Analyst 135, 2768-2778 (2010)

[14] A.K. Geim, K.S. Novoselov, Materials Science 6, 183-191 (2007)

[15] W.A de Heer, C. Berger, X. Wu, P. N. First, E. H. Conrad, X. Li, T. Li, M. Sprinkle, J. Hass, M. L. Sadowski, M. Potemski, G. Martinez, Solid State Communications 143 (2007) 92-100

[16] A.H. Castro Neto, F. Guiena, N.M.R. Peres, K.S. Novoselov, A.K. Geim., Rev. Mod. Phys. 81, 109-162 (2009)

[17] J. L. Tedesco, B. L. VanMil, R. L. Myers-Ward, J. M. McCrate, S. A. Kitt, P. M. Campbell, G. G. Jernigan, J. C. Culbertson, C. R. Eddy, D. K. Gaskill., Applied Physics Letters 12, 122102-122102-3(2009)

[18] Y. Zhang et al., Journal of Power Sources 239, 169-174 (2011),

[19] H. Choi et. al., Nano Energy 1.4, 534-551 (2012)

[20] Z. He et al., Nano Letters 12.9, 4738-4741 (2012)

[21] J. Liu et al, Bioresource Technology 144, 275-280 (2012)

[22] J. Hou, Z. Liu and P. Zhang., Journal of Power Sources 224, 139-144(2013)

[23] L. Xiao et al., Journal of Power Sources208, 187-192 (2012)

[24] F. Schedin et. al., Nature Mat. 6, 652-655 (2007)

[25] B. K. Daas, W. K. Nomani, K. M. Daniels, T. S. Sudarshan, G. Koley and MVS Chandrashekhar., Mater. Sci. Vol. 717-720 665-668 (2012)

[26] L. Liao et. al. Nature, vol. 467, 305-308, 2010

[27] Novoselov, K. S. Rev. Mod. Phys. 2011, 83 (3), 837−849

[28] L. Liao et. al. Nature, vol. 467, 305-308, 2010

[29] M. Y. Han, B. Ozyilmaz, Y. Zhang, P. Kim., PRL 98, 206805 (2007)

[30] B. Verberck, B. Partoens, F. M. Peeters and B. Trauzettel., Phys. Rev. B 85, 125403

[31] S. Ryu, M. Y. Han, J. Maultzsch. T. F. Heinz, P. Kim, M. L. Steigerwald and L. E. Brus., Nano Lett., Vol. 8, No. 12, 2008

[32] D. C. Elias, R. R. Nair, T. M. G. Mohiuddin, S. V. Morozov, P. Blake, M. P. Halsall, A. C. Ferrari, D. W. Boukhvalov, M. I. Katsnelson, A. K. Geim, K. S. Novoselov., Science 30, Vol. 323, No. 5914, 610-613 (2009)

[33] R. Sharma, J. H. Baik, C. J. Perera, M. S. Strano., Nano Letters 10, 398-405 (2010)

[34] R. Sprinkle, J. Hicks, A. Tejeda, A. Taleb-Ibrahimi, P. Le Fèvre, F. Bertran, H. Tinkey, M. C. Clark, P. Soukiassian, D. Martinotti, J. Hass and E. H. Conrad., J. Phys D : Appl. Phys. 43, 374006 (2010)

[35] Y. Lin and P. Avouris., Nano Lett. Vol. 8, No. 8 (2008)

[36] F. Schedin et. al., Nature Mat. 6, 652-655 (2007)

[37] B. K. Daas, W. K. Nomani, K. M. Daniels, T. S. Sudarshan, G. Koley and MVS Chandrashekhar., Mater. Sci. Vol. 717-720 665-668 (2012)

[38] S.K. Lower et. al Geochimica et Cosmochimica Acta, Vol. 64, No. 18, pp. 3133–3139, 2000

[39] Nair et. al., small 6, No.24, 2877-2884 b

[40] C. Riedl, C. Coletti, T. Iwasaki, A. A. Zakharov and U. Starke., PRL 103, 246804 (2009)

[41] Jorge O. Sofo, Ajay S. Chaudhari, Greg D. Barber., Physical Review B 75, 153401 (2007)

[42] M. Wojtaszek, N. Tombros, A. Caretta, P. H. M. van Loosdrecht, B. J. van Wess J. Appl. Phys. 110, 063715 (2011)

[43] R. Balog, B. Jørgensen, J. Wells, E. Lægsaard, P. Hofmann, F. Besenbacher, L. Hornekær., J. Am. Chem. Soc. 131, 8744-8755 (2009)

[44] J. D. Jones, K. K. Mahajan, W. H. Williams, P. A. Ecton, Y. Mo, J. M. Perez., Carbon 48, Issue 8, 2335-2340 (2010)

[45] K. M. Daniels, B. K. Daas, N. Srivastava, C. Willams, R. M. Feenstra, T. S. Sudarshan, MVS Chandrashekhar., J. Appl. Phys. 111, 114306 (2012)

[46]] W.A de Heer, C. Berger, X. Wu, P. N. First, E. H. Conrad, X. Li, T. Li, M. Sprinkle, J. Hass, M. L. Sadowski, M. Potemski, G. Martinez, Solid State Communications 143 (2007) 92-100

[47] [2] A.K. Geim, K.S. Novoselov, Materials Science 6, 183-191 (2007)

[48] [3] A.H. Castro Neto, F. Guiena, N.M.R. Peres, K.S. Novoselov, A.K. Geim., Rev. Mod. Phys. 81, 109-162 (2009)

[49] [4] J. L. Tedesco, B. L. VanMil, R. L. Myers-Ward, J. M. McCrate, S. A. Kitt, P. M. Campbell, G. G. Jernigan, J. C. Culbertson, C. R. Eddy, D. K. Gaskill., Applied Physics Letters 12, 122102-122102-3(2009)

[50] Geim A. K Science 324, 1530 (2009)

[51] S. Stankovich et. al., Carbon 45. Vol. 7 (2007) 1558-1565

[52] B. K. Daas, O. Sabih, S. Shetu, K. M. Daniels, S. Ma, T. S. Sudarshan, MVS Chandrashekhar,. Cryst. Growth Des., 2012, 12 (7), pp 3379–3387 (2012)

[53] B. K. Daas, S. U. Omar, S. Shetu, K. M. Daniels, S. Ma, T. S. Sudarshan, MVS Chandrashekhar., Cryst. Growth Des. 12, Issue 7, 3379-3387 (2012)

[54] J. Rand. Electroanal. Chem, 35 (1972)

[55] K. Ota, S. Nishigori and N. Kamiya., J. Electroanal. Chem., 257, 205-215 (1988)

[56] C. Srinivasan and R. Saraswathi., Current Science 97, Vol. 97, No. 3 (2009)

[57] A.C. Ferrari and J.Robertson., Phys.Rev. B 61, 14095-14107 (2000)

[58] S. Shirvaraman, M.V.S. Chandrashekhar, J.J. Boeckl, M.G. Spencer., Journal of Electronic Materials,Vol. 38, No. 6 (2009)

[59] J. M. Dawlaty, S. Shirvaraman, J. Strait, P. George, M.V.S. Chandrashekhar, Farhan Rana, M.G. Spencer, D. Veksler, Y. Chen., Appl. Phys. Lett. 93, 131905 (2008)

[60] A. K. Vijh., Journal of Power Sources, Vol. 11, Issue 1-2, 171-183 (1984)

[61] D. C. Elias, R. R. Nair, T. M. G. Mohiuddin, S. V. Morozov, P. Blake, M. P. Halsall, A. C. Ferrari, D. W. Boukhvalov, M. I. Katsnelson, A. K. Geim, K. S. Novoselov., Science 30, Vol. 323, No. 5914, 610-613 (2009)

[62] B. Wang, J. R. Sparks, H. R. Gutierrez, F. Okino, Q. Hao et. al., Appl. Phys. Lett. 97, 141915 (2010)

[63] S. Ryu, M. Y. Han, J. Maultzsch. T. F. Heinz, P. Kim, M. L. Steigerwald and L. E. Brus., Nano Lett., Vol. 8, No. 12, 2008

[64] Shu Nie and R.M. Feenstra., J. Vac. Sci. Technol. A 27, 1052 (2009)

[65] B. Verberck, B. Partoens, F. M. Peeters and B. Trauzettel., Phys. Rev. B 85, 125403

[66] R. Sprinkle, J. Hicks, A. Tejeda, A. Taleb-Ibrahimi, P. Le Fèvre, F. Bertran, H. Tinkey, M. C. Clark, P. Soukiassian, D. Martinotti, J. Hass and E. H. Conrad., J. Phys D : Appl. Phys. 43, 374006 (2010)

[67] Y. Lin and P. Avouris., Nano Lett. Vol. 8, No. 8 (2008)

[68] B. Marchon, J. Gui, K. Grannen, G. C. Rauch, J. W. Ager III, S.R.P. Silva and J. Robertson., IEEE Transactions on Magnetics, Vol. 33, No. 5 (1997)

[69] J. O. Sofo, A.S. Chaudhari, G. D. Barber., Physical Review B 75, 153401 (2007)

[70] R. Zan, Q. M. Ramasse, R. Jalil and U. Banger ,. Atomic Structure of Graphene and h-BN Layers and Their Interactions with Metals, Advances in Graphene Science, Dr. M. Aliofkhazraei (Ed.), ISBN: 978-953-51-1182-5, InTech, DOI: 10.5772/56640. (2013)

[71] S. Ryu, M. Y. Han, J. Maultzsch. T. F. Heinz, P. Kim, M. L. Steigerwald and L. E. Brus., Nano Lett., Vol. 8, No. 12, 2008

[72] D. C. Elias, R. R. Nair, T. M. G. Mohiuddin, S. V. Morozov, P. Blake, M. P. Halsall, A. C. Ferrari, D. W. Boukhvalov, M. I. Katsnelson, A. K. Geim, K. S. Novoselov., Science 30, Vol. 323, No. 5914, 610-613 (2009)

[73] C. Riedl, C. Coletti, T. Iwasaki, A. A. Zakharov and U. Starke., PRL 103, 246804 (2009)

[74] K. M. Daniels, B. K. Daas, N. Srivastava, C. Willams, R. M. Feenstra, T. S. Sudarshan, MVS Chandrashekhar., J. Appl. Phys. 111, 114306 (2012)

[75] A. C. Dillon, M. J. Heben., Appl. Phys. A 72, 133-142 (2001)

[76] P. Maity, S. Basu, S. Bhaduri, G. K. Lahiri., Advanced Synthesis & Catalysis 349, Issue 11-12, 1955-1962 (2007)

[77] A. S. Hussey, G. W. Keulks, G. P. Nowack, R. H. Baker., Journal of Organic Chemistry 33, No. 2, 610-616 (1986)

[78] C. Nwosu.,Journal of Technical Science and Technologies, 1(2):25-28, (2012)

[79] K. Okazaki-Maeda, T. Akita, S. Tanaka and M. Kohyama., Materials Transactions, Vol. 49, No. 11, 2441-2444 (2008)

[80] G. A. Somorjai et al., Nature Vol. 258 (1975)

[81] E. Bus, J. T. Miller, J. A. van Bokhoven., J. Phys. Chem. B 109, No. 30, 14581-14587 (2005)

[82] M. Haruta.,Catalysis Today 36, 153-166 (1997)

[83] A. S. Hussey, G. W. Keulks, G. P. Nowack, R. H. Baker., Journal of Organic Chemistry 33, No. 2, 610-616 (1986)

[84] C. Kartusch and J. A. van Bokhoven., Gold Bulletin 42, No. 4, 343-348 (2009)

[85] M. K. Oudenhuijzen, J. H. Bitter, and D. C. Koningsberger., J. Phys. Chem. B 105, 4616-4622 (2001)

[86] P. Claus., Applied Catalysis A : General 291 (2005) 222-229

[87] T. Mitsudome and K. Kaneda., Gold nanoparticle catalysts for selective hydrogenations., Green Chem. Advance Artlcle (2013) DOI:10.1039/C3GC41360H

[88] D. J. Gorin, F. D. Toste., Nature 446, 395-403 (2007)

[89] B. K. Daas, K. Daniels, S. Shetu, T. S. Sudarshan, and M. V. S. Chandrashekhar, Mater. Sci. Forum 717–720, 633–636 (2012).

[90] J. Rand, Electroanal. Chem 35, 209–218 (1972).

[91] K. Ota, S. Nishigori, and N. Kamiya, J. Electroanal. Chem. 257, 205–215 (1988).

[92] C. Srinivasan and R. Saraswathi., Current Science 97, Vol. 97, No. 3 (2009)

[93] C. Casiraghi, A. C. Ferrari, and J. Robertson., Physical Review B 72, 085401 (2005)

[94] J. Schwan, S. Ulrich, V. Batori, H. Ehrhardt, S. R. P. Silva., J.Appl.Phys.,Vol.80,No.1(1996)

[95] A.C. Ferrari and J.Robertson., Phys.Rev. B 61, 14095-14107 (2000)

[96] B. Wang, J. R. Sparks, H. R. Gutierrez, F. Okino, Q. Hao et. al., Appl. Phys. Lett. 97, 141915 (2010)

[97] B. Marchon, J. Gui, K. Grannen, G. C. Rauch, J. W. Ager III, S. R. P.Silva, and J. Robertson, IEEE Trans. Magn. 33(5), 3148–3150 (1997)

[98] A.Siani, K. R. Wigal, O.S Alexeev, M.D Amiridis., Journal of Catalysis 257 (2008) 5–15

[99] A. Tiberj et al.,Sci. Rep. 3, 2355 (2013)

[100] Cançado et al., Nano Lett., 2011, 11 (8), pp 3190–3196

[101] B. J. Wood and H. Wise., Journal of Catalysis 5, 135-145 (1966)

[102] M. Lazar, C. Ducu, V. Almasan, N. Aldea, B. Barz, P. Marginean, C. Sutan, V. Malinnovschi, Rom. Journ. Phys. Vol. 51, No. 1-2, 299-304 (2006)

[103] B. Dren, D. Hug, L. Marot, R. Pawlak, M. Kisiel, R. Steiner, D. M. Zumbühl and E. Meyer., Bellstein J. Nanotechnol. 3, 852-859 (2012)

[104] M. Woitaszek, N. Tombros, A. Caretta, P. H. M. van Loosdrecht and B. J. van Wees., J. Appl. Phys. 110, 063715 (2011)

[105] J.D. Jones, K. K. Mahajan, W. H Williams, P. A. Ecton, Y. Mo, J. M. Perez., Carbon 48, Issue 8, 2335-2340 (2010)

[106] M. Pumera and C. H. A. Wong., Chem. Soc. Rev 42, 5987 (2013)

[107] A.E. Curtin. Kelvin Probe Microscopy Studies of Epitaxial Graphene on SiC(0001). Dissertation, University of Maryland, Digital Repository at the University of Maryland, 2011. (http://hdl.handle.net/1903/12004)

[108] S. Adam, S. Jung, N. N. Klimov, N. B. Zhitenev, J. A. Stroscio and M. D. Stiles., Phys. Rev. B 84, 235421 (2011)

[109] J. Hwang, C. Kuo, L. Chen, K, Chen., Nanotechnology 21, 465705(2010)

[110] A.C. Ferrari and J.Robertson., Phys.Rev. B 61, 14095-14107 (2000)

[111] S. Ryu, M. Y. Han, J. Maultzsch. T. F. Heinz, P. Kim, M. L. Steigerwald and L. E. Brus., Nano Lett., Vol. 8, No. 12 (2008)

[112] M. Wojtaszek, N. Tombros, A. Caretta, P. H. M. van Loosdrecht, B. J. van Wess J. Appl. Phys. 110, 063715 (2011)

[113] R. Balog, B. Jørgensen, J. Wells, E. Lægsaard, P. Hofmann, F. Besenbacher, L. Hornekær., J. Am. Chem. Soc. 131, 8744-8755 (2009)

[114] J. D. Jones, K. K. Mahajan, W. H. Williams, P. A. Ecton, Y. Mo, J. M. Perez., Carbon 48, Issue 8, 2335-2340 (2010)

[115] Jorge O. Sofo, Ajay S. Chaudhari, Greg D. Barber., Physical Review B 75, 153401 (2007)

[116] D.W. Boukhvalov and M.I. Katsnelson., J.Phys.:Condes. Matter 21, 344205 (2009)

[117] P. T. Kissinger and W. R. Heineman., J. Chem. Educ. 60, Issue 9, 702 (1983)

[118] K.M. Daniels, B. K. Daas, N. Srivastava, C. Williams, R. M. Feenstra, T. S. Sudarshan, MVS Chandrashekhar., Journal of Applied Physics 111, 114306 (2012)

[119] O. M. S. Filipe, C. M. A. Brett., Electroanalysis 16, No. 12, 994-1001 (2004)

[120] A. J. Bard, L. R. Faulkner., Electrochemical Methods: Fundamentals and Applications. 2000. Print

[121] A.C. Ferrari and J.Robertson., Phys.Rev. B 61, 14095-14107 (2000)

[122] L. G. Cançado, A. Jorio, E. H. M. Ferreira, F. Stavale, C. A. Achete, R. B. Capaz, M. V. O. Joutinho, A. Lombardo, T. S. Kulmala, A. C. Ferrari., Nano Letters 11, 3190-3196 (2011)

[123] Z. Yang, H. Wu., Chemical Physics Letters 343, 235-240 (2001)

[124] A. Lasia., Modern Aspects of Electrochemistry 35, 1-49 (2002)

[125] V. D. Jović, B. M Jović., Journal of Electroanalytical Chemistry 541, 1-11 (2003)

[126] C. Lin, B. N. Popov, H. J. Ploehn., Journal of The Electrochemical Society, 149, Issue. 2, A167-A175 (2002)

[127] J. W. Lee, T. Ahn, D. Soundararaian, J. M. Ko, J. Kim., Chem. Communications 47, 6305-6307 (2011)

[128] D. Ivnitski, I. Abdel-Hamid, P. Atanasov, E. Wilkins, "Biosensors for detection of pathogenic bacteria," Biosensors & Bioelectronics 14, 1999, pp. 599-624.

[129] O. Lazcka, F. Campo, F. X. Munoz, "Pathogen detection: a perspective of traditional methods and biosensors," Biosensors and Bioelectronics 22, 2007, pp. 1205–1217.

[130] V. Velusamy, K. Arshak, O. Korostynska, K. Oliwa, C. Adley, "An overview of foodborne pathogen detection: In the perspective of biosensors," Biotechnology Advances 28, 2010, pp. 232-254

[131] R. Sharma, J. H. Baik, C. J. Perera, M. S. Strano, "Anomalously large reactivity of single graphene layers and edges toward electron transfer chemistries," Nano Letters 10, 2010, pp. 398-405.

[132] N.Varghese, U.Mogera, A.Govindaraj, A.Das,P.K.Maiti, A.K.Sood, C.N.R.Rao, "Binding of DNA nucleobases and nuleosides with graphene," Chem. Phys. Chem. 10, 2009, pp. 206–210.

[133] G.B.McGaughey, M.Gagne, A.K.Rappe, "Π-Stacking interactions alive and well in proteins," J.Biol.Chem. 273, 1998, pp. 15458–15463.

[134] A.W. Decho, "Microbial biofilms in intertidal systems: an overview," Continental Shelf Research, Volume 20, Issues 10-11, 2000, pp.1257-1273